

## MASTERING THE ANALYTICAL LAB

**FAST, HIGH-RES ORGANOID IMAGING  
WITH LICORbio ATLAS™  
FOR DRUG DISCOVERY**

**ENGINEERING CHEMISTRY'S FUTURE:**

**HOW RADLEY'S TURNS LAB  
CHALLENGES INTO INNOVATION**

**ONE SOFTWARE. ANY REACTOR.  
EFFORTLESS AUTOMATION.**

**radleys**  
accelerating chemistry

**ava pad**





## About Us



*of Pioneering the Scientific Frontier*

**Inkarp, established in 1985, honors 40 years** of dedication to the scientific community in India. Our journey continues to be driven by the pursuit of excellence in **offering cutting-edge scientific research instruments**. We take pride in providing scientists across the country with tools that facilitate discoveries and innovation.

**SPARK**  
SCIENTIFIC PRIVATE LTD

Spark Scientific, a wholly owned subsidiary of Inkarp, focuses on 4 specific markets verticals - **Chromatography consumables, In-Vitro Diagnostics, Life Sciences and General Lab Instruments.**

 **Advion Interchim**  
scientific\*

Advion Interchim's nearly three-decade dedication to serving scientists yields customer-focused life science solutions. **Our deep scientific, engineering, and customer workflow knowledge enables an unrivaled solution portfolio.**

Follow Us On



[www.inkarp.co.in](http://www.inkarp.co.in)



Dear Readers,

Most labs today are equipped with excellent instruments, talented teams, and a constant stream of data. But that does not always translate to mastery. This issue is about that difference. The quiet shift from using tools to actually understanding them.

We begin with a topic that seems simple but is often misunderstood – accuracy versus precision. The cover story explores how modern instruments like balances, pipettes, spectrometers, chromatography systems, and thermal analyzers must manage both. Getting the result right is one thing. Getting it consistently right is another.

The next feature unpacks the idea of traceability in measurement. This is not about the instrument, but about the result. A measurement is only traceable when it connects clearly to a global standard, often through a chain of calibration steps linked to SI units. That traceability is what makes your results valid, comparable, and respected across labs and industries.

We also look at WaveMode, a new development from Nanosurf. It offers better force control without complicating the work. It is especially useful for biological surfaces and materials research where too much pressure can damage the sample or skew the data.

Our interviews this time come from two very different directions. Mr. Ben Jeffrey from Radleys explains how listening to chemists shapes their product design. On the other side, Mr. Tushar Jadhav from Manastu Space shows how deep science, when applied with focus, is helping create cleaner propulsion systems for satellites.

The application section is rich and varied. From analyzing fish oil with Bruker FT-NIR to drying apples with BUCHI, from organoid imaging using LICORbio to nanoscale studies using DriveAFM, the articles stay close to lab workflows. We also feature a study on how Sartorius water systems are helping reduce microplastic content in ultrapure water. Flex SWILE is featured under automation. It simplifies sample preparation for NMR and LCMS methods. The system helps reduce human error and keeps your data more consistent, especially when sample volumes are low or repetitive work is involved.

In the Tech Corner, we look at how a pH meter and a balance from Mettler Toledo can be used together. Preparing buffers and measuring them accurately is one of those lab tasks that seems minor, until it is not. This guide is built to help you get it right without trial and error.

We wrap up with four pieces under chromatography. Peptide purification using puriFlash and Advion CMS, separation of epoxides with RotaChrom CPC, a look at reversed phase polymer columns from Shodex, and profiling of oligonucleotide impurities using Waters systems inside GMP environments.

There is no single way to master a lab. But understanding what your instruments are telling you and knowing why they behave the way they do is a good place to start. This issue is built to support that mindset.

Best regards,



**Arun Mathrubootham**  
Director  
Inkarp Instruments Pvt. Ltd.

## Cover Story

01

01 - The Fine Line: Accuracy vs Precision in the Analytical Lab

## Features

05

05 - Metrological Traceability- Consistent Measurement Results

10 - WaveMode: Simple and Fast Imaging with Accurate Force Control

## Interviews

16

16 - Engineering Chemistry's Future: How Radleys Turns Lab Challenges into Innovation

**Mr. Ben Jeffery**

Global Sales Manager, Radleys

21 - Launching Sustainability: Manastu's MS 289 Blasts into Green Space Propulsion

**CEO Tushar Jadhav**

Co-founder of Manastu Space

## Application Showcase

24

24 - Analysis of fish oil by using bruker FT-NIR analyzers

28 - Lyophilisation of Apples with the BUCHI Lyovapor™ L-200

32 - Advancing drug discovery through rapid, high-resolution visualization of organoids and spheroids with LICORbio ATLAS™ IMAGER

38- Exploring nanoscale organization of normal alkanes on HOPG substrate with DriveAFM

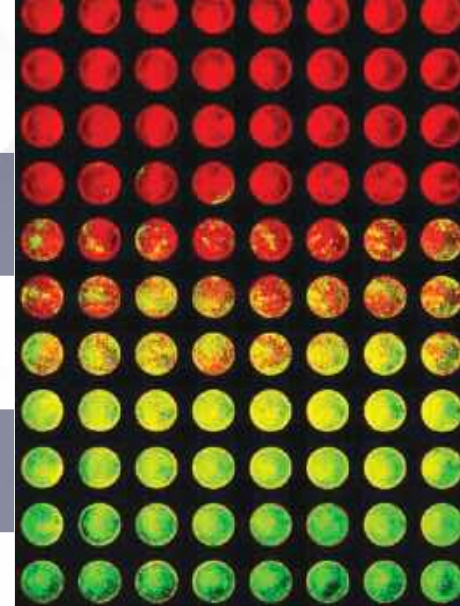
44 - The Role of Sartorius' Lab Water System in Reduction of the microplastic content in ultrapure water

## AI and Automation

NEW

53

53 - Flex SWILE for NMR LCMS sample prep



## Product Highlight

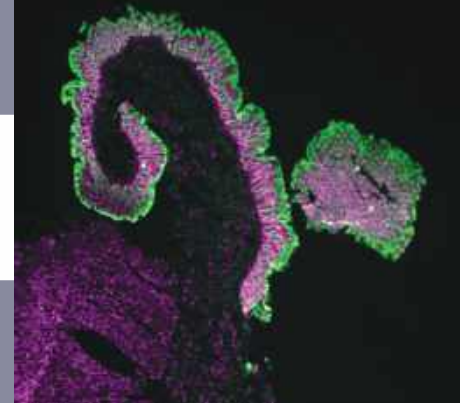
56

56 - Differential Scanning Calorimeter (DSC) NEXTA® DSC series

## Tech Corner

58

58 - Mettler Toledo SevenExcellence™ and MX Balance: Precision-linked pH-balance integration

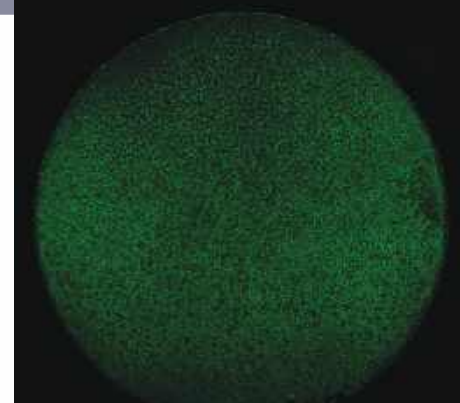


## Advances in Precision Chromatography

NEW

63

63 - Purification Of bioactive peptides from Complex Mixtures using the puriFlash® 5.250 PrepLC and Expression® CMS detector



68 - Preparative separation of diastereomer epoxides Using RotaChrom's Centrifugal Partition Chromatography

71 - Polymer-based Reversed-Phase C18 HPLC Columns for modern applications: Asahipak ODP-50

74 - Robust Oligonucleotide Impurity Profiling in a GMP Setting Using the Waters SQ Detector 2 Mass Detector

## Industry Buzz

81

81 - Pharma updates: Recent novel FDA approved drugs

82 - A sneak-peak at our events

### Editor

Arun Mathrubootham

### Creative Team

Apoorva Nagarajan

Halim Baig

Raju Dasari

### Marketing Team

Venkata Pavan Kumar  
Sanghavi Suresh

# Accuracy vs Precision in the Analytical Lab

In the world of measurement, truth is never absolute. Every scientist knows that no two measurements are ever perfectly identical. Yet, the closer we get to “truth”, the stronger our trust on outcome becomes. This eternal quest for exactitude lies at the heart of analytical chemistry.

In today's laboratories, analytical instruments are not just tools- they are arbiters of reliability. Their ability to measure, quantify and validate defines not only product quality but also scientific credibility. But within this measurement ecosystem lies a subtle tension that has challenged scientists for centuries: the fine line between accuracy and precision.

At first glance, accuracy and precision appear interchangeable - both concern closeness of a measurement. But they represent two very different virtues of good scientific practices in a lab.

## THE BULLS EYE METAPHOR

Imagine targeting a dart board. Darts landing close to each other but far from the center illustrate high precision but low accuracy. Conversely, darts scattered all over the bullseye show poor precision, and only those near the center demonstrate accuracy. The ideal scenario? A cluster on the bullseye—that is both accurate and precise.

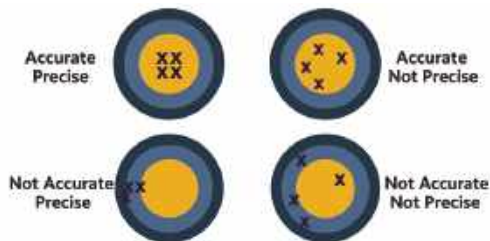
Accuracy refers to closeness to the true value. If a thermometer reads 100 °C when boiling water is truly 100 °C, it's accurate.

Precision, however, refers to repeatability or consistency. A balance that gives 99.9 mg five times in a row may be precise, but if the true value is 100.5 mg, it is not accurate.



In the real world, achieving and maintaining that harmony is one of the greatest analytical challenges!

## Accuracy vs Precision



sciencenotes.org

## THE EVOLUTION OF MEASUREMENT

Historically, measurement was an art even before it became science! Chemists relied on their senses- the shade of a flame, the colour of a precipitate, the viscosity of a liquid- to gauge progress. But with industrialization and the rise of pharmaceutical and chemical manufacturing, empirical judgement gave way to instrumentation.

The analytical revolution began in early 20<sup>th</sup> century with the advent of spectroscopy and chromatography. This ushered in an era where molecules could be separated, detected and quantified with precision, unimaginable to early chemists. Soon followed balances with microgram sensitivity, thermogravimetric analyzers, and spectrophotometers that could resolve minute differences in absorbance.

Today's instruments extend far beyond measurement- they are digital sentinels. Automated calibration, intelligent diagnostics, and AI- assisted data correction have redefined how scientists interpret results. Analytical instruments no longer just produce numbers, they ensure those numbers are trustworthy.

## ANCHORING ACCURACY TO STANDARDS IN METROLOGICAL TRACEABILITY

Accuracy is never a stand-alone idea in measurement science. It can be traced back to a widely accepted reference.

The ability to link a single measurement result to a national or international standard via an uninterrupted series of calibrations, each with its own degree of uncertainty, is the foundation of metrological traceability. It guarantees that one milligram measured in Munich is equivalent to one milligram measured in Mumbai.

This unseen web of trust is essential to all analytical labs. This traceability network is fuelled by certified reference materials, accredited calibration services, and calibrated

When a laboratory reports a value, it is connected to the global definition of that value rather than claiming its own truth.

There are significant ramifications to this interconnectedness. For example, a precise assay of drug potency in pharmaceutical quality control needs to be traceably accurate to international standards in addition to being internally consistent.

This alignment is a silent but crucial victory of global measurement consistency, guaranteeing that drug batches released in one nation meet the same standards in another.

## THE ANALYTICAL ECOSYSTEM

Accuracy arises from a system of measurement rather than from a single instrument. Modern measurement is defined by a variety of instruments, including spectrometers, pipettes, chromatographs, balances, and thermal analysers.

- ▶ The foundation of all analytical work continues to be weighing balances. A mass serves as the starting point for all other measurements in any calibration, solution, or reaction. Measurements down to microgrammes are now possible with remarkable repeatability thanks to developments in temperature compensation, magnetic enclosures.
- ▶ The element of precision in volume control is introduced by pipettes and liquid handling systems. Significant concentration errors can result from even a 1% variation in liquid volume in analytical workflows. Liquid dispensing is now an exact science thanks to digital displays, ergonomic designs, and gravimetric verification.
- ▶ Scientists can measure concentration and purity with high sensitivity using spectroscopic instruments, whether they are UV-Vis, FTIR, or NIR. Beyond big labs, their development into small, self-calibrating instruments has made high-accuracy measurements more accessible to all.

## CONCLUSION

► The mainstays of analytical separation, chromatography systems, have also changed. These devices, which range from manually operated valves to fully automated gradient systems with feedback control, now function as integrated measurement engines and provide unparalleled reproducibility and quantification accuracy.

► Once only used for material testing, thermal analysers are now essential tools for pharmacological and polymer characterisation. The degree to which accuracy and precision are ingrained in contemporary analytical design is demonstrated by the precision of thermogravimetric analysis (TGA) and differential

Together, these instruments create a measurement web – a network where each tool validates the other, collectively ensuring that scientific claims rest on firm, quantifiable ground.

## THE INVISIBLE PARAMETER OF UNCERTAINTY

There is a degree of uncertainty associated with every measurement. Uncertainty is not a weakness; rather, it is a measure of the degree of confidence in a result. Therefore, understanding uncertainty rather than eradicating it is the key to analytical excellence.

International standards like ISO/IEC 17025 are used by accredited analytical labs to express measurement uncertainty. Environmental influences, instrument drift, the calibration chain, and operator handling are all taken into consideration by the uncertainty budget. Labs make their results globally comparable and scientifically tenable by revealing uncertainty.

Uncertainty reporting is a sign of maturity in the context of contemporary analysis. It makes a subtly strong statement of integrity by indicating that the lab not only measures but also comprehends the boundaries of its measurement.

Even as instruments become smarter, one truth remains unchanged – the scientist defines the science.

Accuracy begins not with calibration but with mindset. Every pipette volume, sample mass, or wavelength scan is a promise to uphold reproducibility. Errors can creep in anywhere: improper labelling, contaminated glassware, temperature drift, or even a momentary lapse in concentration. Each of these small human oversights can distort what the instrument records as fact.

That's why analytical training now emphasizes measurement literacy – understanding not just how to operate instruments, but how to critically interpret their data. This shift marks a transition from “button pressing” to data stewardship. The modern analytical chemist is both operator and analyst, ensuring that every value carries the weight of verification.

As laboratories embrace automation, AI-driven analytics, and digital traceability, the definition of accuracy continues to evolve. Tomorrow's analytical instruments will do more than measure — they will interpret, validate, and learn. But their core mission will remain the same: to help scientists see the truth more clearly.

Accuracy, in essence, is not about being right once – it's about being right consistently. It's about creating a shared language of numbers that the world can trust, across labs, borders, and generations.

And in that pursuit, every analyst, every calibration, and every precisely weighed sample plays its part in writing the next chapter of modern measurement.

## ERROR TYPES IMPACTING MEASUREMENTS

Although they are unavoidable, errors can be divided into several categories:

**Systematic Errors (Determinate):** These are caused by defective tools, flawed procedures, or incorrect calibration, and they consistently introduce bias (high or low). Even with extremely accurate measurements, results can be distorted by repeatable systematic errors.

**Random errors (Indeterminate):** Random errors are caused by unpredictable variations in the tools, surroundings, or handling. They reduce precision even though they can be averaged out.

For method validation and quality assurance, it is essential to detect, reduce, and measure both errors.

### Methods of Measurement and Statistical Instruments

Several statistical techniques are used by analytical chemists:

A data set's central tendency and spread are measured by the mean and standard deviation; precision is indicated by close clustering (small deviation).

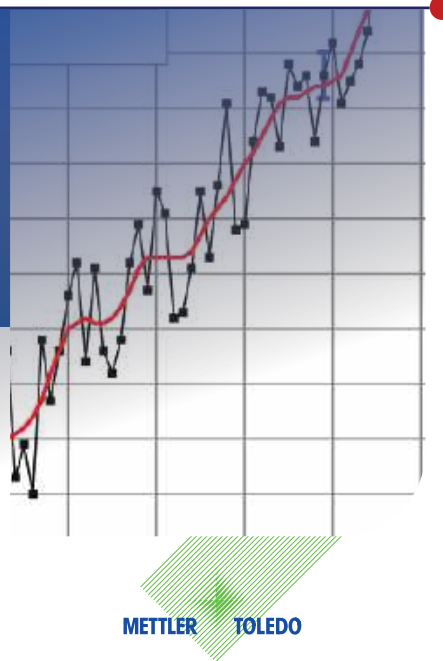
Quantify variability and certainty using the Confidence Interval and **Relative Standard Deviation (RSD)**, which are essential for method comparison.

**Tests for reproducibility, repeatability, and control charts:** Monitor consistency over time and with various operators and instruments.

To guarantee true accuracy and precision, quality control samples and outlier tests like the Q test should be used on a regular basis.

# METROLOGICAL TRACEABILITY

## CONSISTENT MEASUREMENT RESULTS



The international Vocabulary of Metrology (VIM) defines traceability in the context of metrology as:

*Property of a measurement result whereby the result can be related to a reference through a documented unbroken chain of calibrations, each contributing to the measurement uncertainty.*

This definition clarifies some important facts:

- ▶ “Metrological traceability” is a property of a “measurement result”. This means, that, although this is sometimes stated, a measurement device or instrument cannot be “traceable” – it is only a result that is (or is not) traceable.
- ▶ Methods, standards, institutes and measurements are not “traceable”, but are needed to establish traceability of measurement results.
- ▶ Measurement uncertainty is an indispensable prerequisite for metrological traceability. Measurement uncertainty characterizes the dispersion of possible results with respect to the unknown true value with a certain likelihood.

▶ Metrological Traceability is inherited and passed on along an unbroken “traceability chain”, in which, for each link, the measurement uncertainty must be stated. This chain of calibrations starts with the definition of a “reference”, then extends across calibrations of a whole hierarchy of standards, ending at the measurement result, which is finally attributed as being “traceable”.

▶ The “reference” for traceability is the starting point of a measurement unit. Ideally the reference is one of the units of the International System of Units [SI], (Figure 1), but it can also be another agreed reference or reference procedure (e.g. the Rockwell hardness measure). So, a full statement regarding metrological traceability might read “the result is metrologically traceable to the SI”.

▶ Metrological traceability always requires a “reference”. This can be the definition of a unit or a realization of a unit (a “measurement standard” [VIM, 5.1]). According to this definition, an organization cannot be a “reference”. So, statements like “traceable to NIST”, “traceable to PTB” or “traceable to the BIPM” are not valid statements of metrological traceability. Nevertheless, it can be safely assumed that each of these

- ▶ organizations provide measurement results that are metrologically traceable to the SI. Consequently, “metrologically traceable to the SI” would be an appropriate substitute for the above statements.



Figure 1: The International System of Units (SI)

To reliably establish metrological traceability, the following elements are necessary [NIST GMP 13]:

- ▶ A reference (preferably within the International System of Units, the SI)
- ▶ an unbroken chain of calibrations and measurements that refer to the reference
- ▶ measurement uncertainty calculated for every step and passed on to the next step
- ▶ every contributing calibration and measurement must be performed according to a documented and accepted procedure
- ▶ proof of competence of the laboratory executing each procedure, usually given as accreditation of the laboratory for the respective procedure (or a CMC registered at the BIPM)
- ▶ quality assurance of all procedures in place.

Furthermore, it is important to understand that the word “traceability” in many languages (e.g. English, German, French, Italian, Spanish and others) is used for two completely different concepts (=meanings). This is made obvious in ISO 9000 [ISO 9000, 3.6.13, NOTE 2], where it is made clear that while one definition of “traceability” applies in the quality management context, the second definition of traceability (which is the one from the VIM quoted above) applies in the context of metrology, the field of measurements. It is therefore recommended for clarity to use the full term “metrological traceability” (or “measurement traceability”) in these cases.

This is also made clear in NOTE 8 to the VIM definition [VIM]:

“The abbreviated term “traceability” is sometimes used to mean ‘metrological traceability’ as well as other concepts, such as ‘sample traceability’ or ‘document traceability’ or ‘instrument traceability’ or ‘material traceability’, where the history (“trace”) of an item is meant. Therefore, the full term of “metrological traceability” is preferred if there is any risk of confusion.”

## WHAT ARE THE EFFECTS AND BENEFITS OF METROLOGICAL TRACEABILITY?

The effect of metrological traceability is the consistency or comparability [VIM 2.46] of measurement results.

This is especially relevant in the following cases:

### Consistency With Historical Results

A well-known application of this case would be historical climate data. Today it is assumed that temperature measurements over the past >100 years show a significant trend. However, this interpretation of the data is only acceptable if the measurements of the past 100 years truly refer to the same “reference” (i.e. are metrologically traceable), in this case to the agreed temperature unit, Kelvin or degrees Celsius. This is made clear in Figure 2, where temperature values over more than 100 years are given in the

same unit, and uncertainty values are also indicated (blue bars at three data points). With these prerequisites only, a trend is proven to exist.

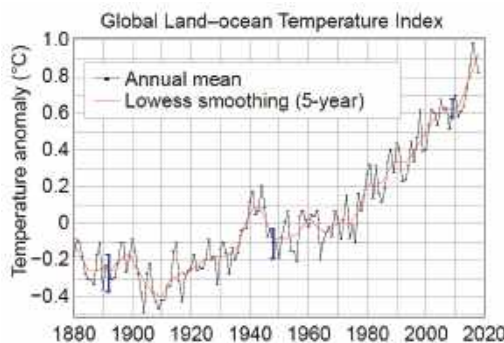


Figure 2: Global Land-ocean Temperature index with uncertainty information (blue uncertainty bars on three points, confidence level 95 %) which prove the non-equality of temperature values over the period under display.

#### Consistency With a Result from a Different Source (Laboratory, Instrument, etc.)

Assume a man-made object with specified dimensions is shipped from a supplier to a plant where an incoming measurement is performed. If the outgoing measurements of the supplier and the incoming measurements of the receiver do not refer to the same "reference" (i.e. are not metrologically traceable), an objective judgement if the object fulfils the specified requirements is impossible.

The same applies if e.g. a balance in a QC laboratory is used to verify measurement results of properties that have been produced with the help of another balance in the production floor.

#### Agreement With a Given Limit

Assume the speedometer of a car does not display the same unit in which the official speed limits are set. If one wants to comply with a given limit, the measurement instrument must display in the same unit as the limit value (i.e. it must be metrologically traceable to the same unit definition). Of course mathematically exact conversions (e.g. from m/s to km/h) do not adversely affect the property of being traceable to a unit.

#### Traceability Ensures Integrity in International Trade

Also, in the field of commercial trade transactions, metrological traceability is an important prerequisite. The International Office of Weights and Measures (BIPM) states:

"Metrological traceability therefore embodies the concepts of measurement uncertainty and calibrations against a hierarchy of reference standards.

Metrological traceability is one of the elements that establishes international confidence in the worldwide equivalence of measurements. The framework described in this document enables legislators, regulators and exporters/importers to take advantage of an international set of mutually supportive systems, which demonstrate equivalence of measurements, thereby significantly reducing technical barriers to trade (TBTs), which might otherwise result from a lack of equivalence." [BIPM]

## IS METROLOGICAL TRACEABILITY A REQUIREMENT?

ISO 9001 [ISO 9001; 7.1.5.2] stipulates metrological traceability (there named "measurement traceability") if it is "a requirement or is considered ... to be an essential part of providing confidence in the validity of measurement results." This condition was added in the 2015 version of the standard and leaves the decision whether metrological traceability is relevant, up to the user.

However, as can be concluded from section 2, non-traceable measurements make no sense: They are not valid because they cannot be used for comparing historical measurements, comparing measurement results from different sources in the short term, comparing measurement results to given specifications or to give limits and tolerances.

So, in all such cases, traceability must be considered essential for the validity of conclusions made upon them.

## HOW CAN METROLOGICAL TRACEABILITY BE ACHIEVED?

In practice, traceability of a measurement result is achieved by:

- ▶ Using measurement instruments which have a calibration certificate from an accredited calibration provider
- ▶ Using the instrument in the calibrated range
- ▶ Using the instrument within its calibration time interval
- ▶ Using the instrument in a competent way that does not adversely affect traceability
- ▶ Using trained and competent staff to make the measurements,
- ▶ Applying an accepted and documented procedure for execution of the measurement
- ▶ Applying quality assurance measures to that procedure
- ▶ Calculating the measurement result and its associated measurement uncertainty according to the given procedure.

It is important to understand that “just having the instrument calibrated by an accredited provider” does not make the measurement results traceable, since this only fulfils the first point of the list above.

## HOW CAN METROLOGICAL TRACEABILITY BE MAINTAINED?

Any calibration result and the associated uncertainty given in a calibration certificate is valid only at the point in time when the calibration is executed. It is therefore a “snapshot” of the actual performance at the time and place of calibration. That means that any change in the performance of the instrument at any point in time after the calibration invalidates the data in the calibration certificate.

To account for this circumstance, it is necessary to calculate an uncertainty in use (of measurement), which is valid throughout the calibration interval.

This is done by considering an additional uncertainty component to the calibration uncertainty. This component accounts for:

- ▶ Differences between the environmental circumstances during calibration and during use
- ▶ Changes of the behavior of the instrument during the calibration interval to come.

### It is obvious that:

- ▶ The longer the interval is, the larger this uncertainty component ought to be
- ▶ The rougher the handling of the instrument is the larger this uncertainty component
- ▶ Any change in the way the instrument is used, must lead to a re-evaluation of the interval or the uncertainty (or both)

A careful evaluation of the factors that might affect the performance of the instrument in use could help optimizing the following parameters:

- ▶ Uncertainty of the measurement result
- ▶ Downtime (time needed for a calibration of the instrument)
- ▶ Calibration interval
- ▶ Risk of falling out of limits during long calibration intervals
- ▶ Direct cost of a calibration.

From this, it becomes clear that this is a multivariate consideration that only the user of the instrument is able to make. Calibration labs are frequently asked for a recommendation for a calibration interval by their customers.

However, this is impossible to state, since all the parameters necessary to decide on a calibration interval are in the responsibility of the user and are unknown to the calibration lab. This is the reason behind the requirement given in [ISO 17025], that a calibration lab shall not normally state a calibration interval. Furthermore, ISO 9001 clearly addresses the management system of the user of the instrument when requiring that measurement equipment shall be calibrated “at specified intervals” [ISO 9001, 7.1.5.2, a)].

It is commonly assumed, but not required, that a calibration interval should be a “time interval”. The texts of the standard documents might also interpret in a way to understand “interval” as e.g. a specific number of uses or an interval measured in “hours in operation”. However, it is a challenging task to monitor this usage aspect and to schedule recalibrations accordingly.

## HOW CAN METROLOGICAL TRACEABILITY BE PROVEN? – THE FEEDBACK LOOP

Setting a calibration interval according to section 5 is based on assumptions of future behaviour of the instrument. An as-found calibration of the instrument at the end of the interval is the prerequisite for a check if these assumptions hold true and were valid and if “maintaining traceability” indeed was effective throughout the interval. This consideration might then lead to either a re-consideration of the next interval or to a re-consideration of the uncertainty assigned to the measurement results during the next interval (or to the confirmation that everything was assumed right).

In this respect, it is especially important that the instrument is first calibrated without making any change to its behaviour. This is called an “as-found calibration” which concludes the past calibration interval. Should any interventions be necessary that might influence the metrological behaviour (e.g. an adjustment, change of parts, cleaning of sensitive elements), another calibration is necessary immediately afterwards. This is called an “as left calibration” which is the starting point of the next calibration interval. Should no intervention be necessary (or not be possible), there is only one calibration which concludes the past and opens the next calibration interval at the same time. Consequently [ISO 17025, section 7.8.4 d)] requires an as-found calibration executed before adjustment or repair “if available”. The exception could be if the instrument is in a state that prevents the calibration or endangers the integrity of the calibration technician or of the calibration equipment.

In this case, the user can face difficulties to prove the traceability of their recent results prior to the damage.

## CONCLUSION

Metrological traceability is a key concept of modern metrology. It assures universal consistency of measurements. Traceability to the International System of Units (SI) as common ground is the preferred basis. Accredited calibration providers have proven their competence and provide metrological traceability. However, more efforts are necessary on the side of the users of all measurement devices to keep traceability maintained once it was established.

## REFERENCES

1. [VIM] JCGM 200:2012: International vocabulary of metrology – Basic and general concepts and associated terms (VIM) 3rd edition
2. [BIPM]: Joint BIPM, OIML, ILAC and ISO declaration on metrological traceability, <https://www.bipm.org/en/news/full-stories/2018-11-quadruplicate.html> [SI] SI-Brochure
3. [NIST GMP 13]: NIST IR 6969, GMP 13, 2008, <https://nvlpubs.nist.gov/nistpubs/ir/2019/NIST.IR.6969-2019.pdf>
4. [ISO 9000]: ISO 9000:2015: International Standardization Organization, 2015, Geneva, Switzerland
5. [ISO 9001]: ISO 9001:2015: International Standardization Organization, 2015, Geneva, Switzerland
6. [ISO 17025]: ISO/IEC 17025:2017: International Standardization Organization, 2015, Geneva, Switzerland
7. [Figure 1]: Graphical representation of the SI. Creative Commons Licence CC BY-ND 4.0; courtesy BIPM, France.
8. [Figure 2]: Land-ocean temperature index, 1880 to present, with base period 1951-1980. The solid black line is the global annual mean and the solid red line is the five-year lowess smooth, i.e. a nonparametric regression analysis that relies on a k-nearest-neighbor model. The function is evaluated using a fraction of data corresponding to a ten year window of data, giving an effective smoothing of approximately five years. The blue uncertaintybars (95% confidence limit) account only for incomplete spatial sampling. This is based upon Fig. 1A in Hansen et al. (2006) and Fig. 9a in Hansen et al. (2010). The graph shows an overall long-term warming trend. NASA Goddard Institute for Space Studies [Public domain]
9. [https://commons.wikimedia.org/wiki/File:Global\\_Temperature\\_Anomaly.svg](https://commons.wikimedia.org/wiki/File:Global_Temperature_Anomaly.svg)

# WAVEMODE: SIMPLE AND FAST IMAGING WITH ACCURATE FORCE CONTROL

The introduction of Nanosurf's CleanDrive technology (Figure 1) enabled the development of novel characterization methods for the DriveAFM

- ▶ *Photothermally excited dynamic mode*
- ▶ *Photothermal torsional resonance imaging*
- ▶ *PicoBalance for mass determination*
- ▶ *High-frequency visco-elastic analysis*
- ▶ *Photothermal off-resonance imaging -WaveMode.*

## WHEN IMAGING IN AFM WE OFTEN WANT TO KNOW: WHAT FORCE ARE WE EXERTING ON THE SAMPLE?

In static mode, we can theoretically control the force precisely. However, this mode has the disadvantage of exerting high lateral forces, which often disturbs the sample. In regular dynamic mode, we minimize these lateral forces but cannot control the force applied to the surface. The only way to get both benefits is force spectroscopy.

Force spectroscopy requires varying the tip-sample distance to acquire a force distance curve at every pixel. Moving the

mass of the entire Z-scanner limits force spectroscopy in speed, as the mechanical motion can excite resonances, cause artefacts and the cantilever holder or the sample to perform the force distance measurement hence vastly increasing the speed, while minimizing lateral forces. This allows us to achieve high imaging speeds with superior resolution and accurate force control. This is beneficial for several applications. On biological samples it allows for gentle imaging conditions. In materials sciences it allows a high reproducibility of experiments as we can control the maximum contact force and do not rely on a damping ratio in a nonlinear system like in dynamic mode.

## AFM IMAGING MODES

The most relevant application of AFM in industry and research is mapping the sample topography. Any AFM-based imaging method relies on a feedback mechanism to track the sample surface. Within the pool of commercially available imaging modes, we typically distinguish between static, off and on-resonant methods. Table 1 compares these three categories regarding their imaging speed limitations, force control capabilities, and susceptibility towards artifacts, or robustness. On-resonance methods, whilst being considered fast, have the disadvantage of not offering precise force

control. Non-linear dynamics in the cantilever response cause shifts in resonance frequency and reduction of amplitude. In classical dynamic mode measurements these effects cannot be separated and hence the interaction force cannot be reconstructed.

Traditional off-resonant methods are characterized by their superior force-control capabilities while usually being limited in speed. These implementations for off-resonant tapping modes utilize the Z-scanner to achieve sinusoidal tip or sample movement. Consequently, the maximum force-distance curve rate is limited by, and typically well below, the AFM Z-scanner resonance frequency (typ. < 8 kHz).

With WaveMode, Nanosurf exceeds this limit by utilizing the photothermal excitation (PTE) method to create a sinusoidal movement of AFM probe itself. In contrast to dynamic mode imaging, the cantilever is excited well below its resonance frequency to avoid nonlinear dynamics effects. Compared to conventional force-distance curve acquisition, the limit of the maximum force-distance curve repetition rate in WaveMode is not set by the Z-scanner resonance frequency but by the cantilever resonance frequency, which is typically in the range of tens to thousands of kHz.

In combination with high-speed electronics acquisition of force-distance curves at rates of > 50 kHz can be achieved. The Wave-Mode NMA technical note will provide additional information about WaveMode based high-speed nanomechanical mapping.

## PHOTOTHERMAL EXCITATION: CLEANDRIVE EXPLAINED

To excite cantilevers photothermally a second laser is required. In the DriveAFM this laser is called the CleanDrive laser. CleanDrive provides major advantages compared to the classical piezo-driven excitation approach: superior stability, a linear amplitude vs. frequency response, and a high excitation bandwidth (up to 8MHz).

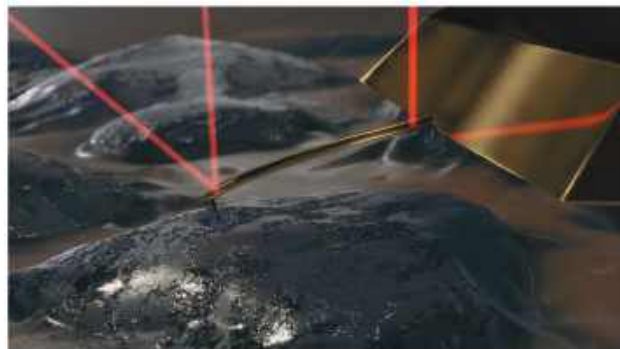


Figure 1. Representation of the CleanDrive setup. As in conventional AFM setups, a laser is focused and aligned to the free end of the cantilever to detect deflection of the cantilever by detecting the reflected beam on the photodetector. For CleanDrive photothermal excitation, a second laser, operating at a different wavelength, is aligned and focused on the base of the cantilever beam. This second laser causes a local heat gradient along the thickness of the cantilever resulting, in combination with the bimetal effect, in bending of the cantilever.

Moreover, it also allows for using a wide range of waveforms to excite the cantilever. CleanDrive relies on the bimetal effect causing a deflection of the cantilever upon local heating by the laser. Therefore, CleanDrive-based imaging methods work best with probes that feature a metallic detector-side coating. To heat the cantilever beam locally, the PTE-laser is aligned to the base of the cantilever (Figure 1), while the readout-laser is located at the probe's free end, measuring the cantilever deflection.

Commercial cantilevers typically feature a metallic reflective coating on the detector side, which is standard in the industry to enhance the cantilever's reflectivity. This pre-existing coating ensures compatibility with CleanDrive excitation without increasing the cost of operation. To facilitate operation of CleanDrive-powered modes, the Nanosurf Studio software offers an automatic laser alignment procedure for both lasers. The only user input required is the cantilever type.

## WAVEMODE

WaveMode uses the CleanDrive laser to oscillate the cantilever sinusoidally. This contrasts with traditional force spectroscopy, which utilizes a triangular motion path.

Limiting the moving parts to just the cantilever allows for up to 100 times higher modulation rates than with traditional

spectroscopy-based force mapping.

Unlike Dynamic Mode imaging, WaveMode operates at frequencies significantly below the cantilever resonance (typically  $\leq 10\%$  of resonance frequency). By comparing two distinct cantilever trajectory curves – one recorded without surface contact (the so called “free wave”) and another during surface interaction – we can correlate deviations between these curves to the forces acting on the sample during imaging.

The measurement process involves recording a reference cantilever trajectory, the “free wave”, while out of contact with the surface. Upon surface engagement, the cantilever deflection profile changes (in-contact wave), resulting in an amplitude reduction. This amplitude reduction serves as the feedback parameter and correlates directly to the tip-sample interaction force.

The tip-sample interaction curve is calculated as the difference between the free wave and the in-contact wave (Figure 2).

Mode	Imaging Speed Limitations	Force Control	Disadvantages	Robustness
Static mode	Limited by AFM hardware	Good force control in aqueous solution	High lateral forces can cause rapid tip degradation and sample dislocation or damage	Depends strongly on stability of setup (drift)
Dynamic mode	Limited by ratio $f_r/Q$	Exact interaction forces very challenging to determine	Possible alternation between repulsive and attractive imaging	Nonlinear behavior, phase instabilities are common
WaveMode	Limited by $0.1*f_r$	Good force control; feedback parameter can be easily linked to interaction force	Requires photothermal excitation laser	Stable excitation and interaction

Table 1: Comparison of common AFM topography imaging modes.

For WaveMode, the only operator input required is the desired imaging force that is then translated to an amplitude reduction.

Other parameters as well as the laser positioning and cantilever calibration are supported by automation routines.

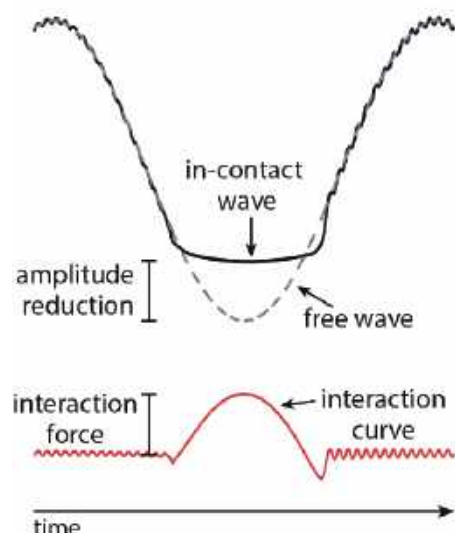


Figure 2. Schematic representation of the signals used in WaveMode imaging. A single oscillation period is shown. The gray dashed line represents the free wave recorded out of contact with the surface. The black line represents the typical deflection profile obtained when in contact with the surface. The amplitude reduction is indicated. The red curve shows a so-called interaction curve that corresponds to the difference between the free wave and the in-contact curve. It illustrates the tip sample interaction force.

## HOW TO CONDUCT A WAVEMODE MEASUREMENT

- ▶ Mount a cantilever and select the respective cantilever type from the Nanosurf Studio cantilever browser.
- ▶ Run the Auto Setup procedure to align the read-out laser as well as the CleanDrive laser. This procedure includes cantilever calibration based on the contact free Sader method.<sup>1</sup>
- ▶ Set the WaveMode excitation frequency in the WaveMode widget of Nanosurf Studio (Figure 3). You have a free choice of excitation frequency, while the highest possible excitation frequency is limited by 10% air and 30% liquid. The Auto button next to the frequency entry field returns a value for the excitation frequency of 7%  $f_0$ , air and 30% liquid with  $f_0$  determined from the thermal noise spectrum. Higher excitation amplitudes allow for faster tapping and

imaging, while lower excitation frequencies enable higher excitation efficiency and larger amplitudes.

- ▶ In the WaveMode widget specify the desired WaveMode Target Amplitude. One can modify this value, and the laser power will be adjusted accordingly. Alternatively, the DC laser power and AC laser power can be manually adjusted in the software. Nanosurf recommends setting an amplitude higher than the highest expected step within the scan area. For clean sinusoidal excitation, the AC laser power should not exceed the DC laser power.
- ▶ For samples with significant adhesion, increasing the amplitude may be necessary. It is critical that the cantilever does not remain in adhesive contact with the surface at the end of each oscillation cycle. Increasing DC and AC laser power and/or decreasing excitation frequency helps to gain larger amplitudes. Manual fine adjustment of the CleanDrive laser spot position on the cantilever can additionally enhance the excitation efficiency.
- ▶ Choose a lift height which is larger or equal to the cantilever deflection amplitude. The Auto button sets the lift height equal to the amplitude.
- ▶ Enter the desired interaction force and approach the surface. For gentle imaging, choose a small contact force which still enables proper topography tracking. Setting larger contact forces enhances the tracking but might lead to faster tip degradation.
- ▶ Before starting imaging go into contact with the surface by setting the idle mode to “z-controller enabled”. Hit the Update button in the WaveMode widget to determine the Free Wave close to the surface. In the WaveMode widget oscilloscope, you should now see the typical WaveMode signals as shown in Figure 2.
- ▶ Decide on imaging parameters. For unknown samples, begin with conservative parameter such as a 1  $\mu\text{m}$  scan

range. When setting the line rate consider that the maximal line rate is determined by the Wave Mode frequency and the points per line.

- ▶ For example:• WaveMode frequency: 15 kHz • Points per line: 500 -> This results in 1000 points for a forward and backward scan. Allow at least 2 oscillations per pixel.  $\text{Max Line Rate} = 15 \text{ kHz} / (2 \cdot 1000) = 7.5 \text{ Hz}$ • A conservative estimate would be a line rate below 5 Hz for 500 x 500 pixel.
- ▶ Enter the desired scan size and line rate and then initiate imaging.
- ▶ Optimize feedback parameters, e.g. the I gain. The Nanosurf Studio software offers a Gain Finder feature that helps finding good imaging conditions. To use this feature, make sure to be in contact with the sample and run the Gain Finder.
- ▶ You can select specific scan areas directly in ViewPort or zoom in on previous scans.
- ▶ The optional ViewPort Plus allows importing reference images or selecting areas of interest from the camera view.

For sequential measurements, the optional Measurement Automation feature enables planning measurement sequences in ViewPort. When recording multiple WaveMode images, the reference wave is updated between images to maintain precise force control.

## CANTILEVER AND PARAMETER SELECTION FOR WAVEMODE IMAGING

Wave Mode, an off-resonance imaging technique, utilizes cantilever actuation via local heating. While various cantilevers can be employed, excitation efficiency varies significantly depending on cantilever type, shape, coating, and spring constant. We have developed specialized cantilevers optimized for WaveMode. These are best used on samples exceeding the following Young's modulus:

WM20PTD: 500 MPa · WM0.8PTD: 50 MPa · WM0.3Al: 10 MPa · WM0.1Au-SS: 5 MPa – 500 MPa These minimal values are conservative estimates; actual limits may be below these values. When setting up Wave Mode, amplitude selection is crucial and depends on cantilever properties, operating environment (air or liquid), sample stiffness, and surface topography. Recommended amplitude guidelines include: Hard inorganic materials:  $A > 10$  nm · Polymers:  $A > 100$  nm · Soft materials: Maximize amplitude Tip-sample adhesion significantly influences amplitude requirements. The selected amplitude must be sufficient to overcome adhesion forces at the conclusion of each oscillation cycle.

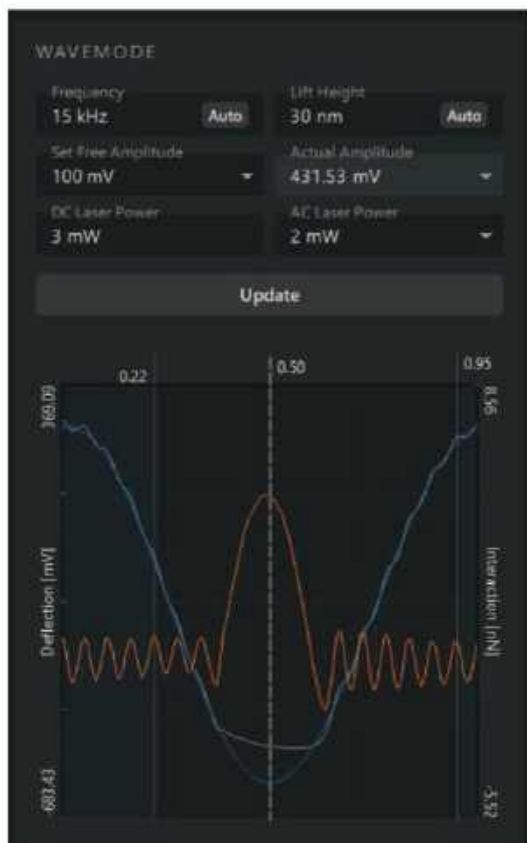


Figure 3. WaveMode widget with the most important WaveMode parameters in the top section and a liveview of the signals relevant for WaveMode imaging in the bottom section: free wave (blue), deflection (white) and the interaction curve (orange).

## A CLOSER LOOK AT THE WAVEMODE

WidgetNanosurf Studio software offers an intuitive interface for controlling the DriveAFM, accommodating both novice and advanced users. Following the completion of alignment and calibration routines, the WaveMode Widget streamlines the configuration of WaveMode operating parameters (Figure 3). This dedicated interface provides convenient access to all essential WaveMode settings:

- ▶ Frequency: WaveMode imaging can be performed with cantilever oscillation frequencies ranging from 200 Hz up to approximately 10% of your probe's resonance frequency. The Auto button determines a safe upper Frequency value based on the cantilever resonance frequency.
- ▶ Lift Height and Update button: For stable feedback and perfect force-control, WaveMode relies on the out-of-contact cantilever trajectory, known as the free wave. Pressing the Update button retracts the cantilever by the specified Lift Height and updates the free wave accordingly. A lift height that ensures free sinusoidal oscillation of the cantilever is mandatory. The Auto button sets the Lift Height value based on the free amplitude.
- ▶ Target Amplitude and Actual Amplitude: Enter the desired cantilever oscillation amplitude in the Target Amplitude field. Upon confirming the entry, the laser power will be adjusted to reach the desired amplitude. The Actual Amplitude field reports the current cantilever oscillation amplitude. This field cannot be edited.
- ▶ DC and AC Laser Power: DC and AC laser power of the CleanDrive laser can be manually adjusted to change the oscillation amplitude according to your needs.

The Play button in the Target Amplitude field adjusts the laser power to achieve the desired target amplitude (in nm). In Operation, you can observe the most relevant signals live in the integrated oscilloscope:

In Operation, you can observe the most relevant signals live in the integrated oscilloscope:

- ▶ **Free Wave (blue):** Displays the probe deflection trajectory without interaction force. This curve can be refreshed by clicking the Update button.
- ▶ **Deflection (white):** Shows the current cantilever deflection trajectory.
- ▶ **Interaction (orange):** The actual tipsample interaction signal i.e., the difference between the Free Wave and Deflection signals.

The interaction signal can be translated into a force-distance-curve. Hence, WaveMode offers the capability of high-speed force-mapping for nanomechanical analysis (NMA). This subject will be covered in separate application note.

## SUMMARY

WaveMode, powered by Nanosurf's CleanDrive technology, represents a significant advancement in AFM by combining precise force control with ease of use. This innovative mode minimizes lateral forces, making it ideal for both biological and materials science applications. The integration of CleanDrive technology ensures superior stability and a linear amplitude vs. frequency response, enhancing the overall imaging process. The full motorization of the Drive AFM paired with the user-friendly Nanosurf Studio software and its automation features significantly simplifies operation, making WaveMode accessible to both novice and experienced users. Overall, WaveMode offers a versatile and efficient solution for achieving reproducible and high-quality imaging results across a wide range of surfaces and applications.

## REFERENCES

- 1) J. E. Sader et al., *Review of Scientific Instruments*, 70, 3967 (1999).

 **nanosurf**

## DriveAFM





## Mr. Ben Jeffery

Global Sales Manager, Radleys

# Engineering Chemistry's Future: How Radleys Turns Lab Challenges into Innovation

**“** I joined Radleys in 2007 as a Technical Sales Specialist, my job has changed over the years through Product Management, UK Sales Manager, and International Territory Manager for Europe, Russia and Africa. I am now the Global Sales Manager, responsible for both the UK and International sales teams and business.

Radleys have a huge variety of customers and applications, from small gin distilleries to huge pharmaceutical research labs, this keeps customer visits and my job fascinating.

I often work with customers and distributors on projects and designs over several years, it's great to see these through from a pencil sketch in a lab, to design, then installation and support many years on.

I really enjoy sharing ideas or problem solving, I get to see such a huge range of laboratories and equipment around the world, that I can often bring some fresh ideas to the table or bench. **”**



## Radleys' Commitment to Innovation:

*Can you share with us the driving force behind Radleys' continuous commitment to innovation in the chemistry research field?*

At Radleys, our drive for innovation comes directly from our customers, scientists working to solve some of the world's biggest challenges. Whether it's pharmaceutical development, material synthesis, or sustainable chemistry, their work demands better tools, more reliability, and greater control. Ever since the development of the Carousel 12 with GSK in the early 90's, we've been working closely with customers to design equipment that makes chemistry safer, cleaner, greener, and more productive. "We don't innovate for the sake of it, we innovate with purpose, inspired by real-world lab challenges." From pencil sketches of small pieces of scientific glassware at the bench to large, automated reaction vessels, we thrive on turning ideas into tangible lab solutions.

*What are the core guiding principles behind Radleys' product design philosophy?*

We want to design innovative chemistry equipment for safer, cleaner, greener and more productive chemical research. These core principles will always be at the heart of our product design. If we get this right, it will help accelerate our customers R&D efforts, helping scientists develop and discover new things.

*Innovation often comes with challenges. What are some of the key considerations Radleys considers when developing new and innovative products for chemistry research?*

Every product must earn its place in the lab by solving genuine challenges and adding real value. We focus on creating tools that make a meaningful difference for chemists and help build lasting partnerships with users and organisations.

Developing great ideas is never simple, but prioritising which ones to move forward with can be just as tough. That's why

our R&D product roadmap is driven by the voice of the customer. We log every idea and piece of feedback to build a clear picture of what matters most.

Our technical specialists and engineers all have real-world chemistry experience, so they truly understand the daily realities of lab work. This ensures our products solve real problems, not theoretical ones.

**“You can see this approach in our latest innovation, AVA Pad, it's a compact, subscription-free controller that brings effortless automation to any jacketed lab reactor. Designed by chemists for chemists, it connects directly to circulators, stirrers, pumps, and sensors, providing full control and data logging from one touchscreen. It's powerful, intuitive, and affordable, simplifying complex chemistry while delivering precise, safe, and reproducible results.”**



## Core Applications of Radleys Products:

*The Mya 4 Reaction Station is one of the key products. Can you elaborate on how it enables precise control and optimization of chemical reactions, particularly for industries focused on drug discovery, material synthesis, and process development?*

Yes, the Mya 4 is one of our flagship products. With independent control of temperature and stirring across four reaction zones, it enables parallel experimentation under tightly controlled conditions. That means faster reaction optimisation, more reproducible data, and more robust scale-up.

In drug discovery, it supports high-throughput screening. In process development, it builds confidence before scaling up. And across all sectors, it allows scientists to do more, learn faster, and waste less. It's a really flexible workstation allowing you to quickly adapt to changing project demands, in seconds you can switch from a small scale synthesis in vials to a 250ml reactor with overhead stirring. This flexibility combined with precise temperature control and active cooling makes it a great tool for any development lab.

*Can you talk about how the Carousel Reaction Stations help pharmaceutical and chemical researchers streamline their workflows, especially when conducting simultaneous experiments?*

Put very simply the Carousel allows you to heat and stir multiple reactions on a single hotplate with a reflux condenser under inert gas. Understanding how this can help researchers really comes down to considering how you would do this work without a Carousel. Your only option would be multiple hotplates with multiple glass condensers, inert gas manifolds, flasks, clamps, Keck clips, tubing etc. The setup of 12 of these would take ages, and would be really tough to get reproducible results from. The Carousel takes away all the pain of those setups, making it faster and easier to setup reactions and saving a huge amount of space. In addition to saving space and time, because they are all on one hotplate

you can be sure that they will all be stirring at the same speed and at the same temperature.

*How does Radleys Reactor-Ready Pilot system help in scaling up from R&D to production, particularly in industries like pharmaceuticals and chemicals?*

Our whole Reactor-Ready range is designed to be flexible and modular. A chemist can quickly change a reactor say from 5L to 20L in minutes rather than hours, without the need for any tools or an engineer. This means you can use one framework for multiple vessel sizes, this saves a lot of space, time and money. Our benchtop system will allow reactors from 100ml to 5L and the Pilot floor standing system can accept from 5L up to a 35L vessel, they all have similar geometry to optimise mixing and be similar to production reactors. Scalable, reproducible results with robust process data when paired with our AVA lab software.

Occasionally it can be the small things that really help people, I remember talking to one customer who said to exchange a vessel stirrer paddle in their existing system took them weeks because they had to fly an engineer in, when they saw how quickly you could change a stirrer paddle in one of our systems without any tools they were keen to get more details.



## Reactor-Ready™ Flex Lab Reactor



## Mya 4 Reaction Station

*Environmental sustainability is increasingly important. Can you discuss the role of the Findenser Air Condenser in eliminating water usage while maintaining consistent temperature control?*

We developed Findenser in conjunction with AstraZeneca, one of their sites was using huge amount of mains water for cooling glass lab condensers. For this particular site it wasn't only the cost of the water supply, but also the cost of treatment. The Findenser replaces traditional water condensers and doesn't use any water or electricity, clearly a big money saving benefit, but also important from a sustainability perspective. Essentially the design utilises a finned aluminium jacket around a custom glass column, both the jacket and column have lots of surface area to it is able to radiate heat really efficiently and replace a water condenser in most reaction reflux situations.

When we launched the product we thought the money saving and environmental impacts would be the key drivers, but as we discussed it with more and more users we found out that one of the biggest issues with traditional water condensers is actually lab flooding when a hose fails or comes off when water pressure changes. You'd be amazed at the number of cutting edge research labs who use condensers with really old tubing, it's easy to cause a huge amount of damage especially when running overnight. Findenser avoids this issue all together, no tubing, no water connections.

## Practical Success Stories:

*Could you share some success stories where Radleys' products have significantly improved operational efficiency or productivity in pharmaceutical, agrochemical, or research labs?*

One that immediately comes to mind is Purolite. They faced some serious challenges scaling up one of their processes from small scale development through to production. On a large scale, they use jacketed reactors. However, their small-scale experiments were done in water or oil baths, giving them poor temperature control with wide batch variations. Their small-scale studies weren't representative of what would happen in process vessels, meaning scale up often involved reworking of formulations.

Consistency of results and scalability to pilot plant scale was key, including the ability to maintain a constant process temperature for exothermic and endothermic reactions. They were also very keen to reduce the minimum batch scale due to limited availability of some of the biomolecules at the R&D stage. As the resin beads are sensitive to grinding, overhead stirring was a prerequisite.

Within a few weeks of being installed the Mya 4 was already making a huge difference in the lab. Used every day for R&D work, Mya 4 enables projects Purolite could not do before. Experiments are now directly scalable to pilot plant scale but also performed in smaller batches, which means less cost and less waste. Process development work is much faster, with multiple temperature profiles run independently.





## Growth and Competition in the Indian Market:

*From your perspective, Ben, what are the most significant opportunities for Radleys in the Indian market moving forward?*

The Generics and CRO markets in India are really interesting for us. The fast changing projects and requirements in these development labs suit our products perfectly. You can see how in a contract lab being able to quickly flex or adapt your reactor from one project to the next really helps speed up workflow and deliver projects on budget and on time. Mya 4 and Reactor Ready are two of our most successful products and they fit into this environment perfectly.

*Given the competitive landscape in India for laboratory equipment how do Radleys differentiate themselves?*

Radleys has glassblowing at its heart, all of our products include glass that we manufacture in house. This combination of glassblowing and technical expertise is really what makes us unique, you have a team of tremendously skilled glassblowers working closely with a team of chemists and engineers to deliver great products. I feel like this is reflected by the customers who choose to use Radleys equipment in their labs, we are trusted by the world's leading pharma companies and have equipment in major sites all over the world, including India.



## 25 Years of Association with Inkarp

*We have been proud to distribute Radleys products for so long. Could you share how Radleys views the value of this enduring relationship with Inkarp?*

Inkarp have been more than a distributor, they've been an extension of Radleys in India. Their market knowledge, technical support capability, and commitment to long-term relationships mirror our own values. Thanks to Inkarp, Radleys equipment is trusted and used in labs across India, from government institutes to global pharma companies. We're proud of this relationship and excited about what we'll achieve together in the future. This year marks 25 years of cooperation between Radleys and Inkarp, I'm excited to see what the next 25 years will hold!





**Mr. Tushar Jadav**

Co-Founder & CEO,  
Manastu Space

*In the fast-evolving landscape of India's private space sector, Manastu Space stands out for its mission to make satellite propulsion cleaner, safer, and more sustainable. From replacing hydrazine with their proprietary green propellant MS 289 to developing catalysts and propulsion systems in-house, the company represents a complete, systems-driven approach to innovation.*

*In this two-part interview, CATALYSTCue speaks with Mr. Tushar Jadhav, CEO & Co-founder of Manastu Space, on building a green propulsion ecosystem, followed by an in-depth conversation with Ms. Sivakami Senthil, Head of Propellant Department, and Mr. Henry Sam, Head of Catalyst Department. Together, they take us behind the scenes of India's first indigenous green propulsion system, sharing insights into the chemistry, engineering, and perseverance that fuel their journey.*



# Launching Sustainability: Manastu's MS 289 Thrusts into Green Space Propulsion

***Let's start with your background and how Manastu Space began.***

Sure. I'm from Nashik, about 150 kilometres from Mumbai. I did my schooling there and then joined IIT Bombay for aerospace engineering. After graduating in 2014, I joined DRDO in Bangalore as a scientist, working on jet engines for cruise missiles and fighter planes for around two years. The journey towards Manastu really began during my time at IIT Bombay. I was part of the IIT Bombay Student Satellite project — first as a team member, then as project manager. We worked closely with ISRO, handling everything from design reviews to budget management. It was completely student-led, so we had to motivate and lead the team without any formal incentives.

That experience taught us a lot about leadership, team management, and perseverance. After multiple iterations and learning from setbacks, our student satellite launched on an ISRO PSLV in 2016 — a dream-come-true moment. That was when we realised this is what we wanted to dedicate our lives to.

In 2017, we officially founded Manastu Space, starting as a small team inside IIT Bombay. Early years were challenging — private space initiatives weren't fully allowed in India and investors were sceptical. But as government policies evolved, especially around 2020, we began attracting more talent, investment, and interest from potential customers.

***That's an inspiring journey. It's clear your early experiences shaped both your technical and leadership approach. With that foundation, how did you shape Manastu's propulsion vision?***

At Manastu, we see sustainability in space as critical. It's not just about exploration — it's about building safe, efficient and long-term infrastructure.

Our first focus was replacing hydrazine, the highly toxic fuel traditionally used in satellites. We developed a green propulsion system — safer, higher performing, and more cost-efficient. Beyond that, we're exploring other technologies and variants to create a full-stack propulsion ecosystem.

***I'm curious about the strategy behind tackling the entire stack — from catalyst to fuel to delivery?***

The key insight was customer value. Customers don't care about individual components; they want a complete, reliable solution. If you solve only part of the problem, other gaps remain.

So we innovated across the entire propulsion stack, ensuring sustainability, performance, and safety all work together to deliver real, measurable value — whether it's saving time, reducing cost, or improving mission reliability.

***That's a strong differentiator. How does this set Manastu apart from other propulsion startups in India or globally?***

Technology matters, but what really counts is the value it provides. Our system offers higher performance — think of it like better "mileage" for satellites — while keeping costs low. Safety is another differentiator: by replacing toxic fuels, we reduce operational risks on the ground.

***Combined, these factors translate into tangible benefits for customers in cost, time, and safety — that's where we stand out.***

***Speaking of tangible products, can you tell us about the I-Booster system?***

The I-Booster is a propulsion system for 100–150 kg class satellites, enabling precise manoeuvring and orbital adjustments. Part of its development was funded by DRDO's Technology Development Fund (TDF), and we've completed development and delivered the system to them. The next step is to demonstrate it in space. We see the I-Booster as one of our flagship products — a green, high-performance solution for 100–500 kg satellites.

***And the propellant used in iBooster is MS-289, correct?***

Yes. MS-289 is our in-house developed propellant. We innovated this because there were no commercially available catalysts or fuels that met our performance and safety requirements. The development was necessary to achieve our sustainability and performance goals.

Sustainability here primarily means reducing toxicity. Hydrazine is carcinogenic; MS-289 is much safer to handle

and transport. It also produces mostly water vapour as exhaust, which adds an environmental benefit.

**Beyond products, your journey has included strategic milestones. Could you highlight some key ones?**

Certainly. Some major milestones include:

- ▶ 2018: First significant grant (~₹25 lakh) from Tata, DST and Lockheed Martin; won a few global competitions.
- ▶ 2020: First contract from DRDO for defence satellite systems — crucial support during COVID.
- ▶ 2021: First small angel investment.
- ▶ 2023: First major investment (~\$3 million).
- ▶ Dec 2024: Launched our first system in space and delivered it to DRDO.
- ▶ Recently: Raised \$3 million in a VC firm, Capital-A.

Each milestone marked growth and validation, both technically and commercially.

**How did COVID impact your operations, and how did you respond?**

COVID hit everyone hard. Our labs and operations shut down, and without hardware a space startup can't function. Funds were tight, but we focused on resilience and innovation. We used the downtime for literature review, planning and advisory consultations, and we developed some COVID-related products — like a conveyor belt with UV sanitisation deployed in hospitals and government facilities. We completed NABL certifications for those products as well.

**So you really leveraged brainpower and manpower to put resources to good use?**

Exactly. That period reinforced our resilience and strengthened the team.

**Looking ahead, what's next for Manastu beyond green propulsion systems?**

Apart from green propulsion, we're working on a few important products and applications in space. These haven't been announced yet, but they focus on creating real customer value. We're figuring out commercialization plans and hope to share details soon.

**Can you throw light on your collaboration with Dhruva Space?**

We're working with Dhruva Space to fly our products into space for testing, which is crucial for establishing product heritage and proving reliability in space conditions.

**How do you see the broader future of green propulsion in India and globally?**

The sector is booming in India, especially in Mumbai, Bangalore, Hyderabad and Chennai. Sustainability should move beyond buzzwords — it must deliver real value: safety, performance and cost benefits.

We like to believe Manastu Space is the future. The industry is evolving, and practical, high-performance green propulsion will play a central role in the next generation of space technology.

*From vision to leadership, Tushar's journey shows how Manastu Space turned a student project into a green-propulsion pioneer. In part -II of this interview, we go behind the scenes with the development team — the core technical talent building the catalysts, propellants and systems that bring India's clean space propulsion to life.*

*His co-founding partner, CTO Ashtesh Kumar, drives the technical wheel right from their college days in aerospace labs to now knocking global space doors of space propulsion.*

## World's safest, agile and most efficient GREEN PROPULSION SYSTEM

## The top-of-the-line benchtop NMR

The highest field available.

Easy-to-use and low maintenance.

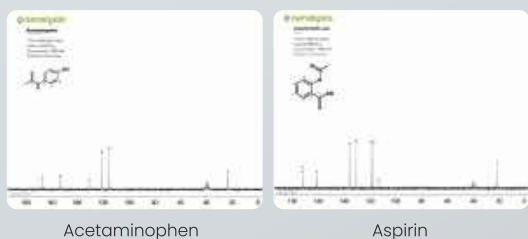
## Nuclei:

$^1\text{H}$ / $^{19}\text{F}$ ,  $^1\text{H}$ / $^{19}\text{F}$ / $^{13}\text{C}$ ,  $^1\text{H}$ / $^{19}\text{F}$ / $^{7}\text{Li}$ ,  $^1\text{H}$ / $^{19}\text{F}$ / $^{31}\text{P}$ , etc.

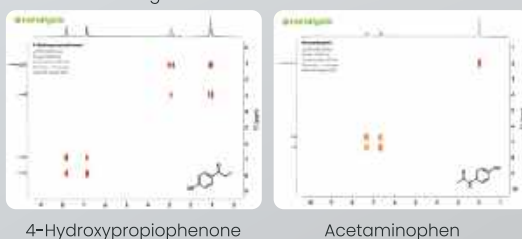
## Technical Specifications

Parameter	Nanalysis-100
Operating Frequency	100 MHz (2.35 T)
Resolution (LW 50%)	< 0.5 Hz (< 0.005 ppm)
Resolution (LW 0.55%)	< 10 Hz (< 0.10 ppm)
Sensitivity (1% Ethylbenzene, 1 scan)	> 250:1 single channel > 220:1 dual channel
Screen size and resolution	15.6", 16:9, 1920 x 1080
Magnet	Permanent, no cryogens
User Interface	Built-in touchscreen and optional remote access. Connectable to external computer if desired.
Nuclei	$^1\text{H}$ / $^{19}\text{F}$ , $^1\text{H}$ / $^7\text{Li}$ / $^{13}\text{C}$ , $^1\text{H}$ / $^{19}\text{F}$ / $^{31}\text{P}$ Please inquire about custom options.
Lock	Internal $^1\text{H}$ and $^2\text{H}$ options
Sample	Standard 5 mm NMR tubes, optional flow cell
Compatibility	File: JCAMP-DX, and CSV Software: Mnova, ACD/Labs, Delta, TopSpin, MATLAB, SpinIt, NMRfx, etc.
Stray Field	< 2 Gauss line outside the enclosure
Operating Temperature	18 – 26 °C

## Example Spectra $^{13}\text{C}$ – 100 MHz



## $^1\text{H}$ COSY – 100 MHz



## Nanalysis-100

Benchtop NMR  
Spectrometer



A close-up photograph of numerous fish oil capsules scattered on a dark, wooden surface. The capsules are translucent with a golden-yellow tint, reflecting light and showing some internal texture. The lighting is dramatic, highlighting the reflective surfaces of the capsules against the dark background.

# Analysis of Fish Oil by using Bruker FT-NIR analyzers

---

Fast-tracking quality assessment in omega-3 production lines.

**M**arine oils are the main source of polyunsaturated Omega-3 fatty acids. Especially EPA (Eicosapentaenoic Acid) and DHA (Docosahexaenoic Acid) are known to be highly beneficial to human health. Since the body is not able to produce Omega-3 fatty acids on its own, it is essential to supplement our diet with DHA, EPA and other valuable unsaturated fatty acids.

### Keywords or phrases:

**FT-NIR Fish Oil Analysis, Omega-3 (EPA/DHA Quantification, Real-Time Quality Control in Marine Oils, Non-Destructive Multi-Component Spectroscopy, Pharma-Grade Omega-3 Validation (USP/PhEur), Bruker FT-NIR Process and Lab Analyzers**

## INTRODUCTION

Omega-3 fatty acids are mostly found in oily fish such as salmon, mackerel, sardines and anchovies. To efficiently separate the Omega-3 fatty acids from the remaining lipids is the most important step in producing high quality fish oil for use in dietary supplements and food products. Here a close control of the process by analyzing the fractions at different stages is important. Moreover, pharma-grade Omega-3 oils need to meet a number of strict purity parameters before being released.

### Advantages of FT-NIR for Fish Oil Analysis

The traditional analyses are generally carried out using standardized chemical and physical methods. However, these methods are often designed for the analysis of only one specific parameter and tend to be tedious, time consuming, expensive and often require hazardous solvents and reagents.

Near infrared (NIR) spectroscopy, on the other hand, is fast (analysis time of the order of less than 1 minute) and can

analysis multi-components with only one measurement. In addition, it is a non-destructive method without any sample preparation and does not require the use of any solvents or reagents. FT-NIR easily allows performing precise real time analysis resulting in huge time and cost savings.

Bruker Optics rugged FT-NIR analyzers for quality control in the lab or production area are easy to use, rugged and reliable.

### Dedicated parameters for Fish Oil commonly analyzed with FT-NIR:

- ▶ No solid stationary phase required
- ▶ Gentle separation technique
- ▶ Wide compound compatibility
- ▶ Multiple operating modes available (ascending, descending, dual-mode)
- ▶ Flexible method development
- ▶ Stable on both acidic and basic pH values

### Benefits of FT-NIR Spectroscopy

- ▶ No sample preparation
- ▶ Sample simply filled in a vial
- ▶ Simple to operate user interface
- ▶ Fast, non-destructive analysis in less than a minute
- ▶ Simultaneous determination of multiple components per measurement
- ▶ No waste, no use of solvents, reagents or gases
- ▶ Highly precise and accurate
- ▶ Direct calibration transfer between instruments

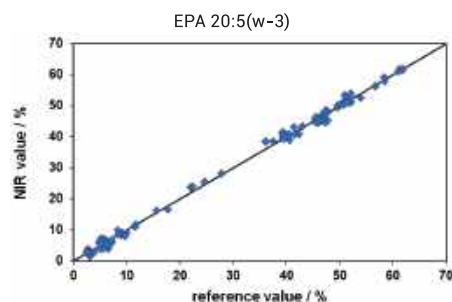
### Quality Assurance in a Validated Environment

To ensure that pharma-grade fish oils and Omega-3 fatty acids meet the strict quality parameters before their release, it is essential to carry out a completely traceable analysis according to GLP.

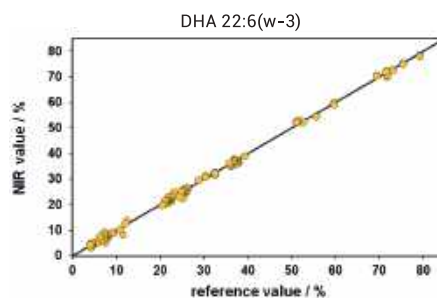
Bruker Optics spectrometers can be fully validated according to US Pharmacopeia and PhEur. The operating software supports Operational Qualification (OQ) and Performance Qualification (PQ) as well as full traceability according to 21 CFR Part 11.

Dedicated validation manuals containing a complete documentation of the hard -and software performance are available on request.

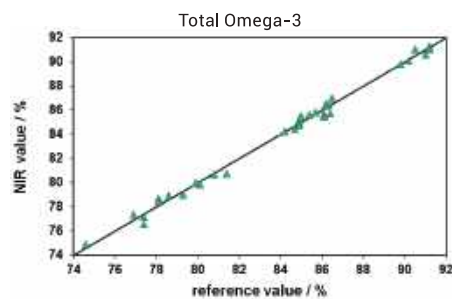
- ▶ OPUS Validation Program for OQ/PQ qualification
- ▶ Qualification according to USP<1119> and PhEur 2.2.40 with certified standards Internal
- ▶ Validation Unit for automatic PQ tests.
- ▶ Validation manual with complete qualification documentation for hard- and software.
- ▶ Compliance with 21 CFR Part 11 Secure, time-stamped audit trails



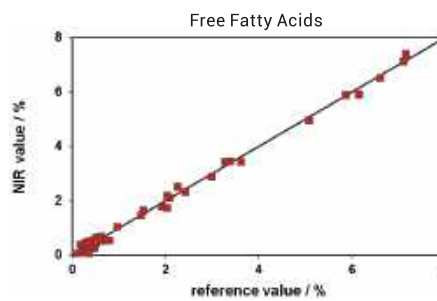
Validation results of EPA with a standard error of 1.1% over a range from 2 - 62%.



Validation results of DHA with a standard error of 0.9% over a range from 3 - 79%.



Validation results of total Omega-3 with a standard error of 0.3% over a range from 75 - 91%.



Validation results of FFA with a standard error of 0.1% over a range from 0.1 - 7.2%.

FT-NIR Spectrometer

## TANGO II

*Measure faster. Work smarter.*



FT-NIR Spectrometer

## MPA III

*FT-NIR Multi Purpose Analyzer*



FT-NIR Spectrometer

## MATRIX-F II

*Keeping an eye on your process*





# Lyophilisation of Apples with the BUCHI Lyovapor™ L-200

---

Optimizing lyophilisation to preserve apple taste, texture, and quality.

Preservation of seasonal fruits for long-term consumption, storage by freeze drying is a common approach aiming on maintaining the original taste, appearance, texture. Here, we developed a freeze-drying method with optimized process time and residual moisture content for apples.

### Keywords or phrases:

Freeze drying, Lyophilisation, Moisture analysis, Aroma retention, Apple preservation, Sublimation process

## INTRODUCTION

The taste of apples is partly determined by the biogenesis of numerous volatile<sup>1</sup> compounds. More than 300 compounds from various crops of apples have been identified as aromatics. However, only a few compounds emitted from apples have been determined to have a decisive impact on sensory quality, so they have been designated as impact compounds in apples.

A considerable portion of these compounds can evaporate during the drying process, resulting in bad taste, which varies between different drying methods and conditions. Quantitative knowledge of the losses of aromatic compounds during drying fruits is also essential to improve the recovery of substances in various commercial activities. Several factors influence the retention of aroma, including the vapour pressure of each compound, its relative volatility, the drying temperature, and the composition of the food product.

Conventional drying methods such as hot air drying, vacuum oven drying, and sun drying, have the disadvantages of reducing the quality and taste of the original food due to loss

of heat-sensitive substances, long drying time depending on weather conditions, and sterility issues<sup>2</sup>. On the other hand, freeze drying is one of the most sophisticated dehydration methods. Freeze drying is a gentle way to remove moisture without disturbing the internal structure of the sample.

Freeze drying is a sublimation process where solid particle is directly converted into vapour form without coming into liquid form. Another important advantage is that freeze drying is accomplished at relatively low temperatures at which fragile compounds are preserved.

Freeze-dried foods are mainly considered of higher quality than other dehydrated products because they can be reconstituted rapidly to products that closely resemble the original taste.

It provides dried products of porous structure, no shrinkage, retention of morphology, superior taste retention<sup>3</sup>, surface area, high yield, long shelf life, high viability, weight reduction, the possibility of sterile handling and better rehydration properties. However, its advantages are directly weighed against its associated high treatment cost.

## EQUIPMENT

- ▶ BUCHI Lyovapor™ L-200 Pro.
- ▶ BUCHI Lyovapor™ Software.
- ▶ Vacuum pump Pfeiffer Duo 6”.
- ▶ Heated Shelves.
- ▶ Stainless Steel trays.
- ▶ Freezer -40 °C – Haier.
- ▶ Balance – Mettler Toledo.
- ▶ Karl Fischer titrator moisture analyzer – Mettler Toledo.

## MATERIALS

- ▶ Fresh red apples, purchased from a local supermarket.
- ▶ Knife.
- ▶ Lime juice with water.

## EXPERIMENTAL

### Sample preparation

Apples contain high levels of an enzyme called polyphenol oxidase. When an apple is sliced open, the cells are ruptured. With the help of oxygen in the air around damaged cells, polyphenol oxidase initiates a series of chemical reactions, transforming polyphenols and eventually forming melanin-brown pigments<sup>5</sup>. Lemon contains ascorbic acid, which not only reduces pH (as does the citric acid also found in lemons) but also the oxidative reaction can be reversed by reduction. The brown colour can't be avoided completely, but it had a better appearance than un used one.

Apples have been cut into pieces approximately 3 mm in width and soaked in lemon juice water for 10 minutes and placed into a tray.

The sample temperature sensor is placed in apple slices to monitor the sample temperature during the freeze drying process. The product trays are kept in deep freezer for overnight freezing at a temperature of -30 °C.

### Lyovapor™ L-200 settings

After 12 hours of deep freezing, the slices were completely frozen. The frozen trays and frozen shelf have been transferred into the Lyovapor L-200 instrument with a PMMA drying chamber at ambient pressure.

The set method was designed considering the critical parameters such as triple temperature at -5 °C, triple point pressure at 0.5 mbar and critical temperature at 55 °C<sup>4</sup>.

The freeze drying process was initiated with the loading step at which shelf temperature needs to be set, e.g. -25 °C due to the freezing in the freezer. By keeping the shelf at the same temperature as samples, sample melting due to heat transfer will be minimized and even drying can be ensured. In the drying process, the shelf temperature was gradually increased from -10 °C to 40 °C to facilitate the sublimation of water from the sample. To keep with the optimal sublimation

and prevent the collapse of the sample, the pressure was maintained at a constant level of 0.300 mbar throughout the primary drying process.

In the secondary drying phase, the pressure was minimized to achieve a low moisture content in the final product. This step is critical to achieve the stability and product shelf life by removing any residual moisture by desorption that could cause degradation or spoilage over time. Details can be found in Figure 2.

During this run, the Lyovapor monitoring app is used as an assisting tool to monitor the overnight lyophilization process. The app helps to keep a close check on the progress of the process and promptly alerts the user in case of any discrepancies in set parameters.

Step	1	2	3	4	5	6
Phase	Loading	Primary drying	Primary drying	Primary drying	Secondary drying	Secondary drying
Duration	0:00	0:00	0:00	0:00	0:00	0:00
Shelf temperature	-25	-10	0	10	20	30
Shelf temperature gradient	0.5 °C/min	0.5 °C/min	0.5 °C/min	0.5 °C/min	0.5 °C/min	0.5 °C/min
Pressure zone	Guaranteed	Recommended	Recommended	Recommended	Maximize	Maximize
Pressure	0.300	0.300	0.300	0.300	0.050	0.050
Safety pressure limit	0.300	0.300	0.300	0.300	0.050	0.050
Safety pressure duration	10 sec	10	10	10	10	10

Figure 1: Parameters of the primary and secondary drying phase set on the Lyovapor™ Software.

## RESULT AND DISCUSSION

### Run Data Plot

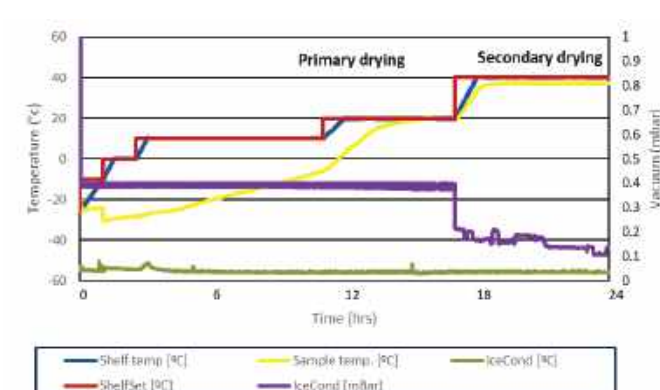


Figure 2: Run data of the primary and secondary drying steps plotting from the Lyovapor™ software.

The figure 1 depicts the process of a freezing drying cycle. After the completion of 17 hours, the sample temperature reaches the shelf temperature of 20 °C. This convergence is a significant indication that the primary drying phase has reached the end. During the primary drying phase, the bulk water is removed from the sample by sublimation which takes lots of energy. The transition into the secondary drying phase begins at 18 hours. In the secondary drying phase, the sample is dried by removing bounded moisture. The amount of this water is rather low and therefore the sample follows the set shelf temperature quickly.

Since freeze-dried products exhibit highly hygroscopic nature in general, the dry apple slices after the freeze drying process are immediately transferred to a sealed or closed container to avoid moisture absorption from the surrounding atmosphere.

## PRODUCT APPEARANCE



Figure 3: Apple slices before (left) and after (right) freeze drying.

The appearance did change slightly before and after the freeze drying. But the consistency can be classified as dry matter. The initial total weight of the sample was 1982 grams. The total weight is drastically reduced to 518 grams after drying. This result goes along with the proposed water content of over 80 % in fruit in the introduction part.

## RESIDUAL MOISTURE ANALYSIS

The freeze-dried apples were analyzed for moisture content by Karl Fischer Titration.

Description	Result
Actual apple weight (without moisture)	502 gr
Moisture content in dry sample	2.64%
Total removed moisture	97%

Table 1: Residual Moisture results of freeze drying apple slices.

## CONCLUSION

With the Lyovapor™ L-200, drying has been completed with 97 % of the moisture removed in 24 h which shows a high drying efficiency. The final dry fruit are dried without changing their appearance, texture and colour with a moisture content of < 2.7 %.

## REFERENCES

1. Krokida, M. K., & Philippopoulos, C. (2006). The volatility of apples during air and freeze drying. *Journal of Food Engineering*, 73(2), 135 – 141. doi: 10.1016/j.jfoodeng.2005.01.012.
2. J Du, H Gary, L Katherine – The Expedition, 2021 – ojs.library.ubc.ca.
3. Di Matteo P., Donsi G., Ferrari G., The role of heat and mass transfer phenomena in atmospheric freeze drying of foods in a fluidised bed. *J. Food Eng.*, 2003, 59, 267 – 275.
4. Pol. J. Food Nutr. Sci., 2011, Vol. 61, No. 3, pp. 165–171, <https://www.proquest.com/openview/-ca25ec10a7832df3199c5f64d4c85d05/1?pq-origsite=gscholar&cbl=2026629>
5. <https://ojs.library.ubc.ca/index.php/expedition/article/view/196106>
6. KARL FISCHER METHOD determination of water – TEST METHOD, <https://law.resource.org/pub/in/bis/S02/is.2362.1993.pdf>

**BUCHI**

**Lyovapor™  
L-200**





**Advancing drug discovery  
through rapid, high-resolution  
visualization of organoids and  
spheroids with LICORbio  
ATLAS™ IMAGER**

---

**High-content imaging of 3D cell models with the LICORbio  
Atlas™ Imager**

**B**iomedical research is undergoing a significant shift towards more physiologically relevant models for studying human biology and disease. Traditional two-dimensional (2D) cell cultures, while useful, often fail to replicate the complex structure and functionality of human tissues. These limitations, as well as the FDA's recently announced plan to phase out animal testing requirements for drug development in favour of New Approach Methodologies (NAMs), have spurred the development and reinforced the adoption of three-dimensional (3D) cell culture systems such as organoids and spheroids.

These 3D cell culture models generally provide a much closer approximation of true human *in vivo* conditions than 2D cell culture and animal models, making them invaluable tools for drug development, disease modelling, and personalized medicine.

This application provides a basic overview of organoids and spheroids, as well as their similarities, differences, applications, and implications for the future of drug discovery. It also highlights technologies like the LICORbio ATLAS™ Imager that bridge the gap between complexity and clarity—delivering high-content, high-resolution imaging of 3D models.

### Keywords or phrases:

3D cell culture imaging, Organoids and spheroids, High-content, high-throughput imaging, Multiplex fluorescence assays, Drug discovery and disease modelling, Spatial biology and quantitative analysis

## INTRODUCTION

### What Are Organoids?

Organoids are miniature, self-organizing 3D structures derived from stem cells or primary tissues that can simulate the structure and function of real organs. They are typically

cultured in extracellular matrix scaffolds (often hydrogels like Matrigel or synthetic alternatives), which provide the necessary support for cell growth and differentiation. Organoids can be generated from various tissues, including the brain, liver, lung, retina, intestine, and kidney, and they contain multiple cell types found in the corresponding organ. This cellular diversity allows organoids to closely mimic the physiological environment of the original tissue.

The practical applications of organoids are incredibly diverse. They are used in drug screening to assess efficacy and toxicity, in disease modelling to study pathogenesis, and in regenerative medicine to explore tissue development and repair mechanisms. Furthermore, organoids have been vital to personalized medicine by enabling the testing of patient-specific therapies to identify the most effective treatment options.

### What Are Spheroids?

Spheroids are free-floating, 3D cell aggregates formed from cell suspensions that spontaneously assemble into spherical structures, with or without an extracellular scaffold matrix. Unlike organoids, spheroids are simpler in structure and often only consist of a single cell type or limited number of cell types. They are typically cultured in non-adherent conditions that promote cell aggregation, such as ultra-low attachment (ULA) plates, hanging drop systems, liquid overlay, spinner or pellet culture, rotating wall vessels, microfluidics, or via magnetic levitation.

Despite their relative simplicity, spheroids are valuable models for studying cellular behaviours like proliferation, migration, and drug response via cell health assays. This makes them particularly useful in drug development, as well as cancer research, where they serve as models for tumour growth and metastasis. Spheroids can also be utilized in high-throughput screening assays due to their ease of formation and scalability.

### Organoids vs. Spheroids

Organoids and spheroids are both 3D cell culture models and offer more physiologically relevant alternatives than traditional 2D cell cultures. However, they differ

significantly in their formation, complexity, and applications. While both models have their strengths, the choice between organoids and spheroids depends on the specific research objectives and the level of complexity required.

### 1. Complexity and Structure

Organoids and spheroids are quite different in terms of relative complexity. Organoids are far more complex, as they contain multiple cell types and exhibit tissue-specific architecture. Spheroids are simpler, often composed of a single cell type, and lack the intricate structures seen in organoids.

Organoids exhibit a high degree of complexity, often developing organized structures that resemble the original tissue. This complexity arises from the self-organizing properties of stem cells, which can differentiate into various lineages and form functional biological tissues. For example, intestinal organoids can develop villus-like structures and exhibit absorptive and secretory functions like the human intestine. Organoids provide a more detailed and accurate representation of tissue architecture, making them suitable for studies requiring complex models, such as disease modelling and personalized medicine.

Spheroids are much simpler in structure. They typically consist of a mass of cells without the distinct layers or compartments seen in organoids. While they can form from various cell types and may exhibit some degree of cellular heterogeneity, spheroids inherently lack the intricate organization and functionality of organoids, limiting their ability to fully mimic the functionality of true human tissues. While spheroid models may be considered reductionist compared to organoids, their ease of generation makes them more practical for high-throughput protocols and drug screening.

### 2. Cellular Composition

Organoids are composed of multiple cell types that are spatially organized to mimic the original tissue. This multi-

cellular composition arises from the differentiation of stem or progenitor cells under specific culture conditions. The presence of various cell types within organoids allows for more accurate modelling of tissue-specific functions and interactions. For instance, brain organoids can contain neurons, glial cells, and other supporting cells, providing a more comprehensive model of neural development and disease.

Spheroids, in contrast, often consist of a single cell type or a limited number of cell types. This simplicity can be quite advantageous for certain applications, such as studying basic cellular behaviours or conducting high-throughput drug screening despite not fully capturing the complexity of true human tissues.

### 3. Applications

Both organoids and spheroids can be found in various biomedical research applications. The choice to use organoids or spheroids generally depends on the specific research question and the level of complexity required. In some cases, combining both models can provide complementary insights into biological processes and therapeutic responses. In general, organoids are suited for long-term culture, genetic manipulation, and modelling organ-specific diseases. Spheroids are advantageous for cell health assays, rapid drug screening, and studying basic cellular behaviours.

Spheroids are widely utilized in cancer research due to their ability to mimic aspects of tumour growth and the tumour microenvironment. They are particularly useful for evaluating drug efficacy and resistance, as they can replicate the 3D architecture of tumours and the gradients of nutrients and oxygen found within them. Additionally, spheroids have the potential to be more common in high-throughput screening, making them valuable tools for drug discovery.

Organoids, however, offer a more advanced model for studying human biology and disease. Their complex structure and cellular composition make them ideal for modelling organ-specific diseases, such as cystic fibrosis in lung organoids or colorectal cancer in intestinal organoids.

Organoids also facilitate personalized medicine approaches, as patient-derived organoids can be used to test drug responses and tailor individual treatments.

While 2D cell culture is still the most popular approach, spheroids can provide value for applications requiring simplicity and rapid scalability. Organoids offer a more detailed and physiologically relevant model for studying complex biological systems and diseases, though they tend to be relatively costly and time-consuming to produce and maintain.

## HIGH-CONTENT, HIGH-THROUGHPUT IMAGING WITH THE LICORBIO ATLAS IMAGER

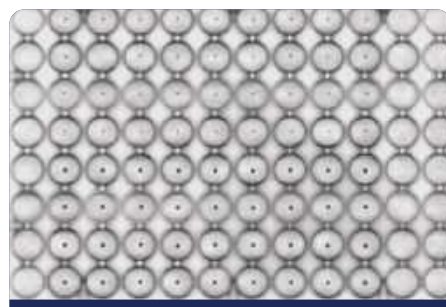
Designed to streamline imaging workflows, the ATLAS integrates advanced optics and automation to support multiplexed assays with minimal user intervention. A unified solution of high-throughput and deep spatial resolution, the system reduces workflow complexity, minimises steps and accelerates image acquisition-delivering results in a fraction of the time and cost compared to conventional imaging platforms.

## KEY FEATURES

- ▶ Acquire entire wells in an image to perform rapid, full-plate screening, and conduct higher-resolution deep dives (5  $\mu$ m) into individual wells and regions of interest.
- ▶ No post-processing manipulation needed, such as stitching or illumination correction.
- ▶ The unique line-scanning technology enables whole-plate imaging in less than one minute.
- ▶ The patented optical system gives you unmatched sensitivity and dynamic range in a single scan. It minimizes background fluorescence and enhances quantitative multiplexing for critical drug discovery applications.

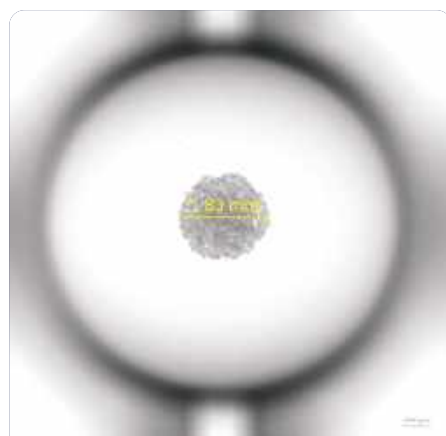
- ▶ Over 30 imaging channels with six lasers spanning UV to near-infrared, plus LED RGB for brightfield and epi-illumination.
- ▶ Perform cell viability and luminescence assays with the built-in luminescent imager.
- ▶ The expansive focus depth enables imaging through entire 3D cell structures such as spheroids, organoids, organ-on-a-chip, and other micro physiological systems.

Shown below are example images acquired using the LICORbio ATLAS Imager, illustrating its ability to capture both 2D and 3D assay data with exceptional clarity and contrast.



Monitoring 3D Cell Culture

PANC-1 and BxPC3 spheroids grown in a 96-well plate, imaged in 630 nm trans channel at 50  $\mu$ m resolution.



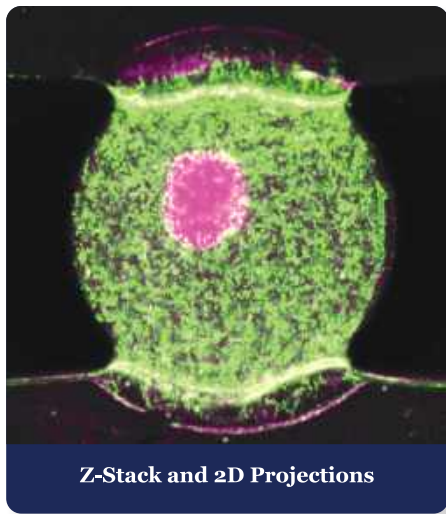
Single Well Imaging in Brightfield

Panc-1 spheroid grown in a 96-well plate imaged in the 630 trans channel at 5  $\mu$ m.



Monitoring 3D Cell Culture

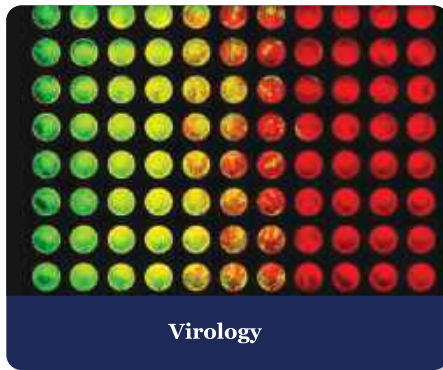
Brightfield image (RGB transillumination) of spheroid in single well image acquired at 5  $\mu\text{m}$  on the LICORbio Atlas Imager. RGB transillumination enables crisp, color detail of the contents of the entire well.



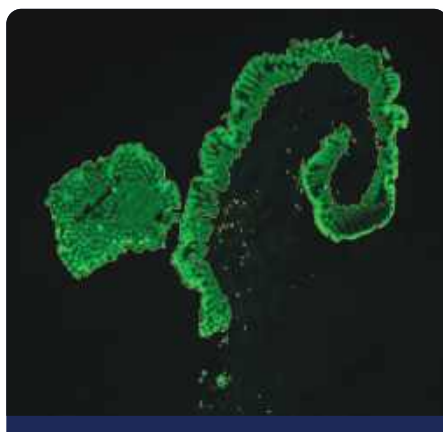
Z-Stack and 2D Projections

Multiplexed fluorescence imaging of a vascularized, liver cancer spheroid in an organiX Plate from AIM Biotech. The sample was imaged using the LICORbio Atlas Imaging System at 5  $\mu\text{m}$  resolution, capturing the entire well in a single image, and Image Studio Software v6.1 was used to create a max projection. The image shows Hoechst (DNA stain) in the 375Ex-460Em channel (blue), GFP expressed in the vasculature in the 488Ex-530Em channel (green), and

Phalloidin555 bound to F-actin in the 520Ex-590Em channel (red). Co-localization is displayed for Hoechst/Phalloidin555 (magenta) and GFP/Phalloidin555 (yellow).



Easily perform fast, reliable, and quantitative virology assays using near-infrared fluorescence imaging.



Tissue Section Analysis

Tissue section at 5  $\mu\text{m}$  shown with automatically generated shape contour using new Morphology Analysis features in Image Studio v6.1. Threshold analysis enables identification of tissue in foreground and autofluorescence for background correction.

### THE FUTURE OF DRUG DISCOVERY

The integration of organoids and spheroids into more drug discovery pipelines marks a significant advancement in

modern preclinical research. These 3D models offer several advantages over traditional 2D cultures, including more accurate prediction of drug responses and better representation of human tissue physiology. This shift in mindset and protocol has the potential to save billions of dollars wasted in clinical drug development, ultimately ensuring safer, more effective drugs get to patients faster. Given the FDA's recent guidance and the increased scrutiny on academic research and pharmaceutical regulatory frameworks, these innovative technologies are poised to play a pivotal role in advancing drug discovery, kickstarting precision medicine, and improving patient outcomes both now and in the near future.

This application note demonstrated capabilities of the brand-new **Atlas™ Imaging System**. This imager delivers both higher-throughput screening and higher-resolution 5  $\mu\text{m}$  multiplex imaging for a fraction of the cost of a confocal microscope or flow cytometer.

The examples highlighted above showcase the **Atlas Imager**'s versatility across diverse research applications—from cell viability studies and spheroid imaging to multiplexed fluorescence assays.

## REFERENCES

1. Devarasetty, M., et al. (2018). Applications of Bioengineered 3D Tissue and Tumor Organoids in Drug Development and Precision Medicine: Current and Future. *BioDrugs*, 32(1) 53–68.
2. Goldrick, C., et al. (2025, 9). 3D multicellular systems in disease modelling: From organoids to organ-on-chip. *Frontiers in Cell and Developmental Biology*. 11.
3. El Harane, S., et al. (2023). Cancer Spheroids and Organoids as Novel Tools for Research and Therapy: State of the Art and Challenges to Guide Precision Medicine. *Cells*, 12(7):1001.
4. Gunti, S., et al. (2021). Organoid and Spheroid Tumor Models: Techniques and Applications. *Cancers*, 13(4):874.
5. Gopallawa, I., et al. (2024). Applications of Organoids in Advancing Drug Discovery and Development. *Journal of Pharmaceutical Sciences*, 113(9):2659–2667.
6. Sun D, Gao W, Hu H, Zhou S. Why 90% of clinical drug development fails and how to improve it?. *Acta Pharm Sin B*. 12(7):3049–3062.



## LICORbio ATLAS™ IMAGER

Data-rich 2D and 3D Cell-Based Imaging, Faster Than Ever.

# Exploring Nanoscale Organization of Normal Alkanes on HOPG Substrate with DriveAFM

---

Mapping the Nanoscale Organization of Long-Chain Alkanes Using DriveAFM

The nanoscale self-organization of normal and ultra-long alkanes ( $C_nH_{2n+2}$ ) on highly oriented pyrolytic graphite (HOPG) was investigated using the DriveAFM microscope equipped with photothermal excitation (CleanDrive) and WaveMode imaging. High-resolution topography and phase data revealed distinct lamellar architectures whose periodicities correspond closely to the molecular chain lengths of the alkanes studied ( $C_{60}H_{122}$ ,  $C_{122}H_{246}$ ,  $C_{242}H_{486}$  and  $C_{390}H_{782}$ ). Subtle topographic modulations of  $\sim 0.2$  nm were attributed to alternating  $-CH_3$  and  $-CH_2-$  groups at lamellar edges, while variations in tip-sample interaction strength exposed hidden periodicities arising from lateral chain folding. These findings demonstrate the sensitivity of DriveAFM in capturing fine variations in lamellar order, molecular orientation, and chain packing that are otherwise inaccessible with conventional imaging. The results highlight how AFM can elucidate the structural dynamics underlying alkane crystallization and provide nanoscale insights relevant to polymer morphology and self-assembly phenomena.

### Keywords or phrases:

Atomic Force Microscopy (AFM), Normal Alkanes, Lamellar Structures, HOPG Substrate, Molecular Self-Organization, Chain Folding

## INTRODUCTION

Normal alkanes  $C_nH_{2n+2}$  are linear chain molecules, which are typically extended, and they form ordered lamellar structures and crystals. When size of the chains increases with  $n$  above 120, such ultra-long alkanes manifest chain folding – the main driver behind of polymer crystallization. The longest alkane  $C_{390}H_{782}$  is a perfect model of linear polyethylene, and crystallization of these species have many common features.

The lamellar 2D organization has been detected in thin and ultra-thin layers of alkanes on highly oriented pyrolytic graphite (HOPG) and other layered crystals such as MoS<sub>2</sub>. On these substrates the molecular orientation exhibits three-fold symmetry that guides the related orientation of the alkane lamellae. As the lamellae are formed of fully elongated chains, their width equals to the alkane length when the molecules are aligned perpendicular to the lamellar edges. The length of different alkanes from  $C_{18}H_{38}$  to the ultra-long one –  $C_{390}H_{782}$  changes as listed in Figure 1a. The lamellar width can be smaller when molecules are tilted at some angle to the lamellar edges. Figure 1b shows a sketch of the alkane lamellae that should have thickness of individual alkane molecule (0.5 nm).

The lamellar order of all these alkanes on HOPG can be revealed in AFM images at room temperature as melting temperature of  $C_{18}H_{38}$  crystals is around 28–30°C and longer alkanes melt at higher temperatures. It is known that lamellar ordering of alkanes, which is facilitated by inter

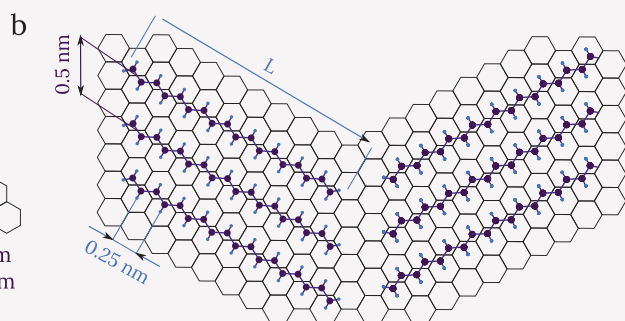
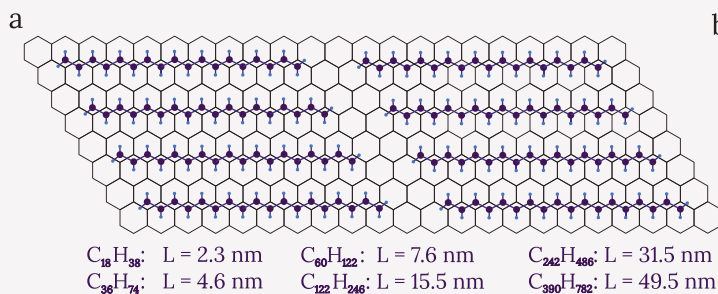


Figure 1.: Self-organization of normal alkane molecules ( $C_nH_{2n+2}$ ) on HOPG surface. The HOPG surface is depicted as a honeycomb lattice, the carbon atoms are dark purple circles and the hydrogen atoms are light blue circles. (a) Horizontal packing with molecular chains in different lamellae parallel to each other. (b) V-shaped packing, with the molecules in different lamellae positioned at angle to each other. Text below the sketch (a) indicates lengths  $L$  of alkane molecules of different molecular weights.

molecular interactions on atomically flat surfaces like HOPG, is preserved at temperatures higher than melting temperature of alkane crystals. This was confirmed by detection of  $C_{390}H_{782}$  lamellar layers on HOPG at temperatures 50 degrees above melting temperature of these alkanes (130°C).

The lamellar edges are formed of  $-CH_3$  end groups, which are bulkier than  $-CH_2-$  groups of the chains. The related height variations should be reflected in topography of lamellar sheets formed on atomically flat substrates. This application demonstrates how the lamellar structures of normal alkanes with different chain length on HOPG are visualized with AFM and what peculiar nanoscale features can be detected.

## EXPERIMENTAL DETAILS

The samples of different alkanes were prepared by spin-casting of their solutions in toluene (concentration is around 10 mg/ml) on freshly cleaved surface of HOPG. All AFM measurements were performed at room temperature and in most cases, we have used DriveAFM microscope in Dynamic Mode by using photo-thermal excitation of the probe (CleanDrive) instead of piezo-electric drive. Few studies were also made in WaveMode, in which intermittent contact has proceed at off-resonance frequency of 3 kHz. Commercially available soft dynamic mode cantilevers with spring constants in the 1-10 N/m range were applied in these experiments.

### Imaging of normal alkanes: $C_{60}H_{122}$

Visualization of lamellar order of normal alkane  $C_{60}H_{122}$  with molecular length of 7.5 nm is displayed in Figures 2a-d. An area of 1  $\mu m$  on side, which is shown in Figure 2a, consists of several terraces covered by barely seen fine linear features. Several nanoscale size droplets most likely represent an alkane material, which was not spread on the substrate. The height image recorded at a smaller location in the center of this area reveals a periodical pattern with the spacing of 7.5 nm. Height and phase images in Figure 2c-d present a location with two HOPG crystalline terraces, which displays

the periodical arrays of linear features with different orientations. The width of these features corresponds to  $C_{60}H_{122}$  length that allows their assignment to the alkane lamellae. The height depressions, which are noticed perpendicular to the lamellar edges on the lower terrace, are ~0.2 nm in height. These features can be assigned to  $-CH_3$  terminals that are slightly higher than  $-CH_2-$  groups of the lamellar sheet. However, the end  $-CH_3$  groups are more mobile than  $-CH_2-$  groups of the chain, and they can be stronger depressed by the probe tip. These local stiffness variations are most likely responsible for the phase contrast in Figure 2d.

### Imaging of normal alkanes: $C_{122}H_{246}$

The multiple lamellar sheets of  $C_{122}H_{246}$  alkanes cover the surfaces of two substrate terraces, which are separated by a diagonal border in the area displayed in the height image, Figure 3a. The wavy structures of 15-16 nm in width are distinguished in the area on right from the border, Figure 3b. They represent  $C_{122}H_{246}$  lamellae as their width is close to  $C_{122}H_{246}$  molecular length. The strips with similar width have formed the raised ribbon with height of 3.5 nm.

Several overlaying strips have composed the ribbon, and they oriented like the wavy structures occupied most of the area. Several dark blocks ~15-16 nm in width represent the missing parts of the lamellae. The terraces of multiple overlaying alkane lamellae, which are noticed on the left from the border, are displayed in the height image in Figure 3c. The steps between top layers are ~0.5 nm that consistent with diameter of individual alkane molecule. Faint contrast variations in this image hints on a regular surface order with the periodical spacing close to the alkane width. To improve structure visualization, we have increased the tip-sample force interactions by lowering set-point amplitude.

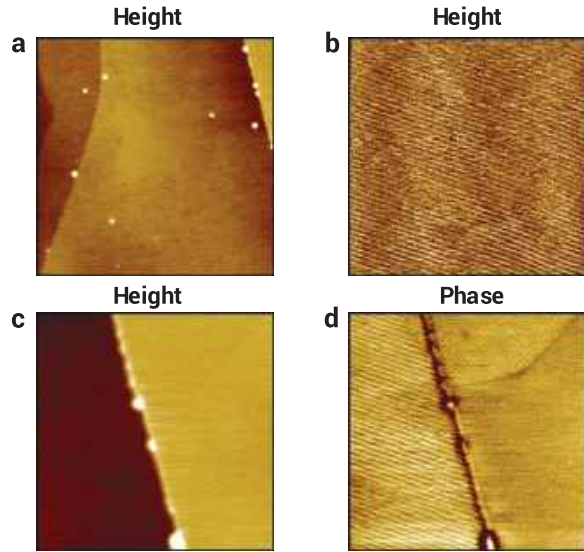


Figure 2.: Height (a,b,c) and phase (d) images of C<sub>60</sub>H<sub>122</sub> layer on HOPG. (a) Terraces of HOPG with fine line features representing the alkane assemblies, small droplets are likely the alkane material, not spread on the surface. (b) Zoom in the center of the image (a) showing a periodic pattern of alkane assemblies with the period of 7.5 nm. (c,d) Height and phase images showing two HOPG crystalline terraces with the arrays of linear features with different orientations.

(a) Image size: 1 x 1  $\mu\text{m}^2$ , height range: 2.4 nm.  
 (b) Image size: 0.4 x 0.4  $\mu\text{m}^2$ , height range: 1  $\text{\AA}$ .  
 (c,d) Image size: 0.4 x 0.4  $\mu\text{m}^2$ , height range: 1.8 nm, phase range 48°.

The related effect is obvious in height image in Figure 3d, which was recorded in the scanning from the top. At the top, scanning was performed at small tip force. Then the tip-force was raised, and the height contrast was drastically improved. The linear features became resolved not only with the spacing of 15–16 nm but also at smaller periodicities. To verify the observation was verified in the bottom of the image when the set-point was raised again and lowered. The related image changes have supported the effect.

The image pattern revealed at high-force imaging can be explained by double folding of alkane molecules that leads to appearance additional spacing of 5 nm. This situation is sketched in Figure 3f.

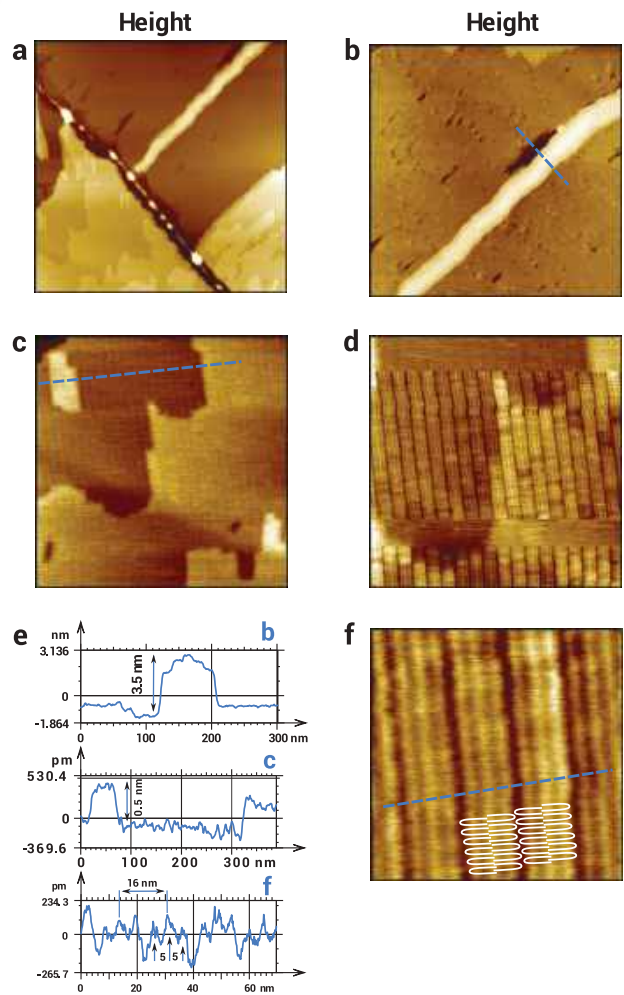


Figure 3.: Height images of C<sub>122</sub>H<sub>246</sub> layer on HOPG. The low tip-force interactions were used for images in (a)–(c). The image in (d) was recorded at low and high tip-forces: the scanning started at the top of the image at low force, later the force was increased, and the visibility of lamellar structures has improved. (e) The cross-sections along the blue dashed lines in images (b,c,f). (f) A tentative pattern of lateral chain folding was overlaid on the height image.

(a) Image size: 1.5 x 1.5  $\mu\text{m}^2$ , height range: 7 nm.  
 (b) Image size: 1 x 1  $\mu\text{m}^2$ , height range: 5 nm.  
 (c) Image size: 0.5 x 0.5  $\mu\text{m}^2$ , height range: 3 nm.  
 (d) Image size: 0.3 x 0.3  $\mu\text{m}^2$ , height range: 1.2 nm.  
 (f) Image size: 76 x 76  $\text{nm}^2$ , height range: 0.5 nm.

### Imaging of normal alkanes: C<sub>242</sub>H<sub>486</sub>

Folding of macromolecules is common for single crystals of ultra-long alkanes and folding of C<sub>390</sub>H<sub>782</sub> chain in 5 segments leads to 10 nm thick lozenge-type crystals of this alkane. A chain folding of flat-lying C<sub>390</sub>H<sub>782</sub> chains, which takes place in few surface locations, was reported only once. Adsorbate of C<sub>242</sub>H<sub>486</sub> on HOPG is characterized by smooth areas covering the substrate terraces and by few raised drop

lets of the alkane that were not spread on the substrate, Figure 4a. A weak stripped pattern is noticed on smooth areas, and it is more pronounced in the height image of a smaller location, Figure 4b. The white lines of around 5 nm in width and ~0.2 nm in height most likely represent the lamellar edges formed by terminal  $-\text{CH}_3$  groups. The  $l'$   $\text{p r o o}$  ~ length of  $\text{C}_{242}\text{H}_{486}$  chains, and this supports of the assignment. This image was recorded at low tip-sample forces. At higher forces, the stripped pattern with depressed lines was observed, Figure 4c. This contrast change can be explained by tip-induced depression of the lamellar boundaries formed by  $-\text{CH}_3$  terminal groups. In addition, a few of short bright rods are observed on the lamellar surface. They can be assigned to individual alkane chains, which were not incorporated into the lamellar layer. Fine lamellar features were detected at the location, where the lamellar order was perturbed, Figure 4d. In addition to the shift of white lines of the lamellar borders, at some locations inside individual lamellae, there are weak features with smaller spacings. These features are indicated with black arrows, and their separations are ~6 nm. Therefore, a lateral folding of  $\text{C}_{242}\text{H}_{486}$  chains looks possible.

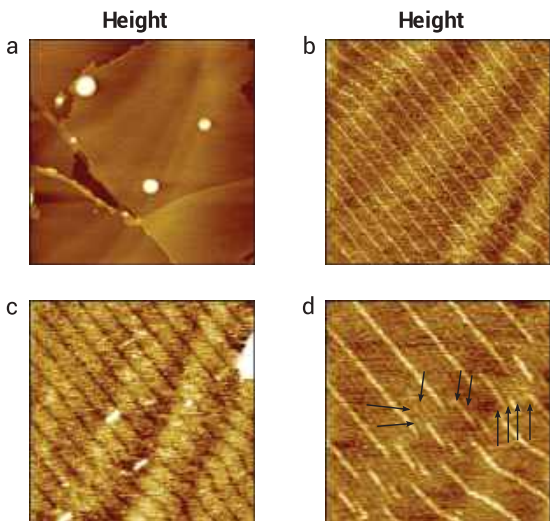


Figure 4.: Height images of  $\text{C}_{242}\text{H}_{486}$  layer on HOPG. The images in (a), (b) and (d) were obtained at low force, and the image in (c) - at higher tip-force. Arrows in (d) point out the fine sub-lamellar features most likely caused by lateral chain folding.

- (a) Image size:  $1.5 \times 1.5 \mu\text{m}^2$ , height range: 11 nm.
- (b) Image size:  $0.5 \times 0.5 \mu\text{m}^2$ , height range: 0.25 nm.
- (c) Image size:  $0.4 \times 0.4 \mu\text{m}^2$ , height range: 0.3 nm.
- (d) Image size:  $0.2 \times 0.2 \mu\text{m}^2$ , height range: 0.25 nm.

## Imaging of normal alkanes: $\text{C}_{390}\text{H}_{782}$

Surface morphology of  $\text{C}_{390}\text{H}_{782}$  layer on HOPG is shown in Figure 5a. Many dark and bright blocks with dimensions of their sides close to 49.5 nm - length of  $\text{C}_{390}\text{H}_{782}$  alkane are detected on this surface. This hints on lamellar order of the top layers. The height image of smaller area (Figures 5b) shows bright features, which can be assigned to the boundaries of lamellae of various size and orientation. The top layer is not complete, and multiple dark vacancies with lamellar dimensions are spread on the surface.

In the attempts to visualize fine details of the lamellar order we have performed imaging at raised tip-forces. The height and phase images, which were recorded at these conditions, revealed depressed lamellar borders as seen in Figures 5c-d. The distance between the bright and dark lamellar edges are close to 49 nm that suggests only small chain tilt with respect to the boundaries.

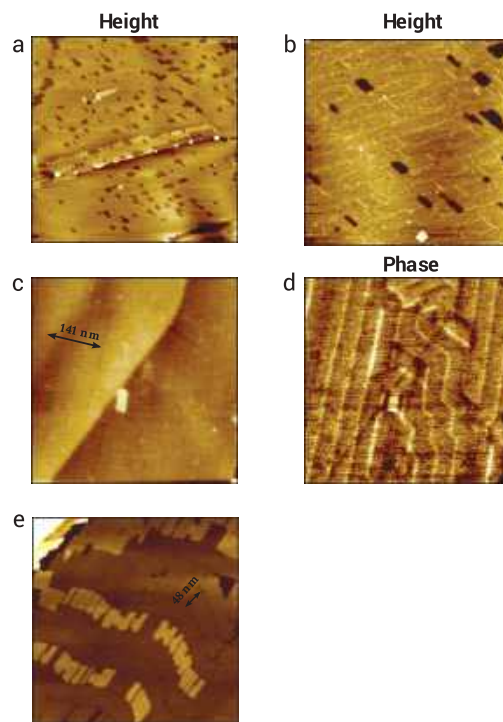


Figure 5.: Height (a,b,c,e) and phase (d) images of  $\text{C}_{390}\text{H}_{782}$  adsorbate on HOPG. The images in (a)-(d) were recorded in dynamic mode in low-force (a-b) and high-force (c-d) operations. The image in (e) was obtained in WaveMode. The inserts in (c) and (e) indicate the width of three and one lamellae, respectively.

- (a) Image size:  $2 \times 2 \mu\text{m}^2$ , height range: 2 nm.
- (b) Image size:  $0.6 \times 0.6 \mu\text{m}^2$ , height range: 0.7 nm.
- (c,d) Image size:  $0.5 \times 0.5 \mu\text{m}^2$ , height range: 0.7 nm, phase range: phase range 5°.
- (e) Image size:  $0.5 \times 0.5 \mu\text{m}^2$ , height range: 4.5 nm.

Fine details in the curved lamellar ribbons were detected in the height image in Figure 5e, which was recorded in WaveMode. This off-resonance mode is characterized by a stronger tip-forces compared to Dynamic Mode. Therefore, more structural features can be visualized. The boundaries of the curved lamellar ribbons are seen with a darker contrast, and individual ribbons exhibit multiple lines with spacings down to 10 nm, which are perpendicular to the boundaries. The parts of the top ribbons epitaxially grown on the underlying lamellae show that they can be split into individual blocks of extended chains. A few dark vacancies with similar dimensions are noticed in the surface as well.

## CONCLUSION

In summary, AFM studies of normal and ultra-long alkanes reveal a set of fine structural features related to the lateral chain folding and lamellar architecture in their layers on HOPG. The formation of these nanoscale structures on atomically flat surfaces can be essential for better understanding of alkane and polymer crystallization.

### Acknowledgements

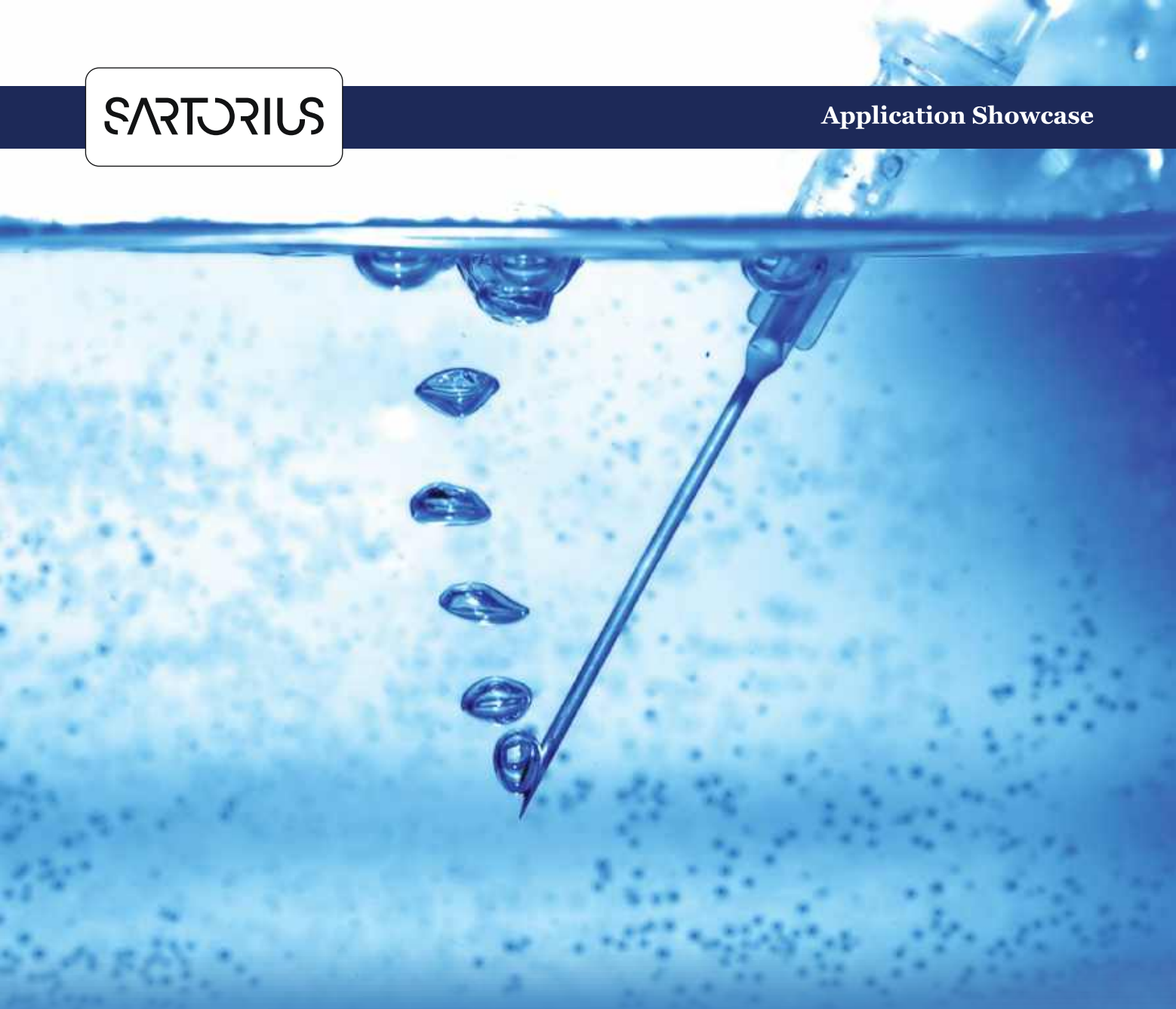
The measurements and the text of this application note were prepared by Sergei Magonov, SPM LABS LLC, USA.



 nanosurf

## DriveAFM

Performance without compromise



# The Role of Sartorius' Lab Water System in Reduction of the Microplastic Content in Ultrapure Water

---

**Ensuring Particle-Free Ultrapure Water Through Advanced Filtration**

Aatto Rautio<sup>1</sup>, Vladimir Stankov<sup>2</sup>, Martin Šteković<sup>2</sup>, Ivana Kučar<sup>2</sup>, Dr. Kunal Kureja<sup>3</sup>,\*

1. Measur Oy, Mannerheimintie 117, 00280 Helsinki, Finland

2. Sample control d.o.o., Puškarićeva ulica 18, 10250 Zagreb, Croatia

3. Sartorius Lab Instruments GmbH & Co.KG, Otto-Brenner-Str. 20, 37079 Göttingen, Germany.

**M**icroplastics in water and the environment is one of the hot topics under the general discussion of environmental professionals. These microplastic particles are present everywhere, also in tap water. Microplastics can already be found inside human bodies and are suspected of causing long-term health problems. Now, the authorities and other professionals are working on new regulations to reduce the amount of microplastic load in the future.

This note describes how well the Sartorius Arium® Pro VF series can remove microplastic particles from normal tap water, deionized water or other suitable water sources using two different test setups and prevent the particles from causing any challenges in laboratory work.

### Keywords or phrases:

Microplastic,  $\mu$ -Raman, ASTM Type I water, Laboratory Water, Arium® Pro VF

Microplastics are tiny fragments (less than 5,000 to 1  $\mu\text{m}$  in diameter)<sup>1</sup> of plastics that end up in nature by degradation of bigger plastic products or from sources like cosmetics, clothing, car tires, and industrial processes (Figure 1). There is rising concern about microplastic pollution in lakes, oceans, and drinking water, which in turn increases the demand for regulation and laboratory testing of microplastics in different kinds of products, environmental samples and other sample types since these particles can

eventually cause for example health hazards.<sup>2</sup>

Microplastics are found everywhere including tap water and other clean water sources, but also inside human bodies. The long-term health effect of microplastics is still unknown, but preliminary evidence suggests that they might affect stress levels and immune responses. For these reasons, it is really important to implement all possible solutions to hinder microplastic count in different locations, such as in laboratory water systems.<sup>3,4</sup>

Many different types of water purification systems have been introduced to the laboratories, but microplastics are a topic that has not been focused on in the past. In general, microplastics levels in different water sources can be still unknown in many areas. Laboratories around the world should be able to be sure that, for example, all possible contamination sources are taken into account when using water in the laboratory.

Currently, new regulations and different standards are under development to get more tools to control the amount of microplastics in the environment. The latest of these is the European Chemical Agency's proposal to ban intentionally added microplastics in different products. The first restrictions of this regulation entered into force in the fall of 2023.<sup>5</sup>

### Ultrapure Water Purification System Overview

#### Application-Oriented and Flexible to Meet the Highest Demands

The Arium® Pro VF series stands as a trusted source of ultrapure water, and it distinguishes itself by offering a flexible and modular system. In comparison to conventional devices, these systems provide remarkable added value.

One standout feature is that all systems within this series not only meet but exceed the stringent ASTM Type 1 water quality standards, ensuring the delivery of the highest quality results in their category. These systems are capable of dispensing up to 2 liters of consistently high-quality ultrapure water per minute, with a conductivity of 0.055  $\mu\text{S x cm}^{-1}$  (equivalent to 18.2  $\text{M}\Omega \text{ x cm}$ ). Moreover, when equipped with the Arium® Sterile Plus final filter,

they deliver ultrapure water that is virtually free from microorganisms.

The Arium® Pro series (Figure 2) embodies the following characteristics:

- ▶ **Modular.** Each system can be specifically selected to suit your application.
- ▶ **Flexible.** They seamlessly integrate into a variety of laboratory environments.
- ▶ **User-Friendly.** These systems feature a touch-activated display with an intuitive menu for easy operation.
- ▶ **Efficient.** With the favorites function, you gain direct access to recurring volumes, streamlining workflows, and saving valuable time in your laboratory.

## Materials

Water samples were filtered using silicon filters with 1  $\mu\text{m}$  pore size (Smart Membranes GmbH, Germany). 10, 25 and 70  $\mu\text{m}$  NIST Traceable Size Standard polystyrene were used for spiking experiments. Particle analyses using Raman microscopy were performed with DXR3xi Raman Imaging Microscope. All spectra were collected using a 532 nm laser, filter, grating set, with the following conditions: 10 mW laser power, 0.05 s exposure time, and the number of spectra was 50. An Olympus magnification apochromatic objective with a 20x magnification was used and brightfield or darkfield illumination mode were used interchangeably for achieving optimal contrast in particle detection.

## Method

This study was done with two main objectives in mind: the first objective was to investigate whether the Arium® device itself leached particles into the final ASTM type I water it produced (Figure 2), and the second objective was to see if the system retained the particles introduced to the system from the feed water (Figure 3).

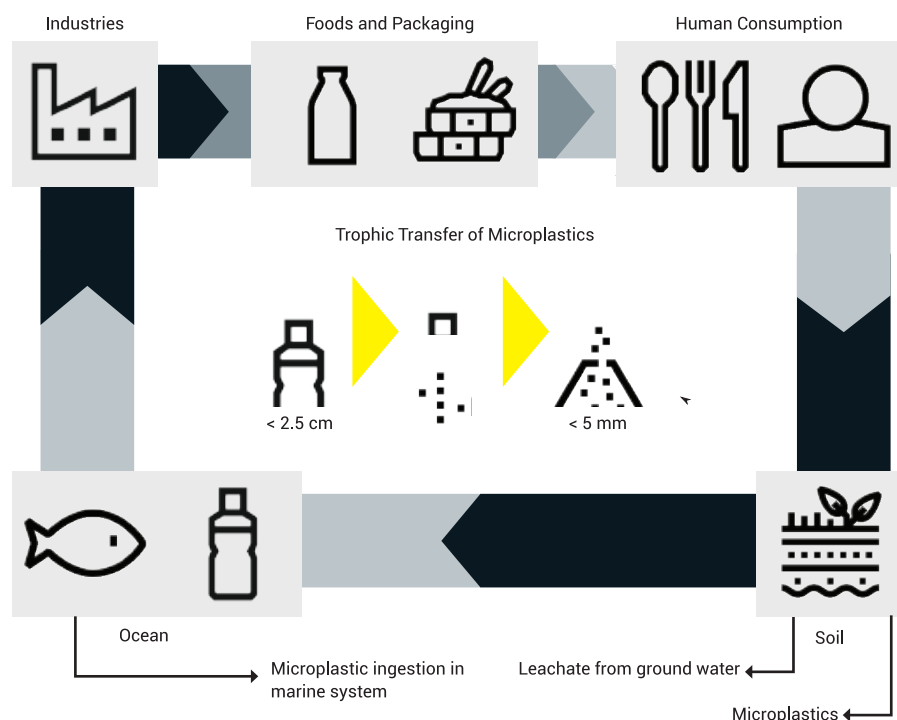


Figure 1: Major sources of microplastics and its transport into food systems.<sup>2</sup>

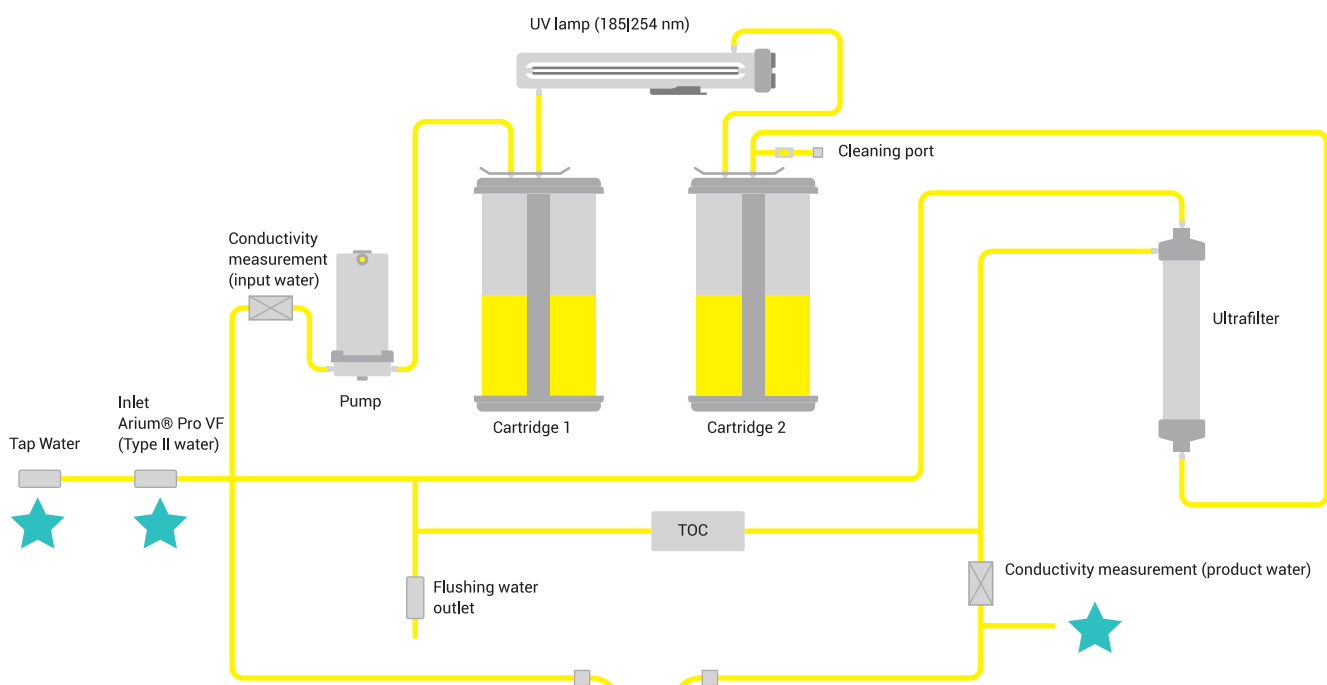


Figure 2: Flowchart of Arium® Pro VF for the second objective. Teal color stars mark the point of sampling.

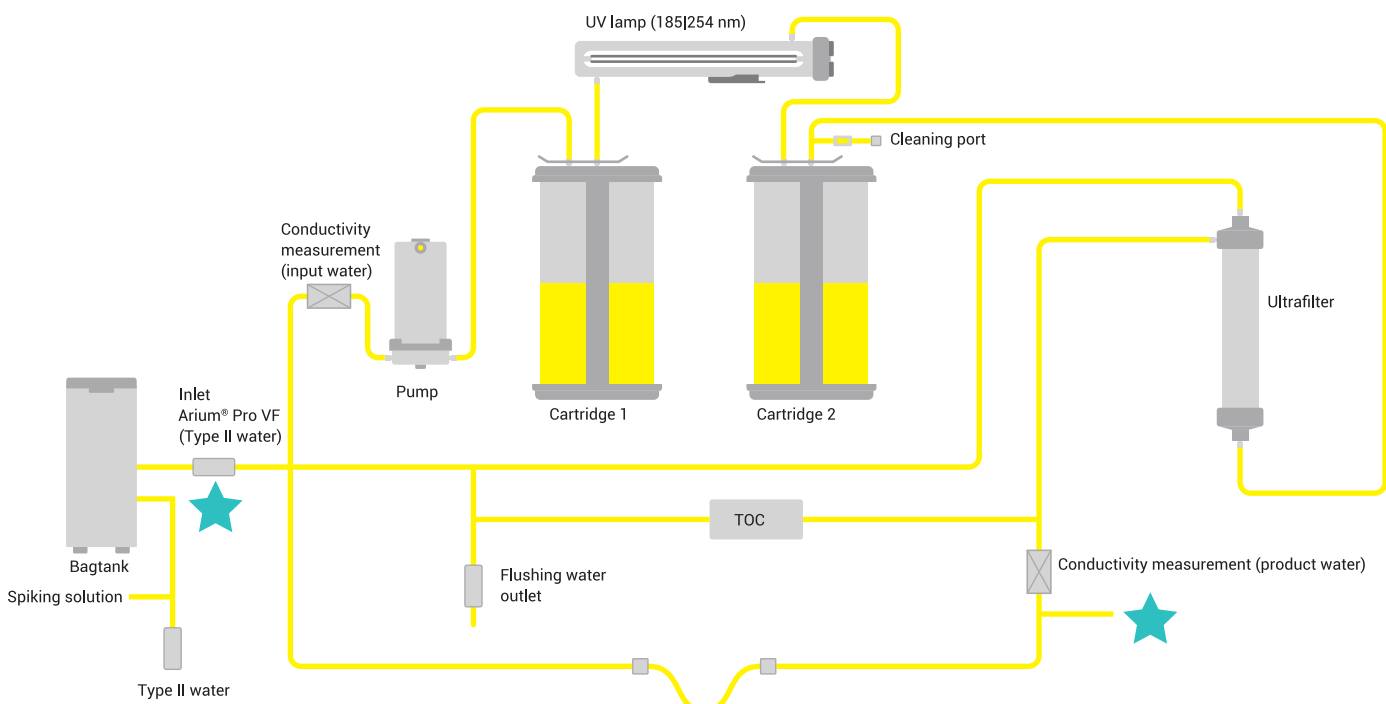


Figure 3: Flowchart of Arium® Pro VF for the first objective. Teal color stars mark the point of sampling.

## RESULTS

The workload was divided into two separate experimental setups. The first consisted of: one tap-water sample, one type II water sample and one Arium®-purified type I water sample (in total three 1L samples, Figure 3). The second setup (Figure 2) consisted of: one type II water sample spiked with 10, 25 and 70  $\mu\text{m}$  polystyrene (PS) microspheres, one Arium®-purified water sample obtained after consuming 9, 14 and 19 L of PS microsphere-spiked type II water (three separate samples) and finally two Arium purified water samples, where the first 1 L sample was taken after consuming 3 L of non-spiked type II water, and the other after 5 L (in total six 1 L samples). Type II water used in the first setup was poured directly in a clean 1 L laboratory glass, while the type II water used in the second setup was fed to the Arium device using a plastic canister. All experiments were performed twice, bringing the total number of experiments to 18.

Next step was to determine method limit of detection (LOD), in terms of numbers of microplastics per type of polymer and per particle size range. This was done by calculating the sum of mean number of particles from seven analyses of 1 L procedural blank samples and three standard deviations.

All water samples were processed as follows: Samples were vacuum filtered through silicon filters with 1  $\mu\text{m}$  pore size, which were subsequently stored in an appropriate container, to avoid particle contamination. Individual filters were placed onto a filter holder, which was then mounted onto a microscope stage and brought to objective focus.

Image of the entire filter surface was obtained by the instrument-controlled camera, after which the individual particles on the filter surface were located using the instrument software. Finally, the particles were analyzed using Raman micro-spectroscopy, yielding information regarding the number, size, and chemical identity of individual particles. Spectral match of a particle spectrum with a spectrum in a spectral library of minimum 70 % was taken as a criterium for including a particle in the reported results.

Limit of detection (LOD) needed to be calculated in order to be able to add context to later results obtained in two experimental setups. In the case of microplastics analyses, method LOD represents the smallest number of particles of a certain polymer type and size range that can be detected using the said analytical method. In this work, seven procedural blank samples were prepared and analyzed, after which the results were used for calculating the LOD:

$$\text{LOD} = \text{mean}_{7 \text{ samples}} + 3 \times \sigma_{7 \text{ samples}}$$

Results of seven analyses, along with the calculated LOD, are shown in Table 1. Particles detected in the blank samples consisted of seven types of polymers: polyethylene (PE), polypropylene (PP), polytetrafluoroethylene (PTFE), polystyrene (PS), ethylene vinyl acetate (EVA), polyamide (PA) and polyethylene terephthalate (PET) (Figure 4).

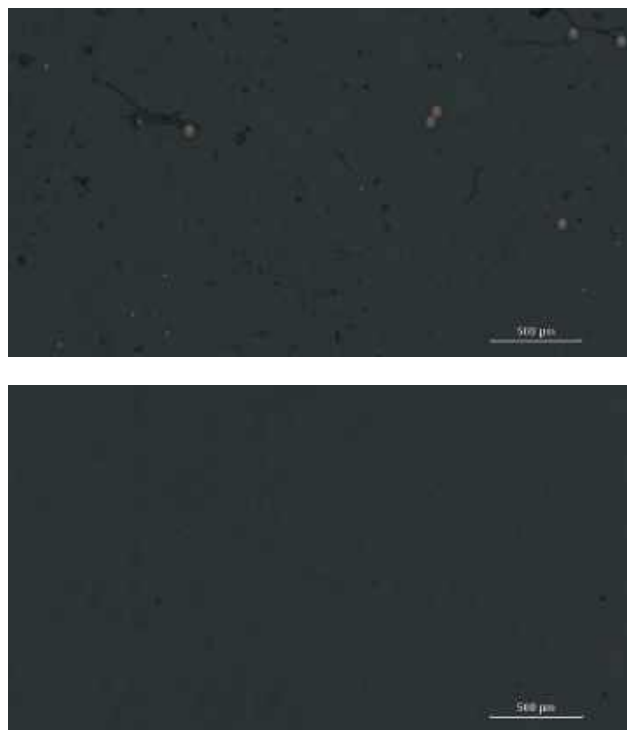


Figure 4: Filter with microplastic particles (top) and filter without any microplastic particles (bottom).

Polymer Type	Size Range ( $\mu\text{m}$ )	Number of Particles									
		1	2	3	4	5	6	7	Average	$3 \times \sigma_7$	LOD
PE	1-50	1	0	1	1	0	4	1	1.1	4.0	5.2
	50-100	1	1	2	0	0	1	1	0.9	2.1	2.9
	100-500	0	0	0	0	0	0	0	0.0	0.0	0.0
	>500	0	0	0	0	0	0	0	0.0	0.0	0.0
PP	1-50	0	0	0	1	0	0	0	0.1	1.1	1.3
	50-100	1	0	0	0	1	0	2	0.6	2.4	2.9
	100-500	2	1	1	1	3	1	5	2.0	4.6	6.6
	>500	0	0	0	0	1	0	0	0.1	1.1	1.3
PS	1-50	1	0	0	0	0	0	0	0.1	1.1	1.3
	50-100	0	0	0	0	0	0	0	0.0	0.0	0.0
	100-500	0	0	0	0	0	0	0	0.0	0.0	0.0
	>500	0	0	0	0	0	0	0	0.0	0.0	0.0
PET	1-50	0	0	0	0	0	0	0	0.0	0.0	0.0
	50-100	0	1	0	0	0	0	0	0.1	1.1	1.3
	100-500	0	0	0	0	0	0	0	0.0	0.0	0.0
	>500	0	0	0	0	0	0	0	0.0	0.0	0.0
EVA	1-50	0	0	0	0	0	1	0	0.1	1.1	1.3
	50-100	0	0	0	0	0	0	0	0.0	0.0	0.0
	100-500	0	0	0	0	0	0	0	0.0	0.0	0.0
	>500	0	1	0	0	0	0	0	0.1	1.1	1.3
PA	1-50	0	0	0	0	0	1	1	0.3	1.5	1.7
	50-100	0	0	0	0	0	0	0	0.0	0.0	0.0
	100-500	0	0	0	0	0	0	0	0.0	0.0	0.0
	>500	0	0	0	0	0	0	0	0.0	0.0	0.0
PTFE	1-50	0	0	0	0	0	0	0	0.0	0.0	0.0
	50-100	0	0	0	0	0	1	0	0.1	1.1	1.3
	100-500	0	0	0	0	0	3	1	0.6	3.4	4.0
	>500	0	0	0	0	0	0	0	0.0	0.0	0.0
Cellulose	1-50	0	0	0	1	2	3	5	1.6	5.7	7.3
	50-100	0	0	0	0	0	6	0	0.9	6.8	7.7
	100-500	3	2	0	0	0	2	2	1.3	3.8	5.0
	>500	0	0	0	0	0	3	1	0.6	3.4	4.0

Table 1: Results for the analyses of seven procedural blank samples, along with the calculated LOD.

First set of experiments, which consisted of one tap-water sample, one type II water sample and one Arium®-purified type I water sample (see Figure 2), was done in order to see if the Arium® purification device leached microplastics into the product water.

Results of the analyses are shown in the Table 2. These results show that all three types of water samples, contained a number of particles smaller than the method LOD. This provides the necessary evidence to state that the Arium system does not leach a detectable amount of microplastic particles into the water it produces.

Polymer Type	Size Range ( $\mu\text{m}$ )	1st Experimental Setup								
		Tap Water			Type II Water			Arium® Water		
		Number of Particles			Number of Particles			Number of Particles		
		1	2	Average	1	2	Average	1	2	Average
PE	1- 50	0	6	3	2	0	1	4	1	2.5
	50 - 100	0	1	0.5	0	0	0	1	1	1
	100 - 500	1	0	0.5	0	0	0	0	0	0
	> 500	0	0	0	0	0	0	0	0	0
PP	1- 50	0	1	0.5	0	0	0	0	0	0
	50 - 100	0	1	0.5	2	1	1.5	0	2	1
	100 - 500	0	1	0.5	2	5	3.5	1	5	3
	> 500	0	0	0	0	0	0	0	0	0
PTFE	1- 50	0	1	0.5	0	0	0	0	0	0
	50 - 100	0	0	0	0	0	0	1	0	0.5
	100 - 500	0	0	0	0	0	0	3	1	2
	> 500	0	0	0	0	0	0	0	0	0
PS	1- 50	0	0	0	2	0	1	0	0	0
	50 - 100	0	0	0	0	0	0	0	0	0
	100 - 500	0	0	0	0	0	0	0	0	0
	> 500	0	0	0	0	0	0	0	0	0
EVA	1- 50	1	0	0.5	0	0	0	1	0	0.5
	50 - 100	0	0	0	0	0	0	0	0	0
	100 - 500	1	0	0.5	0	0	0	0	0	0
	> 500	0	0	0	0	0	0	0	0	0
PA	1- 50	0	0	0	0	0	0	1	1	1
	50 - 100	0	0	0	0	0	0	0	0	0
	100 - 500	0	0	0	0	0	0	0	0	0
	> 500	0	0	0	0	0	0	0	0	0
Cellulose	1- 50	0	0	0	0	1	0.5	3	5	4
	50 - 100	0	1	0.5	0	1	0.5	6	0	3
	100 - 500	1	0	0.5	1	3	2	2	2	2
	> 500	0	0	0	0	0	0	3	1	2

Table 2: Results for the first experimental setup (refer Figure 2).

Second set of experiments was performed in order to see if the system retained the particles introduced to the system from the feed water (refer Figure 3). The setup consisted of one type II water sample spiked with 10, 25 and 70 µm polystyrene (PS) microspheres, one Arium®-purified water sample obtained after consuming 9, 14 and 19 L of PS microsphere-spiked type II water (three separate samples) and finally two Arium®-purified water samples, where the first 1 L sample was taken after consuming 3 L of non-spiked type II water, and the other after 5 L. Results of the analyses of samples in the second experimental setup are shown in Table 3.

Results for the two analyses of water spiked with PS particles show that PS particles were clearly detected before subsequent water purification. In contrast to these results, analyses of Arium®-purified water samples obtained after consuming 9, 14 and 19 L of PS microsphere-spiked type II water showed that PS particles do not get transferred into the final product water. Furthermore, results show that even after swapping PS-spiked type II water with clean type II water, the PS microparticles are not being washed out of the system. This indicates that the Arium® purification system retains all particles introduced to the system and prevents them from ending up in the final product.

Polymer Type	Size Range (µm)	2nd Experimental Setup											
		Type II water + PS			Purified spiked water after 9L			Purified spiked water after 14L			Purified spiked water after 19L		
		Number of Particles			Number of Particles			Number of Particles			Number of Particles		
		1	2	Average	1	2	Average	1	2	Average	1	2	Average
PS	1 - 50	115	53	84	0	0	0	0	0	0	0	0	0
	50 - 100	44	49	46.5	0	0	0	0	0	0	0	0	0
	100 - 500	20	0	10	0	0	0	0	0	0	0	0	0
	> 500	0	0	0	0	0	0	0	0	0	0	0	0

Table 3: Results for the second experimental setup – spiking experiments (refer Figure 3).

Polymer Type	Size Range (µm)	2nd Experimental Setup					
		Purified type II water after 3L			Purified type II water after 5L		
		Number of Particles			Number of Particles		
		1	2	Average	1	2	Average
PS	1 - 50	0	0	0	0	0	0
	50 - 100	0	0	0	0	0	0
	100 - 500	0	0	0	0	0	0
	> 500	0	0	0	0	0	0

Table 4: Results for the second experimental setup – washing the system with clean type II water.

## RETURN ON INVESTMENT

The cost analysis provided over a one-year period, as shown in Figure 5 clearly highlights the advantages of transitioning to in-house treated water. With a daily demand of two litres, the investment in the treatment device starts to yield significant financial benefits in as little as five months, ultimately resulting in substantial cost savings within the course of a year. Furthermore, this approach aligns with sustainability goals by eliminating the need for glass bottles, reducing pollution associated with shipping, and eliminating the necessity for extensive storage space.

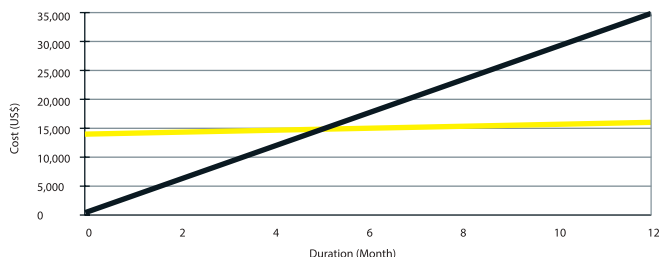


Figure 5: Comparison of expenses between In-house produced Arium®-water Type I (ultrapure water, yellow) and bottled water (VWR: Water Reag. Ph. Eur. 1095507 particle-free, 21.11.2023; 72 US\$ per liter, black). Calculation based on following assumptions: two liters water consumption per working day, 20 working days per month, Arium® Pro VF system plus consumables and annual consumables (list price) and costs of bottled water.

## CONCLUSION

Two different kinds of testing protocols were tested with the Arium® Pro VF system. The first test setup showed that no microplastic contaminations were leached out from the device when deionized water was introduced to the machinery.

The Arium® Pro VF system also removed microplastic particles efficiently from water which was purposely spiked with high amount of microplastics.

The Arium® Pro VF system can be used when laboratories need to be extra sure that no unwanted microplastic particles can contaminate the water used in the laboratory.

## REFERENCES

1. ISO 24187:2023; Principles for the analysis of microplastics present in the environment
2. Sridhar, A., Kannan, D., Kapoor, A., Prabhakar, S. Extraction and detection methods of microplastics in food and marine systems: A critical review, Chemosphere 286, 131653 (2022).
3. Iackburn, K., Green, D. The potential effects of microplastics on human health: What is known and what is unknown. Ambio 51, 518–530 (2022).
4. Gambino, I.; Bagordo, F.; Grassi, T.; Panico, A.; De Donno, A.: Int J Environ Res Public Health, 2022 Apr 26, Occurrence of Microplastics in Tap and Bottled Water: Current Knowledge
5. <https://echa.europa.eu/fi/hot-topics/microplastics>



## Arium® Pro Ultrapure Laboratory Water Purification System

# FLEX SWILE FOR NMR LCMS SAMPLE PREP

The preparation of NMR and / or LC-MS samples is often still done manually and binds highly qualified resources to very time-consuming, tedious and error-prone tasks.

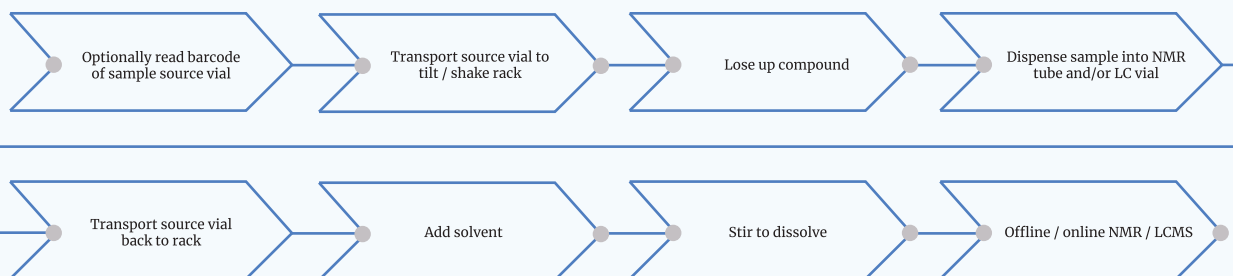
The SWILE technology enables automated true one-to-one gravimetric "pick & decision dispense" of solid compounds directly from sour vials. The scheme at the bottom of this page displays the simplified SWILE workflow including the precision "pick & decision dispense" step. The technology backbone is based on Chemspeed's proprietary overhead gravimetric dispensing tool design in combination with a second analytical on-deck-balance.

In order to exclude any risk of cross-contamination disposable glass tips are used which are stored and provided by the automated SWIN dispenser.

The SWINs are available in different sizes (diameter) and can be adjusted according to the desired target amount to be dispensed. Additionally, a tilt / shake rack is used to loosening up and tilting the powder prior to pick-up.

- ▶ Revolutionary accuracy & precision due to decision dispensing
- ▶ Dispensing range from 100's  $\mu\text{g}$  to about 5 mg with +/- 10  $\mu\text{g}$  resolution with additional on-deck balance
- ▶ No cross-contamination
- ▶ No dead volume
- ▶ Fully inert (glass)
- ▶ Unattended operation

## EXAMPLE WORKFLOW FLEX SWILE NMR



## BENEFITS

- ▶ Proprietary robotic tool exchange interface.
- ▶ Ventilated hood for safety and conditioned atmosphere.
- ▶ Optimized footprint (3x3 ft, 90x90 cm) versus capacity – all while reducing costs and maximizing return on investment.
- ▶ SWILE Robotic Tool can be combined with other tools to accommodate multiple workflows such as on-deck balance, tilt / shake rack, barcode reader, multigripper.
- ▶ Automated sample dispensing into NMR tubes and LC vials (optional on-deck balance for +/- 10 µg resolution).
- ▶ Gravimetric and / or volumetric liquid handling for e.g. dissolution combined with e.g. tumble stirrer, shaking modules.
- ▶ AUTOSUITE SOFTWARE – drag & drop experimentation with easy interface (e.g. python custom device) to e.g. LIMS, ELN, data analysis, Bruker sample case, Agilent / Shimadzu / Thermo / Waters autosamplers.

## CASE STUDY

### AUTOMATING CATALYST DISCOVERY WITH CHEMSPEED

#### How robotic synthesis accelerates insights into NO–CO interaction on Pt-based catalysts

## BACKGROUND

In automotive and industrial emission control, platinum-based catalysts are crucial for oxidizing carbon monoxide (CO) and reducing nitrogen oxides (NOx). Yet, the simultaneous presence of CO and NO dramatically alters catalyst structure and performance, making it challenging to design more stable and efficient materials. Understanding these structure–reactivity dynamics demands both precise synthesis and operando-level characterization.

## THE CHALLENGE

Traditional catalyst preparation methods suffer from variability in impregnation and drying steps, leading to inconsistent dispersion of noble metals such as Pt. Such inconsistencies obscure structure–activity correlations, especially when subtle redox interactions—like the competitive adsorption of NO and CO—must be analyzed with high precision.

Researchers required a reproducible, automated synthesis process that could:

- ▶ Precisely control metal loading and dispersion,
- ▶ Standardize sample preparation across multiple catalyst supports, and
- ▶ Interface seamlessly with operando spectroscopy workflows.

## THE CHEMSPEED ADVANTAGE

Using the Chemspeed Accelerator SLT106 robotic synthesis platform, scientists automated the multi-step synthesis of Pt/Al<sub>2</sub>O<sub>3</sub> and Pt/CeO<sub>2</sub> catalysts.

Key automation–enabled advantages included:

- ▶ Robotic liquid handling and dosing for reproducible impregnation with tetraammineplatinum(II) nitrate.
- ▶ Controlled drying under reduced pressure ensuring uniform metal distribution.
- ▶ Automated repetition of impregnation cycles, improving active site dispersion.
- ▶ Seamless integration of reaction parameters and synthesis metadata for traceability and reproducibility.

This high-throughput synthesis workflow produced a library of catalysts with consistent 1–1.9 wt% Pt loadings and finely tuned dispersion, enabling downstream operando studies without batch variability.

## RESULTS & INSIGHTS

With standardized catalysts from the Chemspeed platform, the team conducted spatially resolved operando X-ray absorption spectroscopy (XAS) and in situ diffuse reflectance infrared Fourier transform spectroscopy (DRIFTS) to map Pt oxidation states along the catalyst bed.

The results revealed:

- ▶ NO competitively adsorbs with CO, hindering CO oxidation activity.
- ▶ NO induces higher oxidation states of Pt, delaying reduction and formation of active Pt clusters.
- ▶ A reductive pretreatment restores catalyst performance, yielding a more uniform reduced Pt state across the reactor bed.

These findings directly linked reaction mixture composition to noble metal redox dynamics, offering critical design parameters for next-generation three-way catalysts.

## IMPACT

By employing Chemspeed's automated synthesis technology, researchers:

- ▶ Reduced synthesis variability and experimental error,
- ▶ Accelerated multi-sample catalyst screening, and
- ▶ Enabled deeper mechanistic understanding through consistent materials and operando data.

## REFERENCES

Gashnikova, D.; Struzek, S.; Maurer, F.; Bauer, M. R.; Maliakkal, C. B.; Kübel, C.; Casapu, M.; Grunwaldt, J.-D. Complementary and Spatially Resolved Operando Spectroscopic Investigation of Pt/al<sub>2</sub>O<sub>3</sub> and Pt/CeO<sub>2</sub> Catalysts during CO/NO Conversion. *The Journal of Physical Chemistry C* 2025, 129 (31), 13923–13938. <https://doi.org/10.1021/acs.jpcc.5c01963>.  
<https://www.chemspeed.com/news/complementary-and-spatially-resolved-operando-spectroscopic-investigation-of-pt-al2-o3-and-pt-ce-o2-catalysts-during-co-no-conversion/>



# NEXTA® DSC series

**Differential Scanning Calorimeter (DSC)**  
**The technology behind world-class performance.**

*NEXTA DSC series, Hitachi's latest series of differential scanning calorimeter (DSC), delivers superior sensitivity with exceptional baseline stability.*

## Features

- ▶ World-class baseline repeatability: Advanced heat-flow sensor and three-layer low-heat-capacity furnace insulation ensure uniform heat transfer, exceptional baseline stability, and unmatched repeatability.
- ▶ World-class sensitivity: Proprietary thermopile-type DSC sensor with multiplexed thermocouples delivers ultra-high sensitivity ( $\leq 0.1 \mu\text{W}$ ), enabling precise measurement of small samples.
- ▶ Wider temperature range for Real View® DSC: A built-in 2 MP camera with a heated viewport enables visual observation from room temperature down to  $-50^\circ\text{C}$ .
- ▶ Modulated DSC separates overlapping transitions and simplifies Cp measurement.

**HITACHI**  
Inspire the Next

## Specifications

Parameter	DSC600	DSC200
Measurement principle	Heat Flux	
Temperature range	-150°C ~ 725°C	
DSC dynamic range	±100mW	±200mW
RMS noise / Sensitivity	0.05µW / 0.1µW	0.1µW / 0.2µW
Calorimetric precision	±0.05% (Calculated from standard deviation (1σ/average value in 10 consecutive measurements))	
Baseline repeatability	±5µW (* Electrical Cooling Unit: -50~300°C, 10°C/min)	
Programmable rate	0.0°C ~ 100°C/min	
Purge gas	Air, Inert gas	
Purge gas control	Mass flow controller, 2 lines	
Auto Sampler *	Max. 50 samples	
Electrical Cooling Unit *	-80°C ~ 500°C	
Auto LN2 Gas Cooling Unit *	-150°C ~ 725°C	
Auto Air Cooling Unit *	Ambient ~ 725°C	

## Real View® Thermal Analysis

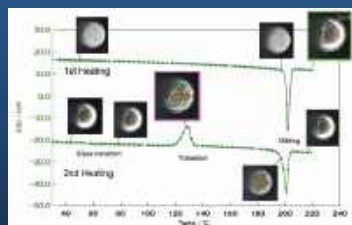
### VISIBLY BETTER THERMAL ANALYSIS

Understand how your samples will perform with Hitachi thermal analyzers.

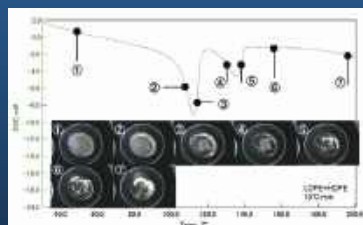
## Advantages

- ▶ Because the information you have obtained has increased, it now becomes easier to analyze data
- ▶ You can obtain the resulting knowledge from phenomena that you have not noticed until now
- ▶ It will be easier to analyze the causes of abnormal phenomena

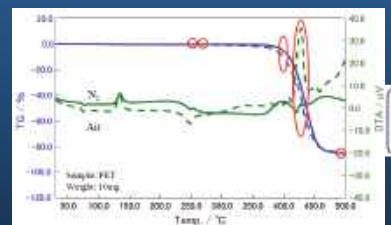
Real View® DSC of Salicilin



Compatibility observation of LDPE and HDPE



Observation of Decomposition Behavior of PET in Real View®





## Mettler Toledo SevenExcellence™ and MX Balance: Precision-Linked pH-Balance Integration

A unified workflow for faster, guided, and fully documented buffer and media preparation

From preparing buffered mobile phases to liquid growth media, making solutions of defined composition and pH is a routine task in many laboratories. Skilled technicians can handle this task easily – but looking up different recipes and filling out documentation takes time.

Combining a SevenExcellence pH meter and an MX balance helps new and experienced users to simplify this task, by providing instructions on screen, adding all information to a common report, and even calculating concentrations and checking that weighing results and pH values are within the desired tolerance.

## INTRODUCTION

This detailed guide shows how a SevenExcellence pH meter and a MX balance can be used together to prepare and measure buffers and similar solutions easily and consistently. A basic example is explained in detail, and options for further development are shown.

### Background

Weigh, dissolve, and measure pH. This is a typical sequence of steps for preparing solutions in the laboratory, especially if the performance of the solution is dependent on the correct pH value or if the pH value itself is the goal of the analysis.

Typical cases include:

- Buffer preparation
- Culture media preparation
- Pharmacopoeia pH checks (typically involve dilution of a certain amount of sample in a certain amount of solvent, then pH must be in a certain range)

Traditionally, this type of workflow would be carried out across different instruments (balance, magnetic stirrer, pH meter) and documented manually (e.g., in a lab notebook – electronic or paper-based – or printed form).

However, working across various instruments and manually documenting the results is time-consuming.

A more advanced alternative is connecting the different devices for seamless workflow and effortless documentation. This solution presents two important advantages:

- Single workflow with user guidance on a single screen
- Single printout report documentation

The following sections provide step-by-step guidance on connecting SevenExcellence to MX laboratory balance and setting up an efficient workflow for formulation and pH measurement. It also offers insights into expansion possibilities with a printer, uMix stirrer, or additional weighing steps.

## MATERIALS

The following equipment is needed:

- SevenExcellence with pH module
- Sensor
- Calibration solutions
- uPlace electrode arm
- Optional uMix stirrer
- SICS capable precision balance (e.g. MX)
- USB-A to RS232 auxiliary instrument adapter cable (51105856) (remove the jackscrews if necessary to ensure fit with the connector on a balance)
- Optional printer (e.g. USB P-25)
- USB-A to RS232 converter cable (30576241)

## METHOD

Attach the USB-A plug of the auxiliary instrument adapter (51105856) to the pH meter. Connect the RS232 plug to the RS232 port of the adapter cable (30576241). Finally, insert the remaining USB-A plug into the USB-A port of the MX balance.

## BALANCE SETUP:

Prepare the MX balance to receive MT-SICS commands. Navigate to Settings and select Services:



Activate MT-SICS Service and choose USB-RS232 converter as Interface.



Activate Transfer data and choose MT-SICS service as transfer option.



Set up SevenExcellence as an Auxiliary Instrument



## SEVENEXCELLENCE SETUP

Prepare SevenExcellence method according to workflow needs.



Activate Transfer data and choose MT-SICS service as transfer option.



Insert method functions to match the desired workflow



Details of Auxiliary Instrument method function for a tare step.



Details of Auxiliary Instrument method function for a weighing step, part 1.



Details of Auxiliary Instrument method function for a weighing step, part 2



The SevenExcellence method provides a great deal of flexibility, including e.g., the display of custom instructions at any point in the method. The above illustration shows a typical scheme for a simple workflow.

The user is instructed what to place on the balance.

After confirmation, the SevenExcellence instructs the balance to execute the corresponding step (Tare or Weigh). Once the sample preparation steps are completed, the concentration is calculated based on actual weight and the pH value is measured.

This basic workflow can be expanded in a variety of ways, including:

- The addition of a printer (strip printer or network printer) to easily document weighing and measurement results on a single printout
- Connecting a uMix stirrer to support the dissolution of the components with magnetic stirring

- Additional weighing steps for further recipe components

This technical note shows how to make sample preparation processes efficient, straightforward, and consistent by connecting SevenExcellence and MX laboratory balance. It also provides guidance on setting up a basic recipe with a gravimetric calculation of concentration and obtaining seamless documentation in a single printout.

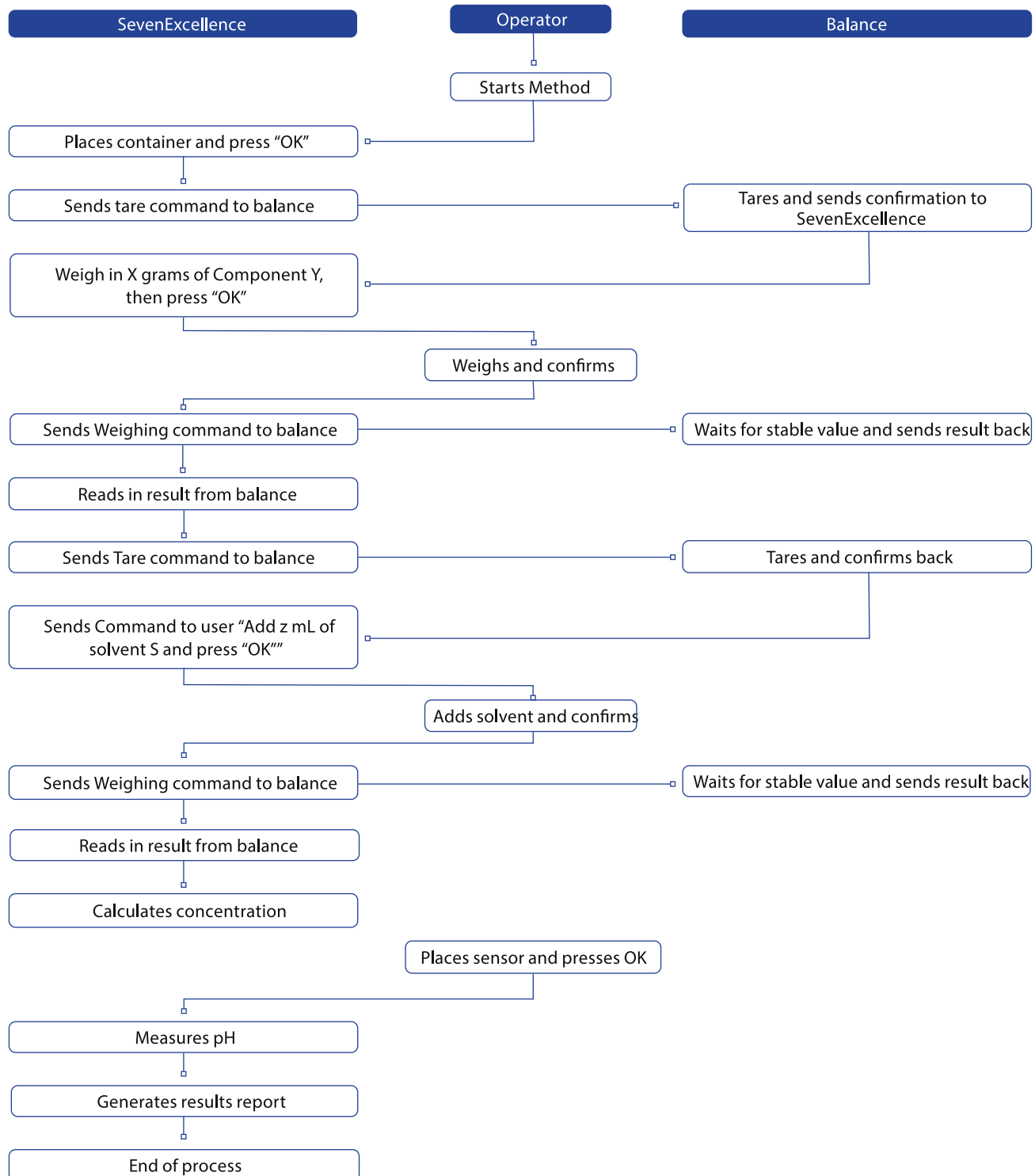


## SevenExcellence pH meter S400-uMix-Kit

### MX precision balance



## STEP-BY-STEP REPRESENTATION OF WORKFLOWV



# THE **BWB** FLASH FLAME PHOTOMETER

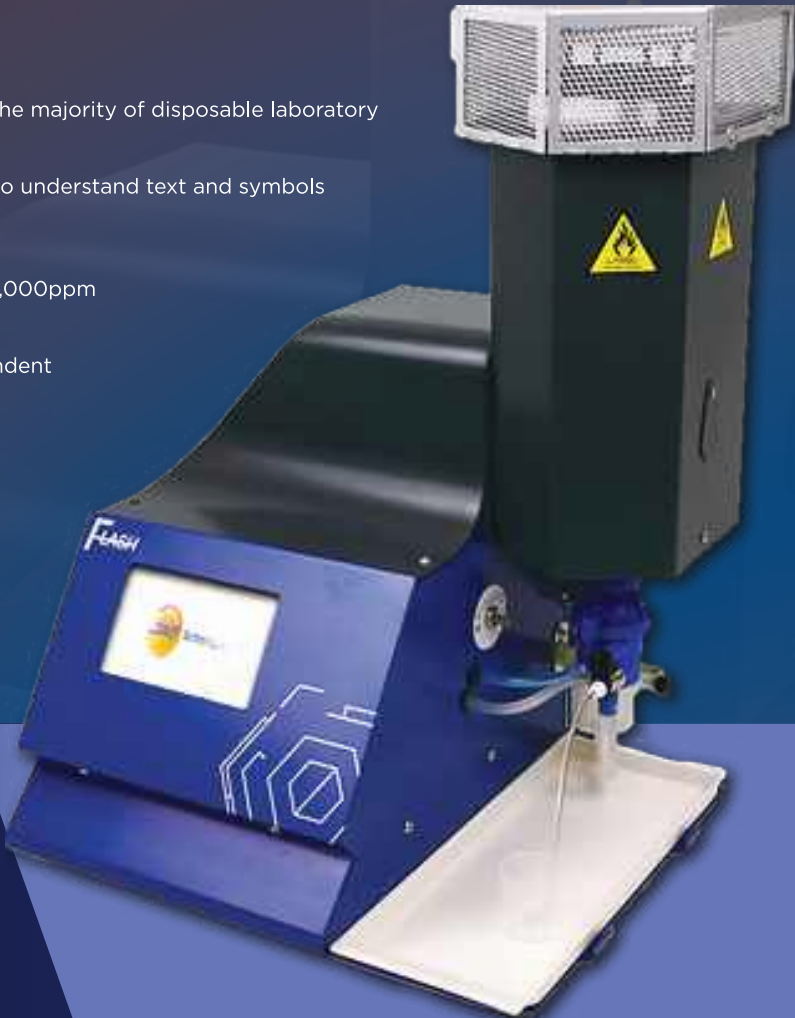
The first simultaneous flame photometer with built in compressor and configurable element analysis to your requirements.

## Features

- ▲ Large 5" touch screen display compatible with the majority of disposable laboratory gloves
- ▲ True ease of use with large buttons and simple to understand text and symbols
- ▲ Built-in air compressor and gas regulator
- ▲ Calibration standards supplied as standard in 10,000ppm concentrations
- ▲ Auto-read technology enables operator independent determination of results
- ▲ User selectable decimal places
- ▲ IQ, OQ, PQ web-based certification available: IQ OQ PQ is completely unique to the analytical instrumentation arena.
- ▲ Complete set of basic labware included to get you started

## Technical Data

Sample rate	2.5 – 4ml/min	
Optimal range	Single point calibration Na 0.1 – 60ppm K 0.05 – 100ppm Li 0.05 – 50ppm Ca 1.0 – 100ppm	
Limit of detection (LOD) and limit of quantification (LOQ)	LOD Na – 0.03ppm K – 0.02ppm Li – 0.02ppm Ca – 0.3ppm	LOQ Na – 0.1ppm K – 0.05ppm Li – 0.05ppm Ca – 1ppm
Fuel requirement	Propane, Butane or Natural Gas* regulated to 19Bar. Flow rate of 0.4l/min <small>*with modifications</small>	



# Purification Of Bioactive Peptides from Complex Mixtures Using the puriFlash® 5.250 PrepLC and Expression® CMS Detector

## High-purity isolation of Casein macropeptides

Changtong Hao,  
Advion Interchim Scientific

**I**n this application note, we use whey protein isolate and two casein macropeptides as an example to demonstrate the isolation and purification of bioactive peptide components with a system comprised of a puriFlash® 5.250 prepLC coupled online to an expression® CMS detector.

### Keywords or phrases:

Mass Spec: expression® CMS Flash:  
puriFlash® 5.250 prepLC, HPLC: AVANT®

**puriFlash®  
5.250**



## INTRODUCTION

In recent years, biopharmaceutical companies have increasingly embraced peptide/protein-based drugs due to their enhanced specificity and selectivity compared to traditional small molecule drugs. However, the purification of peptides/proteins during the drug discovery process is crucial to ensure the safety and efficacy of the final product.

Attaining the highest possible purity levels for the bioactive target compounds is essential in minimizing the risk of toxicity and complying with regulatory standards.<sup>[1,2]</sup> Whey protein isolate, a by-product of cheese production, contains various glycomacrocptides and two significant bioactive peptides, casein macropeptide A (CMPa) with a molecular weight (MW) of 6757 Da and casein macropeptide B (CMPb) with a MW of 6787 Da. Extracting and purifying individual components, such as casein macropeptide, is essential for investigating their bioactivity.<sup>[3]</sup>

In this application note we use whey protein isolate and two casein macropeptides as an example to demonstrate the isolation and purification of bioactive components with a system comprised of a puriFlash® 5.250 prepLC coupled online to an expression® CMS detector. This combination offers higher selectivity and sensitivity compared to traditional detectors such as UV or ELSD, which may not effectively respond to bioactive target peptides and proteins.

## METHOD

### Preparation of Whey Protein Isolate

- ▶ The casein macropeptide isolation procedure used in this application is based on Tadao Saito's work<sup>[4]</sup> with some modifications.
- ▶ A 50 g sample of whey protein isolate purchased from local grocery store was combined with 500 mL of a solvent mixture of 70% water and 30% methanol (v/v). The mixture was sonicated at 70°C for 90 minutes and then filtered under reduced pressure.
- ▶ The resulting filtrate was concentrated to a volume of

- ▶ 300 mL by removing methanol using a rotary evaporator under reduced pressure at 40 °C. It was then stored at 4°C for one hour. Subsequently, an equal volume of cold ethanol was added to the solution, and the mixture was vortexed for 5 minutes before being stored at 4°C for an additional 4 hours.
- ▶ The mixture was filtered under reduced pressure using a 0.5 µm filter. The final filtrate was then concentrated to a volume of 50 mL using a rotary evaporator under reduced pressure.
- ▶ A 100 µL aliquot of the concentrated extract was mixed with 900 µL of deionized (DI) water for analytical HPLC/MS analysis.
- ▶ The remaining filtrate was used for peptide purification using the puriFlash® 5.250 PrepLC system coupled with an expression® CMS detector.

### Analytical HPLC/MS Method Setup

The liquid extract from whey protein isolate was first analyzed using an AVANT® HPLC/CMS system and a chromatography separation method developed for the 4.6 mm column used (Table 1). Figure 1a shows the HPLC/MS chromatogram of the liquid extract. The averaged MS spectra from the peak at 6.44 min indicates that the compound is a multiply charged peptide with at least five masses at  $m/z$  755.2, 849.4, 970.6, 1132.1, and 1358.6 (Figure 1b) forming a charge profile. Through software charge deconvolution, the uncharged mass of the peptide was determined to be 6787.4 Da, indicating casein macropeptide B (CMPb, theoretical mass of 6787 Da) (Figure 1c).

Parameter	Details
HPLC System	Advion Interchim Scientific (AIS) AVANT™ Quaternary UHPLC system
Column	PF15C18HP column, 250x4.6 mm, 15 $\mu$ m HPLC column (AIS)
Mobile Phase	A: 0.1% TFA in water B: 0.1% TFA in ACN
Flow Rate	1.5 ml/min. An adjustable T-splitter was used post column to deliver ca. 1/3 flow to MS and 2/3 of the flow to waste.
Gradient	0.0 min - 27% B 12 min - 35% B 12.1 min - 90% B 15 min - 90% B 15.1 min - 27% B 20 min - 27% B
Injection Volume	15 $\mu$ L
Column Oven	Room temperature (22°C)
MS	AIS CMS-L
Ion Source	Positive ESI
Scan Mode	800–2000 Da

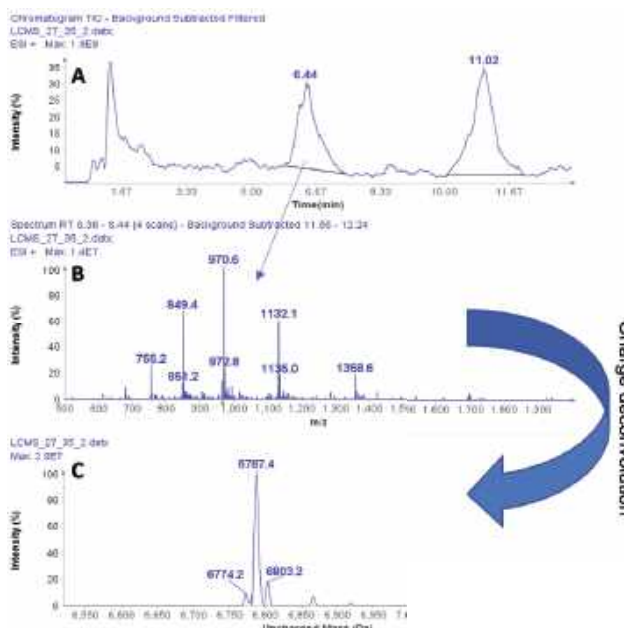


Figure 1: (a) HPLC/MS chromatogram of liquid extract from whey protein isolate, (b) The averaged MS spectra from peak at RT 6.44 min, (c) The deconvoluted, uncharged mass of the peptide eluting peak at RT 6.44 min.

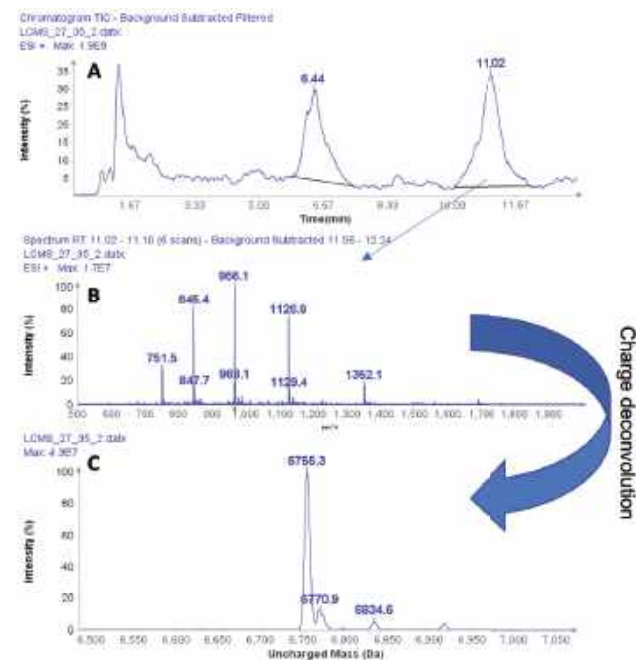


Figure 2: (a) HPLC/MS chromatogram of liquid extract from whey protein isolate, (b) The averaged MS spectra from peak at RT 11.02 min, (c) The deconvoluted, uncharged mass of the peptide eluting at RT 11.02 min.

The averaged MS spectra obtained from the peak eluting at 11.02 min suggest that the compound is also a multiply charged peptide with masses at  $m/z$  751.5, 845.4, 966.1, 1126.8, and 1352.1 (Figure 2b) forming its charge profile. Similarly, charge deconvolution determines the uncharged mass of this peptide to be 6755.3 Da indicating the A variant of casein macropeptide, CMPa with a theoretical mass of 6755 Da (Figure 2c).

## PrepLC/MS Chromatography

In a next step, the analytical separation method was transposed to the larger prep scale from 4.6 mm column ID to 30 mm ID column ID and further optimized for the purification of the two CMPs (casein glyco-macopeptides) on the puriFlash® 5.250 PrepLC/Flash system coupled online to the expression® CMS detector.

The PrepLC-UV/MS chromatogram of the whey protein isolate is shown in Figure 3 and parameters shown in Table 2. Fraction collection was triggered based on the MS signal, chosen for its higher selectivity and sensitivity. XIC of 970–971 Da was used to detect CMPb, and XIC of 965–966 Da for CMPa.

## RESULTS

### Purity Analysis of CMPb

Purity analysis of CMPb in the pooled fractions 11 to 17 is shown in Figure 4. MS analysis shows that four major ions were detected with  $m/z$  at 970.8, 1132.3, 1358.6 and 1968.2 (Figure 4b). With the averaged mass spectra from Figure 4b, the uncharged mass of the peak at 5.94 min was determined to be 6788.4 (CMPb, Figure 4c). However, MS analysis can also detect four minor components at 6758.3, 6773.5, 6804.8 and 6868.4 Da.

The obtained UV purity of CMPb is 86.7% (Figure 4d), but, based on the additional MS data, the compound purity is actually less than that (estimated 80%).

Again, this example shows the value of MS detection of bioactive compounds such as peptide and proteins, and the better specificity of MS detection compared to UV.

Parameter	Details
PrepLC/MS	AIS P5.250 PrepLC/Flash system
Column	PF15C18HP column, 250x30 mm, 15 $\mu$ m PrepLC column (AIS)
Mobile Phase	A: 0.1% TFA in water; B: 0.1% TFA in ACN
Flow Rate	64 ml/min
Gradient (Time vs %B)	0.0 min - 25%   2.0 min - 25%   30.0 min - 50%
Injection Volume	1 ml
Column Oven	Room Temperature (22°C)
UV (nm)	215 nm
MS	AIS CMS-L
Ion Source	Positive ESI
XIC	970-971, 965-966

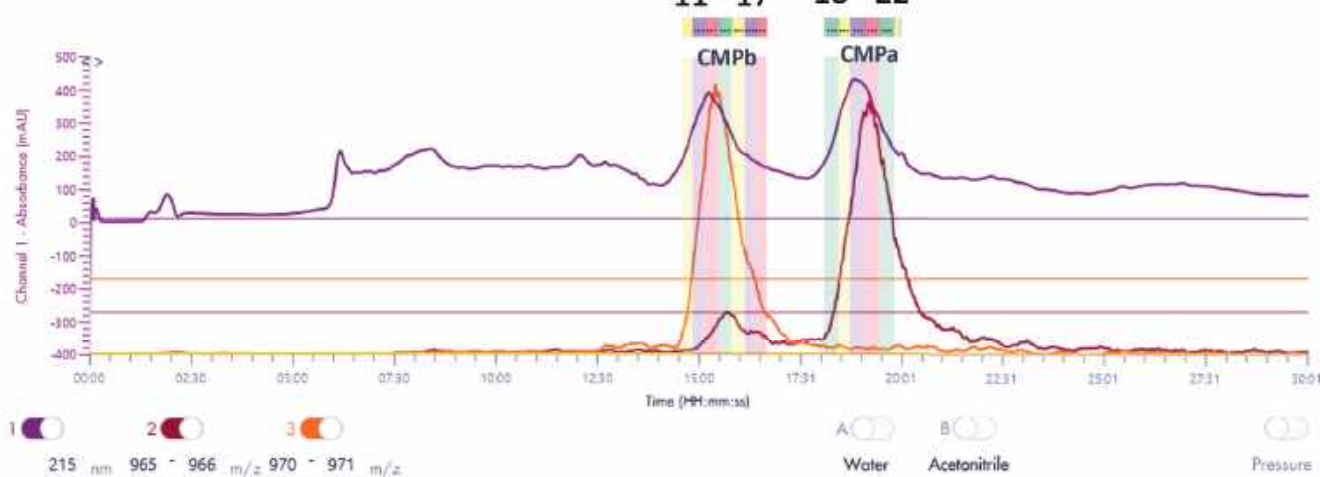


Figure 3: The PrepLC-UV/MS chromatogram of two whey protein isolate

The organic solvent in the combination of fractions 11-17 and fraction 18-22 was removed using a rotary evaporator under negative pressure, and the remaining aqueous solution was dried using a LABCONCO Freezone 2.5L (-50 °C) lyophilizer, resulting in a dry collection of 10 mg each, which was then dissolved in 10 ml of deionized water for subsequent HPLC/UV/MS analysis. The results of the purity analysis are shown in figures 4 and 6.

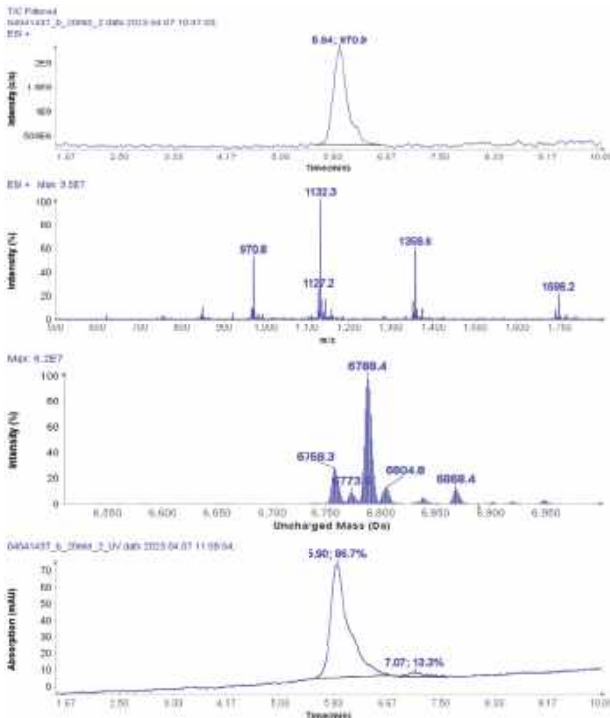


Figure 4: (a) The HPLC-MS chromatogram of pooled fractions of 11-17, (b) Averaged MS spectra of peak eluting at RT 5.94 min, (c) the uncharged mass from (b), (d) The HPLCUV chromatogram of pooled fractions of 11-17.

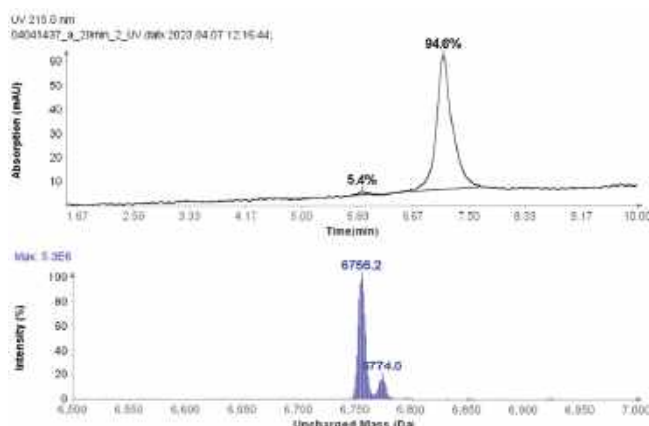


Figure 5: (a) The HPLC-UV chromatogram of pooled fractions of 18-22. (b) deconvoluted uncharged mass of CMPa.

The final overall purity is estimated to be ca. 90%, an excellent value for a bioactive molecule in drug discovery.

Further improvement in purity can be achieved with selective fractions – at the cost of yield. For example, the HPLC-UV/MS analysis of fraction 20 of CMPa (Figure 6a) shows a UV purity of 99.0% (Figure 6d) and no oxidized by-product in the MS analysis.

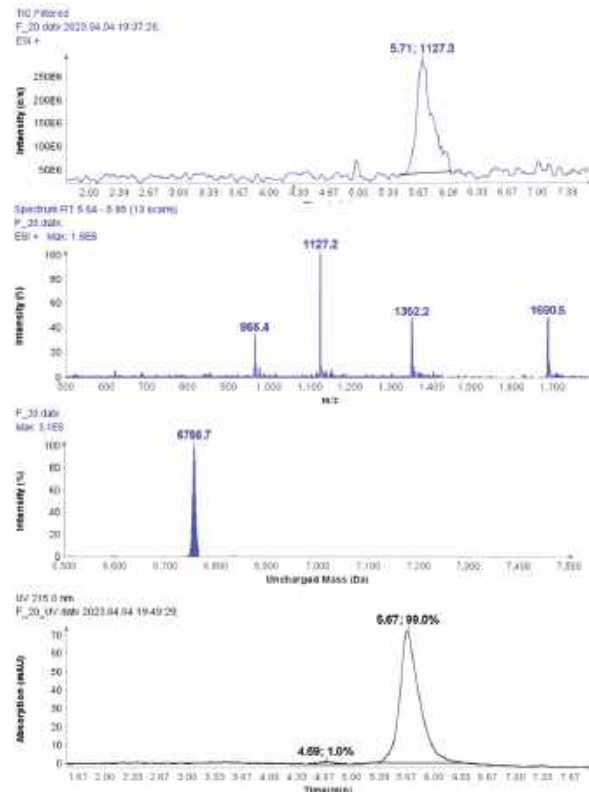


Figure 6: (a) The HPLC-MS chromatogram of fraction 20, (b) Averaged MS spectra of peak at RT 5.71 min, (c) deconvoluted uncharged mass of CMPa (d) The HPLCUV chromatogram of fractions 20.

## CONCLUSION

The puriFlash® 5.250 PrepLC/Flash system, coupled on-line with an expression® CMS detector, achieves outstanding performance, facilitating the selective purification of bioactive macropeptides from a complex matrix with high level of confidence. Compared to UV or ELSD detectors, the mass spectrometer delivers superior selectivity and sensitivity.

An illustrative application of this approach shows the isolation of casein glycol-macro-peptides, resulting in a purity range of 80% (CMPb) to 90% (CMPa) through combined fractions with high yield. Even higher purity of up to 99.0% can be achieved with selective fractions.



# Preparative Separation of Diastereomer Epoxides Using RotaChrom's Centrifugal Partition Chromatography

## Overcome Complex Purification Challenges with RotaChrom's High-Resolution MDM-CPC Technology

**T**his study demonstrates a scalable and environmentally considerate liquid–liquid chromatographic strategy for the preparative separation of nebivolol precursor diastereomers using centrifugal partition chromatography (CPC). By optimizing the biphasic solvent system and operating conditions, the process enabled high-purity isolation of both isomers with excellent recovery and productivity. The method provides a robust alternative to conventional chiral chromatographic separations—eliminating the need for solid stationary phases, minimizing solvent consumption, and ensuring straightforward scalability from laboratory to pilot scale. These results highlight CPC as a sustainable and high-throughput platform for stereoisomeric resolution in pharmaceutical intermediate purification.

### Keywords or phrases:

Nebivolol, diastereomer separation, centrifugal partition chromatography (CPC), liquid–liquid chromatography, achiral resolution, scalable purification, preparative chromatography



## CPC Modeler

## INTRODUCTION

Nebivolol is a selective  $\beta_1$  adrenergic receptor antagonist with nitric oxide-mediated vasodilatory properties utilized in the treatment of hypertension. Diastereomers of an optically active substance are similar in structure, while they usually show significant differences in pharmacodynamic properties. The aim of this study was to develop an achiral liquid-liquid chromatographic (LLC) approach for the efficient and scalable separation of a diastereomer mixture of nebivolol precursors. The starting material consisted of about 57% isomer A epoxide and 31% isomer B epoxide among several other impurities (Figure 1). Centrifugal partition chromatography (CPC) is a preparative LLC technique, where both the stationary and the mobile phase are liquids and resolution is simply governed by the partitioning of solutes between these two immiscible liquid phases. CPC devices use a rotor with interconnected cells instead of a separation column. The rotor can be operated in ascending or descending mode. During the descending mode, the upper phase acts as the stationary phase, while the lower phase functions as the mobile phase, pumped through the column.

In contrast, in the ascending mode, the roles of the phases are reversed, with the upper phase becoming the mobile phase, and the lower phase becoming the stationary phase. This switch in roles, along with changes in flow direction and elution order of the feed components, allows for the effective separation of compounds with limited selectivity. (Figure. 2.). Thus, by adjusting the composition of the utilized solvent system the valuable and unwanted components can be easily fractionated.

The optimal method parameters with lab-scale experiments were found. We screened several different binary and ternary solvent systems to find proper solubility, partition, and selectivity for the diastereomer pair. A lab-scale CPC instrument was used in ascending mode with 14 mL/min flow rate and 2000 rpm rotational speed, 900 mg crude sample was injected in 10 mL mobile phase and the method was 45 min long (Table 1.). In addition, running in ascending mode also facilitated the recovery of the products.

Using our optimized method on a pilot-scale, we managed to isolate both isomers with a throughput of 14.4 g/h, resulting in purity greater than 99% along with a high yield (>90%) (Figure 3). Furthermore, the optimized and tested alkane/alcohol/water biphasic liquid system is considered simple, recyclable, and easily applicable even on pilot-scale or industrial-scale CPC instruments.

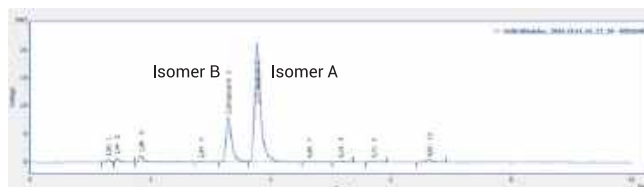


Figure 1. HPLC-UV chromatogram of the crude epoxide mixture, isomers ratio 31:57.

Parameter	Value
Sample	Crude Mixture of Diastereomers
Solvent System	n-Hexane / Methanol / Water
Flow Rate	14 mL / min
Revolution Speed	2000 RPM
Mode	Ascending
Purity (A and B)	99%, 99.9%
Recovery (A and B)	95%, 90%

Table 1. Laboratory-scale CPC runs method parameters.

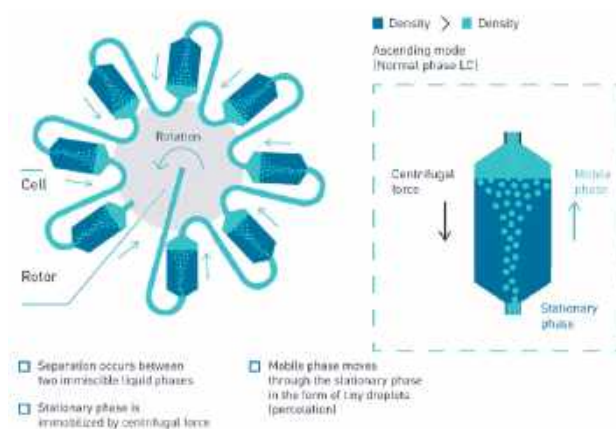


Figure 2. CPC rotor in ascending mode.

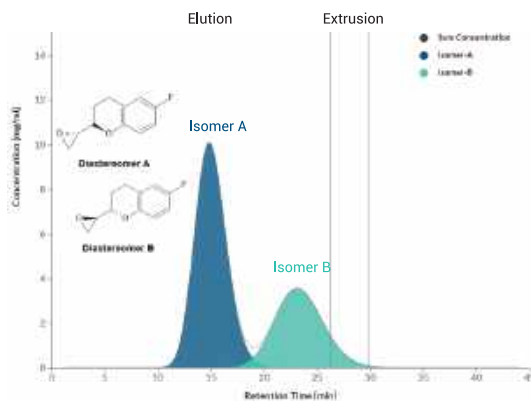


Figure 3. CPC chromatogram of diastereomers in ascending mode.

## CONCLUSION

The developed centrifugal partition chromatography (CPC) method offers an efficient, scalable, and environmentally friendly approach for separating nebivolol precursor diastereomers. By carefully tuning the biphasic solvent composition and operating in ascending mode, both isomers were isolated with high purity (>99%) and excellent recovery (>90%). The method eliminates the limitations of solid-support chromatography, such as column fouling and costly stationary phases, while providing reproducible results suitable for scale-up. Overall, this CPC-based workflow demonstrates strong potential for industrial application in stereoisomer purification and can serve as a model for other complex chiral or diastereomeric separations in pharmaceutical synthesis.



# Polymer-based Reversed-Phase C18HPLC Columns for modern applications: Asahipak ODP-50

## HILIC and SEC-Based Separation Using Shodex Columns

The Asahipak ODP-50 represents a new generation of polymer-based reversed-phase (RP) C18 HPLC columns designed to overcome the chemical and operational limitations of silica-based materials. Its polyvinyl alcohol backbone, functionalized with octadecyl (C18) chains, offers exceptional chemical resistance, long-term stability across a wide pH range (2–13), and superior performance with basic, polar, and high-molecular-weight compounds. This versatility allows for reliable separations in aqueous, organic, or mixed solvent systems—making it suitable for a broad spectrum of analytical and preparative applications. From peptides and proteins to antibiotics and basic drugs, the Asahipak ODP-50 delivers consistent retention, high recovery, and compatibility with mass spectrometry detection due to its low bleed characteristics. These features make it a robust, long-lasting, and cost-effective choice for modern laboratories seeking reproducibility, sensitivity, and sustainability in chromatographic workflows.

### Keywords or phrases:

Polymer-based RP-HPLC, Asahipak ODP-50, C18 column, reversed-phase chromatography, high pH stability, peptide separation, macrolide antibiotics, LC-MS compatibility, column lifetime, polymeric stationary phase.



## Asahipak ODP-50

## INTRODUCTION OF POLYMER RP-C18 COLUMNS

Over 60% of all HPLC applications are Reversed Phase (RP) separations with C18 functional groups. Spherical silica particles proved their use as base material in HPLC columns for many years. To minimize the negative effects of residual silanol groups on the surface, researchers tried end-capping or polymeric coating of the particle and developed hybrid materials. Here we introduce an alternative for these ODS (octadecyl-bonded silica) RP columns:

A polymer particle (for example polyvinyl alcohol) with 5 µm particle size is modified with C18 alkyl chains as functional groups and used as stationary phase. This HPLC column has greater long-term pH stability from 2 to 13. It contains no silanol groups and provides higher resolution for basic substances, for example drugs with tertiary amines (no peak tailing due to unwanted interactions).

Also, the polarity of the polymer gel is slightly more hydrophilic which gives more retention of polar compounds at the beginning of the chromatogram. The polymer-based RP material can be used in 100% water or buffer and a variety of organic solvents (isocratic and gradient separation). It has a pore size of 250 Å which makes it suitable for the analysis of proteins and peptides. The very low bleeding is advantageous for the hyphenation to mass spectrometry (MS) or particle-sensitive light scattering detectors. AC18 column with a stationary phase made of polymer offers more than double the lifetime compared to silica, because it is chemically more resistant.

*Shodex is specialized in polymer-based packing material for Reversed Phase chromatography. The modern column Asahipak ODP-50 (octadecyl-bonded polymer) combines all the advantages of apolymeric RP-C18 column. It is used for small organic molecules, pharmaceuticals, pesticides, hormones, proteins, vitamins and basic drugs.*

## APPLICATIONS ON THE ASAHIPAK ODP-50 COLUMNS

### Proteins and peptides

The Asahipak ODP-50 column has a bigger pore size of 250 Å and is ideal for the separation of molecules like proteins and peptides. Aqueous biological buffers can be used with 100% and organic solvents like acetonitrile or methanol are recommended for flushing. The results show excellent elution volume reproducibility and a high recovery rate.

Column: Shodex Asahipak ODP-50 6D (6.0 x 150 mm, 5 µm)

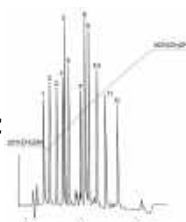
Eluent: (A); 0.05 % TFA aq./CH<sub>3</sub>CN=80/20(B); 0.05 % TFA aq./CH<sub>3</sub>CN=50/50

Linear gradient; (A) to (B), 20 min

Flow rate: 1.0 mL/min

Detection: UV (220 nm) Temperature: 30 °C

Sample: Standard proteins and peptides



Proteins / Peptides	Mw	VR (mL) First Analysis	VR (mL) Second Analysis	Recovery (%)
Lys-Bradykinin	1188	4.63	4.64	97
Bradykinin	1060	5.73	5.7	92
Met-Enkephalin	574	7	7	97
Neurotensin	1673	8.04	8.05	99
Leu-Enkephalin	556	8.47	8.48	100
Substance P	1348	9.24	9.26	93
Bacitracin	1450	11.47	11.44	98
Insulin	5750	12.41	12.25	91
Insulin B chain	3476	12.87	12.89	91
Lysozyme	14300	14.43	14.43	94
Mastoparan	1479	15.97	15.97	98
Myoglobin	17500	18.17	18.18	83

### Antibiotics

Due to the increasing use of antibiotics, it is important to control its purity during production as well as to monitor residues in clinical or food samples to avoid resistance. Macrolide antibiotics give the best peak shape under alkaline conditions with pH 11. Erythromycin can be separated from its derivative Azithromycin. Both are on the World Health Organization's list of essential medicines. The polymeric stationary phase of the Asahipak ODP-60 column is

long-term stable in the range of pH 2 to 13. A smaller particle size of 4  $\mu\text{m}$  was used for better performance.

Column: Shodex Asahipak ODP-40 4E(4.6 x 250 mm, 4  $\mu\text{m}$ )

Eluent: 40 mM Potassium phosphatebuffer (pH 11.0)/CH<sub>3</sub>CN=40/60

Flow rate: 0.5 mL/min

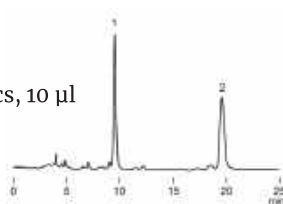
Detection: UV (223 nm)

Temperature: 40° C

Sample: Macrolide antibiotics, 10  $\mu\text{l}$

1. Erythromycin

2. Azithromycin



## Longer lifetime and stability

The Asahipak ODP-50 column has 2.5 times longer lifetime compared to a silica C18 column. This reduces the down time for replacement and the costs per injection. The durability test with NaOH-solution at pH 12 shows the chemical resistance of the column. The retention time and peak form of the tested phenones are stable and reproducible. 100% water can be used in gradient or isocratic runs without dewetting effects. This makes the column suitable also for unexperienced users and for method development in R&D for different kind of samples.

Column: Shodex Asahipak ODP-50 4D(4.6 x 150 mm, 5  $\mu\text{m}$ )

Eluent: 10 mM NaOH aq. (pH 12.0)/CH<sub>3</sub>CN=35/65

Flow rate: 0.6 mL/min Detection: UV (254 nm)

Temperature: 30° C

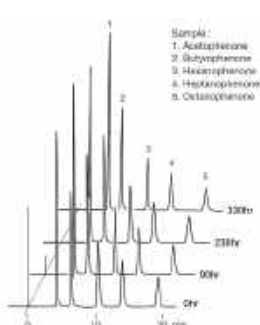
Sample: Durability test with phenones- 1. Acetophenone

2. Butyrophenone

3. Hexanophenone

4. Heptanophenone

5. Octanophenone



## Sensitive mass spectrometry detector (MS)

The Asahipak ODP-50 with a smaller inner diameter of 2.0 mm is used for the LC-MS analysis of basic drugs, scopolamine and atropine (both with tertiary amine group). Polymer-based columns exhibit smaller ionic adsorption (no peak tailing) compared to silica-based columns with residual silanol groups. The separation can easily be performed with less or completely without the addition of salt or non-volatile ion pair reagents. Therefore, there won't be any unpredictable ion suppression during ionization. The lower bleeding of the Asahipak ODP-50 column results in a better signal-to-noise ratio and makes it also suitable for charged aerosol or particle-sensitive light scattering detectors.

Column: Shodex Asahipak ODP-50 2D(2.0 x 150 mm, 5  $\mu\text{m}$ )

Eluent: H<sub>2</sub>O/CH<sub>3</sub>CN=40/60 Flow rate: 0.2 mL/min

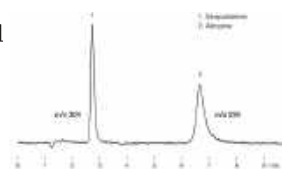
Detection: ESI-MS (SIM, positive mode)

Temperature: 30° C

Sample: Basic drugs, 5  $\mu\text{l}$

1. Scopolamine

2. Atropine



## CONCLUSION

The Asahipak ODP-50 polymer-based RP-C18 column provides a powerful and flexible alternative to traditional silica ODS columns, combining high stability, reproducibility, and wide chemical compatibility. Its performance under extreme pH, excellent recovery of biomolecules, and minimal bleeding makes it particularly well-suited for advanced analytical techniques such as LC-MS. The ability to use 100% aqueous conditions without dewetting further enhances its reliability in both research and routine applications. With its extended lifetime and broad application range—from peptides and proteins to complex pharmaceuticals—the Asahipak ODP-50 stands out as a durable, efficient, and sustainable solution for modern chromatographic analysis.

# Robust Oligonucleotide Impurity Profiling in a GMP Setting Using the Waters SQ Detector 2 Mass Detector

## Streamlined Ion-Pair LC-MS Analysis for Reliable Impurity Detection

Lara Nercessiana, Claire I. Butréa, Damien Mouveta, Cristian I.

Cojocariub, Jonathan Foxb, Arnaud Delobela

a Quality Assistance S.A., Thuin, Belgium

b Waters Corporation, Wilmslow, United Kingdom

**T**his study presents a reliable and easy-to-implement method using the SQ Detector 2 Mass Detector and Empower™ Software for the routine impurity analysis of oligonucleotides in QC laboratories. It offers a practical solution that meets pharmaceutical quality standards while maintaining simple and efficient workflows.

### Keywords or phrases:

- Recombinant Proteins
- Mammalian Expression Systems
- Virus-Sterile Production
- Stem Cell-Derived Biomolecules
- Animal-Free Reagents
- Growth Factors & Cytokines



## ACQUITY UPLC H-Class PLUS System

This study demonstrates the suitability of the Waters™ SQ Detector 2 Mass Detector for oligonucleotide impurity profiling in GMP labs, offering:

- ▶ High-sensitivity mass detection at a fraction of the cost of high resolution mass spectrometry (HRMS).
- ▶ Streamlined GMP oligo impurity profiling, no need for UV integration, or orthogonal separation.
- ▶ Routine-ready MS solution with full Empower Software control, enabling compliance with 21 CFR Part 11.
- ▶ Accurate quantification of truncated oligonucleotides down to 0.1%, with good linearity ( $R^2 > 0.99$ ) and precision of < 6% RSD.
- ▶ Simplified method with robust performance across different instruments, columns, and days.

## INTRODUCTION

Therapeutic oligonucleotides are short synthetic nucleic acid sequences that have gained significant attention for their ability to modulate gene expression.<sup>1</sup> These molecules are chemically modified to enhance their stability and target specificity.

Among the most common modifications are backbone alterations, such as phosphorothioate linkages, and sugar or base modifications. These modifications contribute to the increased resistance to enzymatic degradation. Such modifications introduce considerable analytical challenges, particularly in the accurate assessment of impurities. Oligonucleotide synthesis is typically performed using the phosphoramidite method, a highly efficient stepwise process involving deprotection, coupling, oxidation, and capping steps. Despite the robustness of this method, the synthesis process can produce various impurities, including N-1 species, shortmers, capped sequences, failure sequences, and other side products originating from incomplete or side reactions. These impurities must be

precisely quantified to ensure the safety, efficacy, and regulatory compliance of the final product.

Accurate determination of oligonucleotide purity is a critical step in quality control (QC). Ion-pair reversed-phase liquid chromatography (IP-RP-LC) is widely used for oligonucleotide impurity profiling thanks to its robustness, sensitivity, and compatibility with various detection techniques. However, ultraviolet (UV) absorbance detection alone is insufficient for the comprehensive quantification of all impurities present in the sample. In many cases, full characterization requires the use of multiple orthogonal high-performance liquid chromatography (HPLC) separation techniques to resolve structurally diverse species.

An alternative and powerful approach is to couple IP-RP-LC with mass spectrometry detection, which significantly enhances the analytical capabilities of the method. Among the key factors in method development are the choice of ion-pairing reagents, mobile phase conditions, and detector type. While HRMS, such as quadrupole time-of-flight (QTOF), remains the gold standard for detailed impurity characterization, it may not be ideally suited for routine QC workflows due to its complex handling, cost, and need for a highly trained workforce.

To meet the increasing demand for efficient, cost-effective, and GMP-compliant methods in QC environments, a single quadrupole mass detector, such as the Waters SQ Detector 2 Mass Detector, offers a compelling balance between sensitivity, ease of use, and affordability, and has already been adopted and used for oligonucleotide applications.<sup>2</sup> When coupled with IP-RP liquid chromatography, SQ Detector 2 Mass Detector enables the straightforward quantification of oligonucleotide impurities without the complexity of HRMS platforms.

## EXPERIMENTAL

### Sample Preparation

Oligonucleotide samples matching the sequence of the commercial nusinersen product were selected as model compounds for this study and obtained from an external source. In addition to the full-length product, four truncated

Name	Molar mass (g/mol)	Sequence
FLP	7127.5	5'<T*C*A*-C*T*T*T*-T*C*A*-T*A*A*-T*G*C*-T*G*G>3'
N-1 A	6733.1	5'<C*A*C*-T*T*T*C*-A*A*T*-A*A*T*-T*C*T*-G*G>3'
N-1 B	6708.1	5'<T*C*A*-C*T*T*T*-T*C*A*-T*A*A*-T*G*C*-T*G*C>3'
N-2	6339.7	5'<A*C*T*T*T*C*-A*T*A*A*-A*T*G*C*-T*G>3'
N+1	7521.8	5'<T*C*A*-C*T*T*T*-T*C*A*-T*A*A*-T*G*C*-T*G*G*T>3'

Table 1. List of samples used in the study with their sequences and molar masses.

## LC-MS Conditions

Samples were analyzed using a Waters ACQUITY™ UPLC™ H-Class System equipped with a TUV Detector set at 260 nm, hyphenated to a Waters SQ Detector 2 Mass Detector. Separation was performed on a Waters ACQUITY Premier Oligo BEH™ C18, 130 Å Column (2.1x100mm; 1.7 µm, p/n: 186009485) at a flow rate of 0.3 mL/min using two different sets of mobile phases and conditions for comparison (Table 2). Samples were kept at 5 °C in the autosampler prior to injection on the column (5 µL at 0.1 mg/mL).

Parameter	Conditions 1	Conditions 2
Mobile phase	A: 10% ACN, 5 mM TBuAA, 1 µM EDTA B: 80% ACN, 5 mM TBuAA, 1 µM EDTA	A: 7.9 mM TEA, 380 mM HFIP in H <sub>2</sub> O B: A/MeOH 50/50
Purge solvent	ACN/H <sub>2</sub> O 10/90	MeOH/H <sub>2</sub> O 50/50
Wash solvent	ACN/H <sub>2</sub> O 80/20	MeOH/H <sub>2</sub> O 50/50
Flow rate	0.3 mL/min	0.3 mL/min
Column temperature	60 °C	80 °C

Table 2. Details on the two chromatographic conditions.

The first set of mobile phases used mobile phase A containing 10 % acetonitrile, 5 mM TBuAA, and 1 µM EDTA in water, while mobile phase B was prepared with 80% acetonitrile, 5 mM TBuAA, and 1 µM EDTA in water.

Chromatographic separation was performed at a column temperature of 60 °C. The gradient program started with 1 minute equilibration at 40% B, followed by a linear gradient to 90 % B over 15 minutes. This was maintained isocratically for 2 minutes before immediately returning to the starting conditions in one minute, followed by 6minutes re-equilibration.

The second mobile phase system included mobile phase A, composed of 7.9 mM TEA and 380 mM HFIP in water, and mobile phase B, prepared as a 1:1 mixture of mobile phase A and methanol. The column temperature was maintained at 80 °C. The gradient started at 30% B, increased linearly to 70 % B in 16 minutes held constant for 1 minute, then immediately returned to the starting conditions, followed by an 8minutes re-equilibration plateau.

The LC system was coupled to a SQ Detector 2 Mass Detector operated in negative electrospray mode (ESI-).

The instrument parameters included a capillary voltage of 1.5 kV, source temperature of 150 °C, cone gas flow of 50 L/h, desolvation temperature of 500 °C, and desolvation gas flow of 1000 L/h (Table 3).

In the preliminary phase, MS data were acquired in full scan mode. For the quantification study, specific settings were applied depending on the mobile phase system. For the first set of mobile phases (TBuAA/EDTA), a cone voltage of 60 V was applied, and selected ion recording (SIR) was performed on charge stage 4 of the FLP and its impurities.

Quantification was based on the SIR peak area for all compounds. For the TEA/HFIP system, a cone voltage of 40 V was used, and SIR was acquired on charge states 7 and 8. Quantification was performed as the sum of the two SIR values. All data acquisition and processing were performed using Empower 3 Software.

Parameter	Conditions 1	Conditions 2
Mobile phase	A: 10% ACN, 5 mM TBuAA, 1 µM EDTA B: 80% ACN, 5 mM TBuAA, 1 µM EDTA	A: 7.9 mM TEA, 380 mM HFIP in H <sub>2</sub> O B: A/MeOH 50/50
Purge solvent	ACN/H <sub>2</sub> O 10/90	MeOH/H <sub>2</sub> O 50/50
Wash solvent	ACN/H <sub>2</sub> O 80/20	MeOH/H <sub>2</sub> O 50/50
Flow rate	0.3 mL/min	0.3 mL/min
Column temperatur	60 °C	80 °C

Table 3. SQ Detector 2 mass detector parameters used for the two chromatographic conditions.

### Stability Study

To assess sample stability, repeated injections of the full-length product (FLP) were performed over a 48-hour period using the TBuAA/EDTA mobile phase system before

plotted against the concentration to evaluate the linearity of the response and calculate the individual response factors.

### Accuracy

To assess the accuracy of the method, samples were prepared by spiking the FLP with impurities at defined levels. A mixture of the four impurities in water was spiked into an FLP solution at 0.1 mg/mL (considered 100%) to achieve a final impurity concentration of 1%. The spike solutions were injected in triplicates.

Additionally, a diluted 1% FLP solution was injected separately six times and used as an external calibrant for the MS response. Impurity recovery was calculated as the ratio of the SIR peak area of each impurity in the 1% spiked sample to the SIR peak area of the FLP in the 1% external calibrant solution and corrected by the relative response factor as:

$$\text{Recovery (\%)} = \frac{\text{Area Impurity in 1\% spike-mean (n = 3)} / \text{area impurity in 100\% FLP}}{\text{mean (n = 6)} / \text{area of FLP in 1\% external calibrant}} \times \frac{1}{\text{Response factor}}$$

*The recovery values were reported as the average of the three injections.*

evaluating the method performance. Stability was evaluated by monitoring the FLP UV peak area over time. Evaluation of Method Performance

To ensure a full comparison and robust evaluation of the method, the following tests were performed on two different instruments using two batches of columns over two consecutive days. On the second day, the same experiment was repeated, but the columns were swapped between the systems.

### Linearity

To evaluate the signal linearity and determine the response factors of the different impurities relative to the FLP, a mixture of truncated oligonucleotide species and FLP was prepared and injected. The four different impurities and the FLP were mixed at concentrations of 0.1, 0.5 %, 1%, 2.5% and 5 % and injected using both mobile phase sets. The 0.1% and 1% concentration levels were each injected six times to assess injection repeatability. The resulting peak areas were

## RESULTS AND DISCUSSION

### Method Development

In the initial phase of this study, the chromatographic conditions were optimized for two sets of mobile phases, which are common reversed-phase conditions used for the analysis of oligonucleotides and are based on ion pairing retention mechanisms. As the primary objective was to develop an MS-based method for impurity quantification, chromatographic resolution was not the main focus. Under both conditions, the FLP eluted as a Gaussian peak (Figures 1A and 1B), with a noticeably sharper profile under TBuAA/EDTA conditions. In the preliminary steps, to set up the quantification, data were acquired in full scan mode over a m/z range of 500– 3000. Under TBuAA/EDTA conditions, a predominant charge state was observed, whereas TEA/HFIP produced a wider distribution (Figure 2). The charge state profile obtained using the TEA/HFIP system was particularly sensitive to the cone voltage setting. Lowering the cone voltage to 40 V shifted the

distributions to higher charge states with higher intensities (data not shown). However, the signal was spread across several charge states, decreasing the sensitivity for quantifying impurities. To set up the quantification method, single-ion recording was implemented. Under TBuAA/EDTA conditions, the SIR was based on the ion corresponding to charge state 4. For TEA/HFIP, to mitigate the impact of signal division over several charge states, quantification was based on the summed signals from two charge states (7 and 8). The summation was performed automatically using Empower Software.

In the example of the N-1A impurity, the individual channels m/z 961 and m/z 841 corresponding to charge states 7 and 8, respectively, are shown for the injection of the 100% FLP solution (Figure 3). For further data processing, a method set was created, including the instrument method, the processing method for these channels, and a newly defined “derived channel” based on a formula that calculates the sum of both channels. Once applied, Empower Software automatically performed the summation according to the processing method, generating a new channel C as a sum of channels A and B. During the setup of the method, it was observed that the signal was highly susceptible to system equilibration.

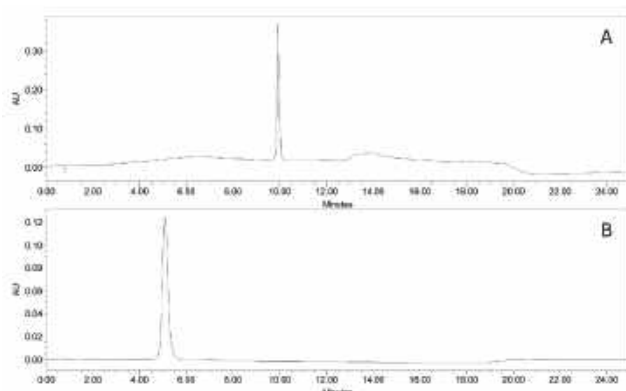


Figure 1. UV260 chromatogram of the FLP in (A) TBuAA/EDTA mobile phases and (B) TEA/HFIP conditions.

Column equilibration with the mobile phase is necessary, and multiple sample injections are required to ensure that both the MS and UV signals are stable.

It was observed that at least 10 injections of a sample were necessary to obtain a stable MS signal. In addition, stability was evaluated by repeated injections of the FLP sample and was confirmed over 48 h as the % RSD on the FLP UV peak area was lower than 2%, indicating that no degradation products were formed.

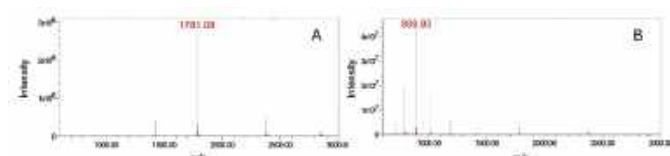


Figure 2. FLP spectra for (A) mobile phase TBuAA/EDTA and a cone voltage of 60 V and (B) mobile phase TEA/HFIP and a cone voltage of 40 V.

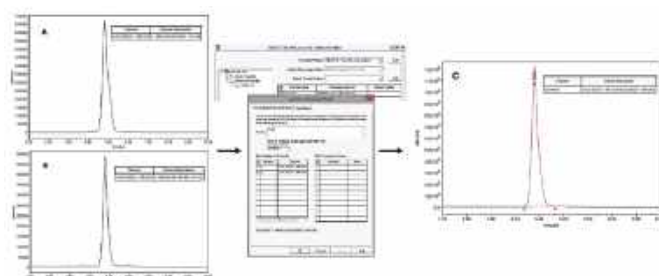


Figure 3. Workflow description of SIR channel sum in Empower. (A) SIR channel at m/z 841 (charge state 8) of FLP solution at 0.1 mg/mL. (B) SIR channel at m/z 961 (charge state 7) of the FLP solution at 0.1 mg/mL. (C) Sum of A and B.

## Method Performance

Once the method was established, both in terms of chromatographic conditions and MS parameters, its performance was evaluated. The first step was to check the MS signal linearity and method sensitivity. Linearity was evaluated for the FLP and four different impurities across a concentration range of 0.1% to 5%. In all cases, a linear response was observed within the studied range (Figure 4). The injection repeatability (% RSD) determined each day for each mobile phase set was below 6% for six injections at 0.1% and below 3% for the six injections at 1% for the FLP as well as the four impurities. From these injections, the signal-to-noise ratio was calculated at the lowest concentration level (0.1%), with all values exceeding 10 and some close to 30, indicating that the method is sufficiently sensitive for impurity quantification down to 0.1% (Table 4). Overall, these S/N values were higher for the TEA/HFIP mobile phase set than for the other set, especially for FLP and the N-1 A impurity. These injections also enabled the

determination of the response factors for impurities (relative to the FLP) based on the slopes of the curves (Table 5). The response factor values were consistent across two days, two column batches, and two SQ Detector 2 Mass Detector instruments. However, the mobile phase significantly influenced the response factors (Table 5). For example, the response factor for the N-1 A impurity was approximately 1.6 for the TBuAA/EDTA system and 0.8 for the TEA/HFIP system.

In the second step, method accuracy was assessed by performing triplicate injections of the FLP solution spiked with known amounts of the four impurities at the 1% level. Overall, the recovery values varied between 86 and 148% (Table 6). For instance, the N-1 A impurity showed an average recovery slightly above 100%, indicating excellent accuracy. In contrast, the N+1 impurity showed higher recoveries, 126 % on average for mobile phases TBuAA/EDTA and 137% for mobile phases TEA/HFIP. These results are consistent with previously published data using single-quadrupole mass spectrometry for oligonucleotide impurity quantification.<sup>3</sup> Finally, it should be noted that the precision of the triplicate injections was acceptable. The percentage RSD determined for the spike impurities are indeed lower than 2% for TBuAA/EDTA mobile phase and lower than 3% for TEA/HFIP mobile phase.

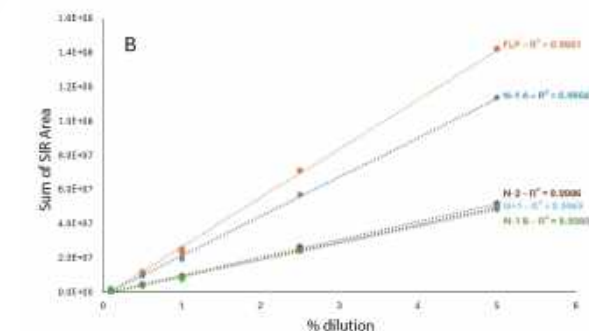
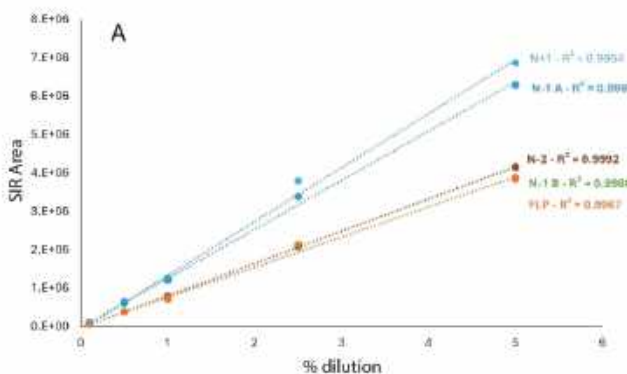


Figure 4. Linearity of response and response factor on day 1 for (A) mobile phase TBuAA/EDTA and (B) mobile phase TEA/HFIP.

	FLP	Impurity N-1 A	Impurity N-1 B	Impurity N-2	Impurity N+1
TBuAA/EDTA	23	41	31	32	53
TEA/HFIP	186	112	34	35	63

Table 4. Method sensitivity assessed by determination of the signal to noise ratio for the different compounds for the two mobile phases set, with charge stage 4 for TBuAA/EDTA and charge state 8 for TEA/HFIP mobile phases.

	Day	FLP	Impurity N-1 A	Impurity N-1 B	Impurity N-2	Impurity N+1
TBuAA/EDTA	Day 1	1.00	1.63	1	1.07	1.79
	Day 2	1.00	1.64	0.96	1.06	1.83
TEA/HFIP	Day 1	1.00	0.8	0.34	0.36	0.35
	Day 2	1.00	0.79	0.35	0.36	0.36

Table 5. Response factors determined for the different impurities on the two mobile phase sets on two days.

Conditions	Impurity N-1 A	Impurity N-1 B	Impurity N-2	Impurity N+1
Day 1	110	126	145	135
Day 2	110	108	148	140

Table 6. Determination of the recoveries for the four different impurities for the two mobile phases on day 1 and day 2.

## METHOD PERFORMANCE AND LIMITATIONS

The developed MS method allowed the accurate quantification of oligonucleotide impurities, with a performance similar to the one presented in a reference study.<sup>3</sup> In addition, MS signal linearity was demonstrated across the range 0.1–5% relative to the FLP concentration. Two sets of mobile phases were compared to evaluate their influence on performance and ease of use.

Suitable method performance was obtained for both sets. However, both have their advantages and disadvantages, and show limited stability over time. With TBuAA/EDTA mobile phases, oligonucleotides eluted as sharp peaks, and the MS spectra showed a predominant charge state, facilitating MS quantification. In contrast, the TEA/HFIP mobile phases resulted in slightly lower chromatographic quality and a more complex charge state distribution profile. This distribution was notably sensitive to the cone voltage settings. However, despite this charge state complexity, higher signal-to-noise ratios were obtained for the TEA/HFIP mobile phase than for TBuAA/EDTA when considering a single charge state (Table 4). Therefore, the selection of the mobile phase should be guided by the specific requirements of the method, particularly in terms of expected sensitivity, chromatographic resolution, and robustness of MS quantification.

## APPLICABILITY AND COMPLIANCE

The developed method enables the quantification of truncated species with acceptable accuracy, precision, and sensitivity using a single quadrupole mass detector. This study presents the example of four impurities, but the results could be extrapolated to other species. For fully phosphorothioate (PS) oligonucleotides, a common impurity is the mono-phosphodiester (mono PO) variant.

One challenge with this impurity is its minimal mass difference with the FLP (16 mass units, corresponding for example to only 2 m/z for charge state 8) making it indistinguishable by a single quadrupole detector without chromatographic separation. This limitation was confirmed by recording the continuum spectra of both the FLP and the mono PO impurity, which showed a large overlap of the signals. For these types of impurities, a high-resolution mass spectrometer or a triple quadrupole mass spectrometer operated in MRM mode is required. For other types of impurities, such as depurinated species, the main limitation is the availability of reference standards.

As observed in this study, the compounds showed different response factors that were influenced by the mobile phase. In the absence of standards, assumptions must be made regarding response factors, introducing uncertainty into the purity calculation.

Finally, the SQ Detector 2 Mass Detector is user-friendly and ideal for routine analyses, such as purity assays. Its integration with Empower Software and full 21 CFR Part 11 compliance make it well suited for GMP applications. Although method setup during development can be somewhat demanding, particularly with TEA/HFIP mobile phases, where summing two SIR channels is necessary to enhance sensitivity, these adjustments are straightforward to implement (Figure 3).

Once optimized, the method can be executed reliably and efficiently in routine workflows, ensuring both compliance and robustness.

## CONCLUSION

The Waters SQ Detector 2 Mass Detector combined with Empower Software provides a reliable, accurate, and GMP-compliant solution for oligonucleotide impurity profiling. The method enables quantification of truncated oligonucleotide impurities down to 0.1%, with strong linearity and precision, without requiring complex instrumentation. Once optimized, the workflow is robust, stable, and efficient, making it ideally suited for routine QC laboratories. The approach supports regulatory compliance while maintaining operational simplicity and cost effectiveness.

## REFERENCES

1. Crooke ST, Witztum JL, Bennett CF, Baker BF. Cell Metabolism, Vol 27, Issue 4, 2018, DOI: 10.1016/j.cmet.2018.03.004
2. Miller M., Lefebvre P., Leightner A., Lauber M.A., Fasth M., Rainville P.D., Shave D. Increasing the Productivity of Oligonucleotide Purification through Column Scaling and Method Optimization. 2024. Waters application note 720008266.
3. Rentel C, Gaus H, Bradley K, Luu N, Kolkey K, Mai B, Madsen M, Pearce M, Bock B, Capaldi D. Nucleic Acid

# LAB TIPS AND TRICKS

## AVOID THE MIX-UP: LABEL FIRST!

Every analytical chemist has faced that quiet moment of doubt – the one where two identical vials sit on the bench, and you can't quite remember which holds what sample.

That's why the golden rule stands: **Label first. Pour later.**

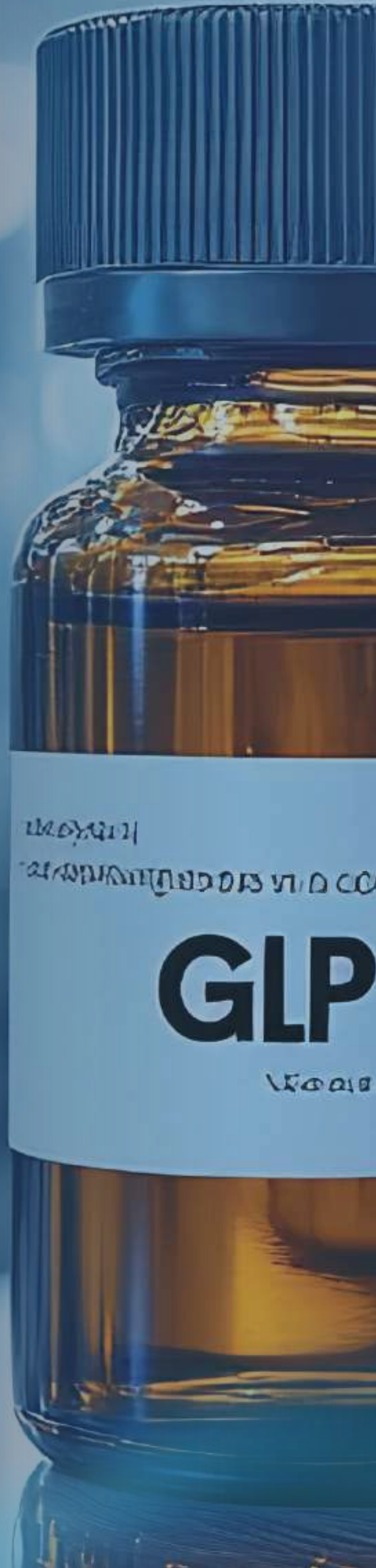
### Why It Matters:

- **Avoid mix-ups:** Clear labels prevent the all-too-common scenario of identical-looking liquids leading to analytical errors or safety hazards.
- **Regulatory compliance:** GLP and ISO standards emphasize accurate labelling at every step – from reagent prep to waste segregation.
- **Safety first:** An unmarked flask of nitric acid or acetone poses immediate risks, especially in shared workspaces.
- **Traceability:** Proper labelling ensures every step of your workflow can be traced back, aiding audits and reproducibility.

### Best Practices

- Use pre-printed or barcoded labels for consistency in analytical labs. Many instruments (like HPLC autosamplers or titrators) can now read barcodes directly for automated data logging.
- Label before adding any reagent or sample. Never assume you'll "remember which one's which" – even during short workflows. Include key identifiers: sample code, date, analyst initials, and concentration or dilution factor if applicable.
- Choose label materials wisely. For analytical or environmental testing, use solvent-resistant, cryo-safe, or waterproof labels to ensure legibility after exposure to solvents or low temperatures.
- Avoid labelling caps only. Caps can be accidentally swapped between vials – always label the body of the container.
- Digital integration: If your lab uses a LIMS (Laboratory Information Management System), link physical sample labels with digital entries for full traceability from preparation to reporting.

**Pro Tip:** Use solvent-resistant lab markers or printable labels. Faded or smudged writing is as risky as no label at all.



## Updates

### *Recent Novel FDA Approved Drugs*

#### **Paltusotine (Palsonify)**

Paltusotine is an oral small-molecule somatostatin receptor 2 (SST2) agonist developed by Crinetics Pharmaceuticals for treating *acromegaly* and related endocrine disorders. Designed to replace monthly injectable therapies, it offers convenient once-daily dosing while effectively reducing growth hormone and IGF-1 levels.

#### **Remibrutinib (Rhapsido)**

Remibrutinib is an oral, highly selective *Bruton's tyrosine kinase (BTK)* inhibitor developed by Novartis. It is being investigated for the treatment of *autoimmune* diseases such as chronic spontaneous urticaria and multiple sclerosis, offering targeted immune modulation with fewer off-target effects.

#### **Imlunestrant (Inluriyo)**

Imlunestrant is an *oral selective estrogen receptor degrader (SERD)* developed by Eli Lilly. Designed for *ER-positive breast cancer*, it works by blocking and degrading estrogen receptors, aiming to overcome resistance seen with traditional endocrine therapies.



PharmaLab Chem  
Vapi Gujarat 2025



India Expo Centre,  
Greater Noida, Delhi NCR-2025

**CATALYST** Cue invites scientists and industry specialists to share their expertise through articles on emerging scientific breakthroughs and instrumentation.



Please write to us at ***info@inkarp.co.in***

**CATALYST** Cue is now available in digital format.



***Scan the QR Code  
to leave your valuable feedback***

For latest news, insights, and discussions in the world of science, follow us on

*Disclaimer: CATALYSTCue provides a platform for diverse perspectives. The views and opinions expressed in the articles and interviews are solely those of the authors.*

# Hei-PLATE Mix 'n' Heat Core+

Stirring and Heating with a Pt1000\* – Simple and Precise

## Key Features

- Dual Functionality: Gently stirs up to 1,400 rpm and heats precisely up to 300°C.
- Smart Controls: Illuminated keys show active functions; dynamic knobs adapt to turning speed for fine or rapid adjustments.
- Safety First: Includes locking function to prevent accidental setting changes and a residual heat indicator above 50°C.
- Patented Kera-Disk® Plate:
  - Made of anodized aluminum – chemical- and scratch-resistant
  - 135 mm diameter fits a wide range of accessories
  - Enables faster, uniform heating
- Digital Precision: Two selectable modes – FAST or PRECISE – ensure stable temperature control without overshoot.
- External Sensor Ready: Compatible with the Pt1000 temperature sensor for direct sample monitoring.



**Inkarp Instruments Pvt Ltd**

Plot No - 5A/10-11, 3rd Floor, IDA Nacharam Road No. 1, Nacharam - Chilka Nagar Road, Hyderabad – 500076.

📞 040 27172293/5088 📩 info@inkarp.co.in